Integrated Traffic Control at Motorway Bottlenecks using Variable Speed Limits and Efficient Vehicles Lane Assignment

Dimitrios-Ilias Skoufoulas

Supervisor: Prof. Ioannis Papamichail

A thesis submitted in fulfillment of the requirements for the degree of
Production Engineering and Management
in the

Chania, 2018

Abstract

Motorway traffic congestion, typically initiated at bottleneck locations, is a major problem for modern societies, causing serious infrastructure degradation. According to empirical investigations, capacity flow in conventional traffic is not reached simultaneously at all lanes. Thus, traffic breakdown may occur on one lane, while capacity reserves are still available on other lanes. Naturally, once congestion appears on one lane, it spreads fast to the other lanes as well, as drivers on the affected lane attempt to escape the speed drop via lane changing. After congestion has occurred, retarded and different vehicle acceleration at the congestion head causes the so-called capacity drop phenomenon, which breeds a reduction in the mainstream flow of a motorway, while a queue is forming upstream of the bottleneck location. The most efficient way to mitigate this problem is the development and implementation of proper traffic control strategies. This thesis investigates via microscopic simulation the integrated use of two feedback control strategies utilizing Vehicle Automation and Communication Systems (VACS) in different penetration rates, aiming at maximising throughput at bottleneck locations. The first control strategy employs Mainstream Traffic Flow Control (MTFC) using appropriate Variable Speed Limits (VSL) that are communicated to all vehicles within specific controlled sections of the motorway. The second control strategy delivers appropriate lane-changing actions to selected connected vehicles, again within specific controlled sections. Simulation results demonstrated the effectiveness of the integrated use of strategies for all performance indexes considered.

Acknowledgments

Finalizing this thesis, I would like to thank my supervisor Prof. Ioannis Papamichail as well as Prof. Markos Papageorgiou for their motivation, guidance, immense knowledge and for trusting me to become a member of the Dynamic Systems and Simulation Laboratory (DSSL). I would like to thank all members of DSSL for sharing thoughts and support on several issues all this period. Specifically, I would like to thank Vasileios Markantonakis for his patience and his guidance throughout the development of this work.

Most of all, I would like to thank my family for their support and encouragement all these years, as well as my friends and my girlfriend for being there for me.

Contents

List of Figures

4

List of Tables

1. Introduction

1.1 Motivation

A crucial problem for modern societies is the daily traffic congestion on motorways, especially during rush hours. The continuous increase of car ownership and demand that contribute to the daily appearance of recurrent and not recurrent motorway congestion are the main reasons of the problem. Since the expansion of the traffic congestion is increasing in both space and time, the consideration of the immediate effects is essential in order to improve the quality of life in urban areas.

Ironically, daily recurrent congestion reduces substantially the available infrastructure capacity during rush hours, i.e., at the time this capacity is most urgently needed, causing delays, increased environmental pollution, and reduced traffic safety (Papageorgiou and Kotsialos, 2000). The negative outcomes are huge especially for economy and social life. For instance, in 2014 at U.S.A. urban citizens had to travel an extra 6.9 billion hours and purchase an extra 3.1 billion gallons of fuel for a congestion cost of $160 (Schrank et al., 2015).

Generally, traffic congestion appears when too many vehicles attempt to use a common transportation infrastructure with limited capacity (i.e. bottleneck locations). Congestion leads to queueing phenomena, reduced safety and respectively delays and infrastructure capacity is not fully exploited. In the worst-case, congestion leads to a degraded use of the available infrastructure, therefore accelerating the congestion increase, which leads to further infrastructure degradation and so forth (Papageorgiou, 2004). Sometimes congestion becomes generalized and covers a significant part of the motorway network, often spilling over from one motorway to another via the corresponding interconnections.

According to empirical investigations, capacity flow in conventional traffic is not reached simultaneously at all lanes. Thus, traffic breakdown may occur on one lane, while capacity reserves are still available on other lanes. This implies that the potentially achievable cross-lane capacity is not fully exploited. Naturally, once congestion appears on one lane, it spreads fast to the other lanes as well, as drivers on the affected lane attempt to escape the speed drop

via lane changing. After congestion has occurred, retarded and different vehicle acceleration at the congestion head causes the so-called capacity drop phenomenon, which breeds a reduction in the mainstream flow of a motorway, while a queue is forming upstream of the bottleneck location.

The degradation and underutilization of the freeways networks which accordingly lead to reduced throughput in periods of congestion can be countered via suitable control measures and strategies (Papageorgiou, 2004).

In the last two decades, a significant and increasing interdisciplinary effort by the automotive industry, as well as by numerous research institutions around the world, has been devoted to the planning, developing, testing and deploying a variety of Vehicle Automation and Communication Systems (VACS) that are expected to revolutionize the features and capabilities of individual vehicles within the next decades (Roncoli et al., 2014).

Simulation studies on VACS point out that they can affect traffic flow both positively and negatively; they may lead to a deterioration of the overall traffic conditions. On the other hand, they may offer significant benefits if deployed appropriate by traffic management (Diakaki et al., 2015). Specifically, VACS may be exploited to interact with recommendations of driving behavior, or even executing traffic control actions. This gives the possibility of having access to control actions that are not available with conventionally driven cars (e.g., individual vehicle speed or lane-change advice) (Roncoli et al., 2014). However, currently penetration rates of VACS around the globe are still limited.

Microscopic simulators models have been widely accepted for several transportation system designs, traffic operations and strategy planning. Basically, these simulators are exceptionally useful when strategies under construction require new constrictions or costly investments (Park and Qi, 2006). AIMSUN (Transport Simulation Systems, 2014), VISSIM (AG Planung Transport Verkehr, 2011), CORSIM (FHWA, 1997), etc. are the most commonly used commercial vehicular microscopic simulation models. Simulation models require suitable calibration and validation in order to provide reliable results. Calibrating a traffic simulation model can require significant time and effort, particularly as the model complexity increases.

1.2 Thesis objectives

The objective of this thesis is the investigation via a microscopic simulator the integrated use of two feedback control strategies for a hypothetical motorway stretch featuring a lane-drop bottleneck. The calibration of the macroscopic model is based on a try-and-error procedure

that involves manual tuning. Hypothetical traffic demand was used in order to build the simulation scenario and evaluate the simulation output. We evaluate these two control strategies via testing them on a motorway stretch involving a lane-drop area, in order to mitigate the traffic congestion of the motorway. These strategies comprise Mainstream Traffic Flow Control (MTFC) and Lane-changing Control (LCC). The first one was proposed in previous work (Carlson et al., 2011) with ramp metering in bottlenecks locations using Variable Speed Limits (VSL) as an actuator and tested in a macroscopic simulator. Then, this strategy was tested in a validated microscopic flow model for a highway work zone (Papamichail et al., 2017). Concerning the Lane-change control, it was proposed by Roncoli et al. (2016) and it was tested utilising a macroscopic simulator. For the implementation of LCC actions, the presentence of VACS is essential because they have the technology to execute these commands.

1.3 Thesis outline

This thesis is composed of five Sections. Section 1. is the introduction which describes the problem we consider, includes the reasons and targets for this specific study. In addition, for the control strategies we intend to investigate, we mention the relevant studies in which they are developed and proposed. After that, Section 2. is a brief description of the AIMSUN microscopic simulator and the employed behavioral models. Section 3., describes the control strategies used in this work. More specifically, the Mainstream Traffic Flow Control (MTFC) using Variable Speed Limits (VSL) and the Lane-changing Control (LCC) we implement. Section 4. follows with the simulation results. The network is described, the simulation parameters are introduced and the results for each case are exhibited. Finally, Section 5. summarizes the conclusions of our study.

2. Microscopic Simulator

2.1 Introduction

The behavior of the proposed strategy in Section 3 is examined through a microscopic simulation process using AIMSUN (Advanced Interactive Microscopic Simulator for Urban and Non-urban Networks) by Transport Simulation Systems (Transport Simulation Systems, 2014).

Transport professionals and researchers use widely AIMSUN which is a commercial microscopic traffic simulation software. The system provides modeling of traffic network in-depth while it includes separate type of vehicles and drivers, a wide range of network geometries, model incidents, conflicting manoeuvre and so on (Transport Simulation Systems, 2003). It provides the ability to users to exchange information dynamically with Aimsun tools (e.g. Aimsun API and microSDK).

AIMSUN microscopic simulator requires a simulation scenario and the setting of simulation parameters to define the experiment. Basically, scenario is the container for the input data and experiments to execute the simulation, while it is composed of several parameters. For the ones mentioned above, the main parameters are the network description, traffic demand data (a group of traffic stages), public transport plan and traffic control plans. As for the simulation parameters, there are fixed values that define the experiment like simulation time, warm-up period, statistics intervals and some variable parameters to calibrate the models. Common outputs are measures such as average travel time and speed (Transport Simulation Systems, 2003).

The AIMSUN Application Programming Interface (API) offers the ability to users to exchange information dynamically with Aimsun. It connects externally to the microsimulator during the simulation to get and set information about vehicles, demand, control, traffic management etc. The microsimulator API is offered in both C and Python. Another tool that developers can use is a microsimulator (microSDK) to modify the behavioral models of the desired vehicles which is offered in C++ (Transport Simulation Systems, 2014). With this last

tool, a user can change the AIMSUN's default behavioral models that will be overwritten by the new developed behavioral models for specific sections or the whole network.

2.2 Behavioral models

The behavioral models are used to approach different aspects of human driver behavior while they comprise several sub-models. The accuracy of these models depends on the quality of the traffic-flow models. The most critical components are the car-following and lane-changing models (Panwai and Dia, 2005).

2.2.3 Car-following model

The car-following behavior describes the way a pair of vehicles interact with each other. "*Microscopic traffic models describe the motion of each individual vehicle, that is, they model the action such as accelerations and decelerations of each driver as a response to the surrounding traffic by means of an acceleration strategy toward a desired velocity in the free-flow regime, a braking strategy for approaching other vehicles or obstacles, and a car-driving strategy for maintaining a safe distance when driving behind another vehicle. Microscopic traffic models typically assume that human drivers react to the stimulus from neighboring vehicles with the dominant influence originating from the directly leading vehicle known as follow-the-leader or car-following approximation*" (Kesting and Treiber, 2008).

The AIMSUN microscopic simulator contains a default car-following model based on the Gipps model (Gipps, 1981). This model has realistic physical meanings for all its parameters, but it fails to reproduce the speed and capacity drop of the network (Wang et al., 2005). On account of this, the Intelligent Driver Model (IDM) (Treiber et al., 2000) is implemented and replaces the default car-following models, as the reproduction of the capacity drop phenomenon is essential for our experiment.

An ordinary differential equation formulates the IDM car-following model; therefore space and time are treated as continuous variables. According to Kesting and Treiber (2008) this model class is characterized by an acceleration function $\dot{v}$ that depends on the actual velocity $v(t)$, the (net distance) gap s(t) and the velocity difference $\Delta v(t)$ relevant to the leading vehicle:

$$\dot{v}(s, v, \Delta v) = f(s, v, \Delta v) \tag{1}$$

Notice that $\Delta v(t)$ is defined as the approaching rate, that is, positive if the following vehicle is faster than the leading vehicle.

IDM is defined by the acceleration function:

$$\dot{v}_{IDM}(s, v, \Delta v) = a \left[1 - \left(\frac{v}{v_0} \right)^4 - \left(\frac{s^*(v, \Delta v)}{s} \right)^2 \right]$$

(2)

The expression that combines the acceleration strategy is $\dot{v}_{free} = a \left[1 - \left(\frac{\dot{v}}{v_0} \right)^4 \right]$ toward a desired velocity v_0 on a free road with the parameter a for maximum acceleration with a braking strategy $\dot{v}_{brake}(s, v, \Delta v) = -a \left(\frac{s^*}{s} \right)^2$ which is dominant if the current gap s(t) to the preceding vehicle becomes smaller than the desired minimum gap:

$$s^*(v, \Delta v) = s_0 + vT + \frac{v \Delta v}{2 \sqrt{ab}}$$

(3)

The minimum distance s_0 in congested traffic is significant for low velocities only. The dominating term of Equation (3) in stationary traffic is vT which corresponds to following the leading vehicle with a constant desired (safety) time gap T. The last term is only active in non-stationary traffic and implements an "intelligent" driving behavior including a braking strategy that, in nearly all situations, limits braking decelerations to the comfortable deceleration b. Note, however, that IDM brakes stronger than b if the gap becomes too small. This braking strategy makes IDM collision-free. All IDM parameters v_0, T, s_0, a and b are defined by positive values (Kesting and Treiber, 2008).

2.2.4 Lane-changing model

The transfer of a vehicle from one lane to the adjacent has a significant impact on traffic flow. Modeling the behavior of a vehicle within its present lane is relatively straightforward, as the only variables that matter are the speed and location of the preceding vehicle. Lane changing is complex because the decision to change lanes depends on a number of objectives, and at times these may conflict (Gipps, 1986). The default Lane-changing model in AIMSUN is based on the Gipps Lane-changing Model (Gipps, 1986).

The aforementioned model cannot capture the merging behavior in a critical flow regime (Chevallier and Leclercq, 2009), a fact that led us to replace it with heuristic rules that were introduced by Roncoli et al. (2014) which are applied in the sections where the default model is unable to provide realistic driver behavior. The rest of the network uses the default Gipps lane-changing Model.

13

Gipps lane-changing model

The Gipps lane-changing model models the lane change as a decision process analyzing the necessity of the lane change, the desirability of the lane change and the feasibility conditions for the lane change that are also local, depending on the location of the vehicle on the road network (Barcelo and Casas, 2005).

Each time a vehicle has to be updated the model draws up the question for the necessity of the lane changing. The answer to this question is depending on several factors, the turning feasibility at current lane, the distance to the next turning and the traffic conditions in the current lane. As for the traffic conditions they are measured in terms of speed and queue lengths. When a driver is going slower than he wishes, he tries to overtake the preceding vehicle. On the other hand, when he is traveling fast enough, he tends to go back into the slower lane (Barcelo and Casas, 2005).

Once the lane change action is considered necessary it has to answer two more questions. The desirability of lane change by checking the possible improvement in the traffic conditions after the transfer and the possibility of lane change by testing if there is enough gap to safely move to the neighboring lane.

In order to represent the driving behavior more realistically, there are three different zones inside each section with different rank of lane-changing motivation (Barcelo and Casas, 2005). The zones are:

- Zone 1: This is the farthest from the next turning point. The lane changing decisions are governed by the traffic conditions of the lanes involved; the feasibility of the next desired turning movement is not yet taken into account. To measure the improvement that the driver will get on changing lanes several parameters are considered: the desired speed of the driver, speed and distance of the current preceding vehicle and speed and distance of the future preceding vehicle.

- Zone 2: This is the intermediate zone. Vehicles not driving in valid lanes (i.e. lanes where the desired turning movement can be made) tend to get closer to the correct side of the road from which the turn is allowed. Vehicles looking for a gap try to adapt to gaps located either downstream or adjacent.

- Zone 3: Vehicles are forced to reach their valid lane, looking for gaps upstream and reducing speed if necessary, even coming to a complete stop in order to make the change possible.

Heuristic lane-changing model

The default lane-changing model of AIMSUN is overwritten by the Heuristic rules in the lane-drop network section, in this way the merging behavior is more realistic. In the lane-drop regions, drivers need to change lane in order to enter in the mainstream network.
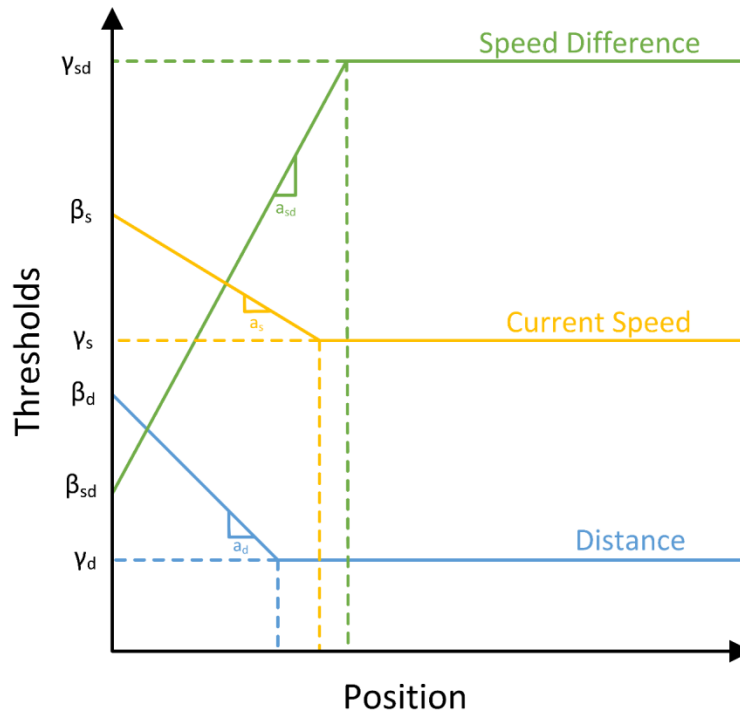
Figure 1: Heuristic rules based on current speed, distance and speed difference.

The heuristic rules consist of a set of inequality conditions between the vehicle's current state, and its threshold values. In particular, linear functions of the vehicle's current position determine the threshold values of the three variables of interest i.e. current speed, relative speed with respect to the target-lane vehicles, and available gap in the target lane. The concept of the rules is illustrated in Figure 1., where two regimes can be noticed. In the first region the threshold values are linearly dependent on the position of the vehicle while in the second regime the threshold values remain constant. Note that in the first region the current speed and the distance thresholds are decreasing while the threshold of the relative speed difference is increasing with respect to the position of the vehicle. The current state of the vehicle needs to have greater values of current speed and distance than the threshold values of these linear rules while the speed difference has to be lower than the respective threshold value. Once these conditions are simultaneously satisfied then the vehicle is mandated to

move to another lane. As it can be observed, the conditions are easier to be satisfied as the vehicle moves further downstream where the threshold values are relaxed (Perraki, 2016).

For the determination of these rules some parameters have to define in order that a realistic merging behavior is achieved. These parameters are the slope as well as the initial and the final value of the linear equations. Considering that our network is similar in lane-drop areas with (Perraki, 2016) we used that calibration as an initial step. Then based on a trial and error process we achieved a realistic driving behavior in this area. The calibrated values of the rules are given in Section 4.2.

3. Control strategies

3.1 Bottlenecks on Motorways

A (latent) bottleneck on a motorway is a location where the flow capacity q_{cap}^{up} upstream is higher than the flow capacity q_{cap}^{down} downstream of the bottleneck location (see Figure 2.). Bottlenecks may be due to a number of reasons, i.e., merging of on-ramps, infrastructure layout (e.g., lane drop, tunnel, strong grade, and curvature), specific traffic conditions (e.g., strong weaving), regulatory measures (e.g., fixed speed limits), or external capacity-reducing events such as overspilling off-ramps or incidents.

The nominal bottleneck capacity q_{cap}^{down} is the maximum traffic flow that can be maintained at the bottleneck location if the traffic flow q_{in} arriving from upstream happens (or is controlled) to be equal to q_{cap}^{down}. However, if the arriving flow q_{in} ($q_{in} \leq q_{cap}^{up}$) is higher than the capacity q_{cap}^{down}, the bottleneck is activated, generating congestion starting at the bottleneck location and spilling back for as long as the upstream arriving flow is sufficiently high (see Figure 2.). The congestion forming at an active bottleneck has two kinds of detrimental effects on the motorway capacity and throughput (Papageorgiou and Kotsialos, 2000).

- Capacity drop at the congestion head: For most bottleneck types previously mentioned, bottleneck activation leads to a speed breakdown upstream of the bottleneck location. As a consequence, vehicles have to accelerate from lower speeds (within the formed congestion) to higher speeds (downstream of the bottleneck). This is deemed to lead to a capacity drop, i.e., an active bottleneck outflow q_{out} that may be 5%–20% lower than the nominal capacity q_{cap}^{down} (see Figure 2.).
- Blocking of off-ramps (BOR): In most cases, the tail of the formed congestion propagates upstream and covers several on-ramps and off-ramps upstream of the bottleneck (see Figure 2.). As the traffic flow along the congested area is lower than the upstream arriving flow (else the congestion tail would not move upstream), the

17

off-ramp flows drop accordingly. Thus, vehicles that are bound for exits upstream of the active bottleneck are also delayed due to the congestion and in fact contribute to an accelerated spatial increase of the congestion.

To avoid or delay the activation of a bottleneck and the related capacity drop phenomenon, various traffic control measures have been proposed and applied (Papageorgiou et al., 2003).
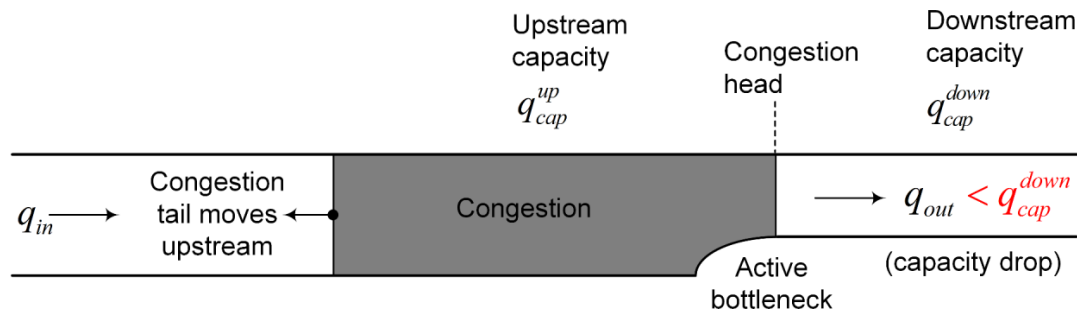
Figure 2: Active bottleneck notions.

3.2 MTFC via VSL

3.2.1 MTFC concept

The basic idea of MTFC as it is presented in (Carlson et al., 2011) is to enable the mainstream traffic flow at selected locations (e.g., upstream of bottlenecks) to take values ordered by an appropriate control strategy to establish optimal traffic conditions (maximum throughput) for any appearing demand. A local aspect of this basic idea is shown in Figure 3. The bottleneck of Figure 3. is not activated (and no MTFC is needed) as long as $q_{in} \leq q_{cap}^{down}$, in which case, we have $q_{out} \approx q_{in}$. If q_{in} grows bigger than the bottleneck capacity q_{cap}^{down}, the bottleneck would be activated in the absence of control as in Figure 2., and q_{out} would be reduced due to capacity drop; on the other hand, MTFC can implement a controlled outflow q_c that is equal to the bottleneck capacity (or accordingly less if the bottleneck is due to a merging on-ramp). Clearly, the mainstream congestion cannot be avoided via MTFC because $q_{in} > q_{cap}^{down}$ (otherwise, MTFC would not intervene).

- The congestion outflow in the MTFC case is higher than in the no-control case because the capacity drop is avoided.
- For the same reason (higher outflow with MTFC), the created congestion in the MTFC case (a) has higher internal speed and (b) is space-time shorter than that in the no-control case. Thus, MTFC leads to less blocking of less off-ramps, which marks

potential improvement for the detrimental effects of BOR on the infrastructure capacity.

Nevertheless, the fact that MTFC leads to the formation of (controlled) mainstream congestion implies that BOR effects may be reduced but not fully avoided. In other words, MTFC is a control measure against capacity drop in the first place, whereas any improvements related to BOR effects are due to shorter and lighter mainstream congestion.
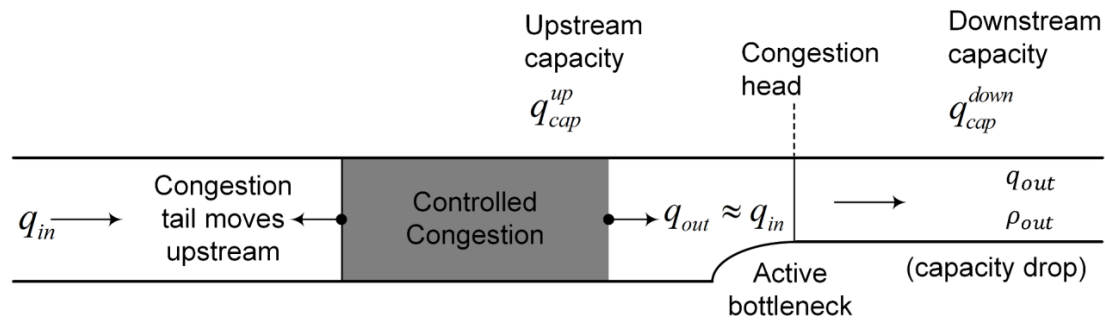
Figure 3: Local aspect of MTFC

VSLs may be used to slow down the motorway traffic flow sufficiently to create the ordered mainstream control flow q_c. The proposed real-time merging traffic control framework is based on previous work (Papamichail et al., 2017) using Variable Speed Limits (VSL) as a control actuator for efficient real-time merging traffic control at highway work zones. In our case, we use this strategy at a hypothetical highway bottleneck due to a lane drop, which is similar to the work zone merging zone.

The application of a low VSL at some stretch (application area) upstream of the lane-drop area may lead to a controlled congestion. An acceleration area, downstream of the application area, ensures that vehicles have enough space to accelerate from low speeds in the VSL application area to the critical speed corresponding to capacity flow through the bottleneck. In addition, for safety reasons, VSL may also be applied upstream of the application area (safety area) so as to enable a gradual speed decrease for arriving vehicles; see Figure 4.
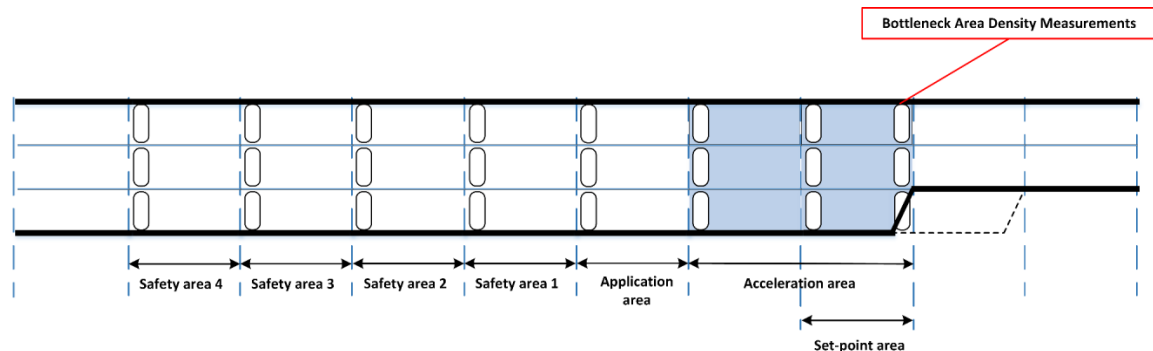
Figure 4: MTFC control infrastructure

In order to apply feedback control and maintain the bottleneck density ρ close to its critical value ρ_{cr}, real-time measurements or estimates of ρ are needed. A frequently practiced way of estimating ρ is by use of ordinary loop detectors measuring traffic occupancy, placed at appropriate positions (Vigos et al., 2008).

3.2.2 Controller design

In a similar manner to what was proposed in the past for the case of mainstream traffic flow control of ramp merging bottleneck (Carlson et al., 2011, Carlson et al., 2013) and (Papamichail et al., 2017) for the case of work zone control; a PI controller is used here for MTFC at a motorway bottleneck location due to a lane drop.

The measured (or estimated) density $\rho(k^Q)$ (or occupancy) at the bottleneck location at each discrete time instant k^Q (=1, 2, …) is compared against the desired set-point $\hat{\rho}$.. The set-point is typically selected around the critical density value, at which capacity flow is achieved at that location; and the aim of the feedback regulator is to keep the bottleneck density close to the selected set-point which guarantees maximum throughput. The PI-type regulator is given by:

$$vsl(k^Q) = vls(k^Q - 1) + K_I\left(\hat{\rho} - \rho(k^Q)\right) + K_P(\rho(k^Q - 1) - \rho(k^Q)) \qquad (4)$$

where $vsl(k^Q)$ represents the output of the regulator at a discrete number instant k^Q. K_I and K_P are the integral and proportional gains, respectively. The output of the regulator is truncated so as to remain within a range of admissible VSL values $[vsl_{min}, vsl_{max}]$. The truncated values are used at the next time-period as the values to avoid the well-known windup phenomenon for PI regulators.

So, at each discrete time k^Q, the controller calculates the VSL values which will be posted at the gantries via the use of Variable Message Signs (VMS), but some practical VSL implementation aspects are then taken into account. Posted VSL can only take predefined discrete values (e.g. 90, 80, 70, … km/h).

Furthermore, the difference between two consecutively posted VSL at the same gantry is limited (e.g. to ±10 km/h), so as to avoid abrupt speed changes. Also, the difference between two VSL posted at consecutive gantries at the same control period is limited (e.g. to 10 km/h), as often required in practice, in order to achieve a safe approach of vehicles within the safety area.

Regarding the gantries, at the beginning of the acceleration area (see Figure 4.) there is a gantry with constant VSL. The decision of the PI regulator (4) is placed at the gantry in the

start of the application area. The real-time density estimates needed for the regulator are provided by the most downstream detectors of the stretch (see Figure 4.). As far as the safety areas, the VSL gantries are placed at the upstream end of each section.

3.3 Lane-changing Control

As mentioned in section 3.1 if the arriving demand is higher than the bottleneck capacity, the bottleneck is activated, i.e. congestion is formed upstream of the bottleneck location. It should be empathized, however, that according to empirical investigations, capacity flow in conventional traffic in not reached simultaneously at all lanes. The Lane-change Control (LCC) is a new strategy that can be exploited for traffic management. This control strategy aims the distribution of traffic flow among the lanes in the immediate proximity of a bottleneck, so as to exploit the capacity of each and every lane, thus increasing the overall (cross-lane) capacity. The LCC is not feasible with conventional means, because it calls for the possibility to communicate with vehicles, so the use of VACS is essential.

The Lane-changing Controller uses real-time measurements for the calculation of optimal lateral flows for each segment-lane, but the implementation of the corresponding lane-changing advice is a bit challenging. More specifically we have to define the way that we select the cars to implement the lane-changing. This is related to the penetration rate of VACS in each segment, so the availability of able cars to execute the commands. Another question is which cars are more suitable to take the command regarding the traffic condition near them, so the lane-changing has the least negative impact in the lane we advise each vehicle to enter (target lane). For this matter in each control period, we calculate for all VACS the gaps between the leader and follower in their target-lane. We use this information to select the more suitable cars for lane-changing. As for the calculation of optimal lateral flows in the next sections, we present the methodology of the proposed strategy.

3.3.1 Multi-lane macroscopic traffic flow model

The multi-lane macroscopic traffic flow model described in (Roncoli et al., 2015) and its simple mathematical form and the further formulation of traffic dynamics aspects makes it an efficient tool for optimal control problem formulations such as those used by the strategy utilized in the present work.

The multi-lane network is subdivided into segment-lane entities with the index $i = 0, ..., N$ for segments and $j, m_i ..., M_i$ for lanes, where m_i and M_i are the minimum and maximum indexes of lanes for segment i. A discrete time step T^f for a simulation horizon K indexed by

21

$k^f = 1, \ldots, K$ where the simulation time is $t = k^f T^f$. The motorway is discretized in space by defining the segment-lane entities, which are characterized by the following variables:

- Density $\rho_{i,j}(k^f)[veh/km]$, the number of vehicles in the segment i, lane j, at time step k^f, divided by the segment length L_i

- Longitudinal flow $q_{i,k}(k^f)[veh/hour]$, the traffic volume leaving segment i and entering segment $i+1$ during time interval $(k^f, k^f + 1]$, thus remaining in lane j

- Lateral flow $f_{i,j}(k^f)[veh/hour]$, i.e. the traffic volume in the segment i and moving from lane j to lane $j+1$ (vehicles changing lane remain in the same segment during the current time interval $(k^f, k^f + 1]$)

- External flow $d_{i,j}(k^f)$ entering the network in cell i either from the mainstream or from on-ramp, remaining in lane j during time interval $(k^f, k^f + 1]$
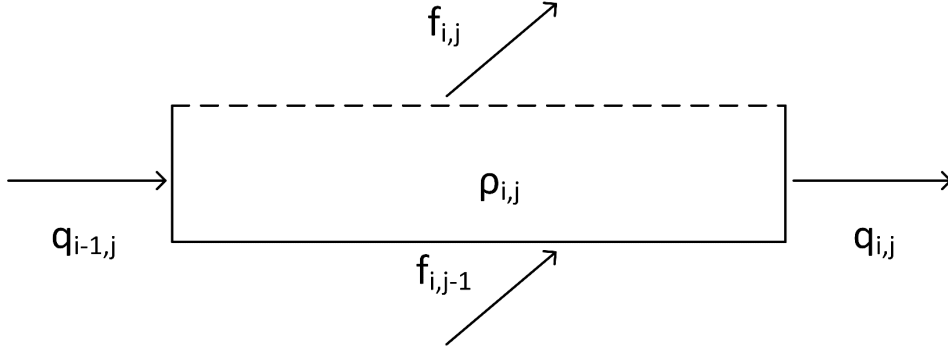

Figure 5: The segment-lane variables used in the model formulation

The density $\rho_{i,j}(k^f)$ is updated based on the following conservation Equation:

$$\rho_{i,j}(k^f + 1) = \rho_{i,j}(k^f) + \frac{T}{L_i}\left[q_{i-1,j}(k^f) - q_{i,j}(k^f) + f_{i,j-1}(k^f) - f_{i,j}(k^f)\right]$$
$$+ \frac{T}{L_i}d_{i,j}(k^f) \tag{5}$$

Depending on the network topology, some terms of the (5) may not be present. To account for any possible network topology, including lane drops and lane additions on the right and on the left sides of the motorway, it is assumed that $j = 0$ corresponds to the segment(s) including the rightmost lane. Consequently, m_i and M_i are defined as the minimum and maximum indexes j, respectively, for which a lane exists in segment i. According to that definition, the total number of cells from the origin to segment i is $H_i = \sum_{r=0}^{i}(M_r - m_r + 1)$, and the total number of cells for the whole stretch is $\bar{H} = H_N$.

22

It is important to highlight that, in order to ensure numerical stability, the time step T^f must respect the Courant–Friedrichs–Lewy (CFL) condition (Courant et al., 1928), precisely:

$$T^f \leq \min_{i,j} \frac{L_i}{v_{i,j}^{free}}$$

(6)

where $v_{i,j}^{free}$ is the maximum speed allowed in the corresponding segment-lane. Equation (5) is the only dynamic equation considered in this first-order traffic flow model.

The net lateral flow $f_{i,j}(k^f)$ is considered only in one direction, namely, from the right to left lanes; therefore, $f_{i,j}(k^f)$ is actually the difference between the flow leaving and entering lane j at its left side. This simplification is useful for the subsequent control problem formulation since lateral flows are treated as control inputs. Consider the well-known relationship:

$$q_{i,j}(k^f) = \rho_{i,j}(k^f)v_{i,j}(k)$$

(7)

Using the Equation (7) and the assumption of one-way lateral flows the Equation (5) is obtained:

$$\rho_{i,j}(k^f + 1) = \frac{T^f}{L_i}v_{i-1,j}(k^f)\rho_{i-1,j}(k^f) + \left[1 - \frac{T^f}{L_i}v_{i,j}(k)\right]\rho_{i,j}(k^f)$$
$$+ \frac{T^f}{L_i}\left[f_{i,j-1}(k^f) - f_{i,j}(k^f)\right] + \frac{T^f}{L_i}d_{i,j}(k^f)$$

(8)

which treating speeds $v_{i,j}(k)$ as known parameters, can be seen as a Linear Parameter Varying system in the form:

$$\underline{x}(k^f + 1) = A(k^f)\underline{x}(k^f) + B\underline{u}(k^f) + \underline{d}(k^f)$$

(9)

where

$$\underline{x} = \begin{bmatrix} \rho_{0,m_0} \cdots \rho_{0,M_0} & \rho_{1,m_1} \cdots \rho_{N,M_N} \end{bmatrix}^T \in \mathbb{R}^{\bar{H}}$$

(10)

$$\underline{u} = \begin{bmatrix} f_{0,m_0} \cdots f_{0,M_0} & f_{1,m_0}(k^f) \cdots f_{N,M_{N-1}} \end{bmatrix}^T \in \mathbb{R}^{\bar{F}}$$

(11)

$$\underline{d} = \left[\frac{T^f}{L_0} d_{0,m_0} \ \dots \ \frac{T^f}{L_0} d_{0,M_0} \quad \frac{T^f}{L_1} d_{1,m_1} \ \dots \ \frac{T^f}{L_N} d_{N,M_N} \right]^T \in \mathbb{R}^{\bar{H}} \tag{12}$$

and time index k^f is omitted to simplify the notation. $A \in \mathbb{R}^{\bar{H} \times \bar{H}}$ composed of elements $a_{r,s}$, which represent the connection between pairs of subsequent cells connected by a longitudinal flow, and $B \in \mathbb{R}^{\bar{H} \times \bar{F}}$, composed of elements $b_{r,s}$, which reflects the connection of adjacent cells connected by lateral flows, are defined as:

$$a_{r,s} = \begin{cases} 1, & \text{if } r = s \text{ and } (j < m_{i+1} \text{ or } j > M_{i+1}) \\ 1 - \dfrac{T^f}{L_i} v_{i,j}, & \text{if } r = s \text{ and } (i = N \text{ or } m_{i+1} \le j \le M_{i+1}) \\ \dfrac{T^f}{L_i} v_{i-1,j}, & \text{if } r > H_0 \text{ and } s = r - M_{i-1} + m_i - 1 \\ 0, & \text{otherwise} \end{cases} \tag{13}$$

$$b_{r,s} = \begin{cases} \dfrac{T^f}{L_i}, & \text{if } j > m_i \text{ and } s = r - i \\ -\dfrac{T^f}{L_i}, & \text{if } j < M_i \text{ and } s = r - i + 1 \\ 0, & \text{otherwise} \end{cases} \tag{14}$$

where $r = \sum_{r=0}^{i-1} H_r + j - m_i$.

3.3.2 Optimal control problem formulation

The linear system (Equation (9)) described in Section 3.3.1 is used for formulating an optimal control problem with the purpose of manipulating the lateral flows to avoid creating congestion resulting from the activation of a bottleneck. Under the assumptions that the overall traffic flow entering the controlled area does not significantly exceed the bottleneck capacity and that the controller succeeds in avoiding the creation of congestion, one can assume that the speed in all cells remains at a constant value (e.g., the free-flow speed) $v_{i,j}(k) \equiv \bar{v}, \forall i, j, k$. In addition, one can assume that the measurable inflows $\underline{d}$ are constant; the actual slow time variation of $\underline{d}$ will not affect the control performance significantly. With these assumptions, the system in Equation (9) can be viewed as a linear time-invariant system:

24

$$\underline{x}(k^f + 1) = A\underline{x}(k^f) + B\underline{u}(k^f) + \underline{d} \qquad (15)$$

The following quadratic cost function (over an infinite time horizon) that accounts for the penalization of the difference between some (targeted) densities and the corresponding prespecified (assumed constant) set point values is defined, as well as a penalty term aiming at maintaining small control inputs, that is, small lateral flows (weighted by ϕ):

$$J = \sum_{k=0}^{\infty} \left\{ \sum_{\hat{\imath}} \sum_{\hat{\jmath}} a_{\hat{\imath}\hat{\jmath}} \left[\rho_{\hat{\imath}\hat{\jmath}}(k) - \hat{\rho}_{\hat{\imath}\hat{\jmath}} \right]^2 + \varphi \sum_{i=0}^{N} \sum_{j=m_i}^{M_i-1} \left[f_{i,j}(k) \right]^2 \right\} \qquad (16)$$

where

$(\hat{\imath}, \hat{\jmath}) =$ targeted cells,

$\hat{\rho}_{\hat{\imath}\hat{\jmath}} =$ desired set point, and

$a_{\hat{\imath}\hat{\jmath}} =$ corresponding weighting parameter

Equation (16) is rewritten in matrix form as

$$J = \sum_{k=0}^{\infty} \left\{ \left[C\underline{x}(k) - \hat{\underline{y}} \right]^T Q \left[C\underline{x}(k) - \hat{\underline{y}} \right] + \underline{u}^T R\underline{u}(k) \right\} \qquad (17)$$

where $Q = Q^T \geq 0$ and $R = \varphi I_{\overline{F}} > 0$ are weighting matrices associated with the magnitude of the state tracking error and control actions, respectively, while C, composed of elements $c_{r,s}(k)$, where:

$$c_{r,s} = \begin{cases} 1, & \textit{if density} \\ 0, & \textit{otherwise} \end{cases} \qquad (18)$$

reflects the cells that are tracked and $\hat{\underline{y}}$ is a vector that contains the desired set points.

The problem, defined as the minimization of the cost in Equation (17) subject to the linear dynamics in Equation (15), is solved through a Linear Quadratic Regulator (LQR), under the assumption that the original system is, at least, stabilizable and detectable. In Section 3.3.3 the aforementioned properties for our system are analyzed.

<u>Optimal solution</u>

The solution to the proposed (LQR) problem obtained via dynamic programming in (Roncoli et al., 2016) results in the following feedback–feedforward control law:

$$\underline{u}^* = -K\underline{x} + \underline{u}_{ff} \tag{19}$$

where

$$K = (R + B^T P B)^{-1} B^T P A \tag{20}$$

$$P = C^T Q C + A^T P A - A^T P B (R + B^T P B)^{-1} B^T P A \tag{21}$$

$$\underline{u}_{ff} = \left(R + B^T P B\right)^{-1} B^T F (C^T Q \hat{\underline{y}} - P \underline{d}) \tag{22}$$

$$F = (I - (A - BK)^T)^{-1} \tag{23}$$

The feedback control law (19) is very effective for practical application since it requires the computation of the feedback gain matrix K offline. Note that the optimal gain (20) and the Algebraic Riccati Equation (21) are the same that can be found in classic Optimal Control books (Anderson and Moore, 1971).

Note also that, regulator (19) is a so-called state-feedback regulator, which requires availability of measurements for all state variables (densities for each cell) in real time. In the case of incomplete measurements, one may employ a traffic state estimator to produce the missing measurements, e.g., in the context of connected vehicles (Bekiaris et al., 2016).

3.3.3 Stabilisability and Detectability

As already implied Stabilisability and Detectability are essential properties for solving the original problem as an LQR and provide a stabilizing feedback control law (19). The way to address both of the properties in our case is developed in (Roncoli et al., 2016) and also presented in the next paragraphs.

26

Stabilisability

The property of Stabilisability is defined in the Book of (Williams and Lawrence, 2007) as:

The linear state equation (19) *[or the pair* (A, B)*, for short] is stabilizable if there exists a state feedback gain matrix K for which all eigenvalues of* $A - BK$ *have strictly negative real part.*

where the system for the definition:

$$\dot{x} = Ax(t) + Bu(t)$$
$$y(t) = Cx(t)$$

(24)

Also, in the Book by Williams and Lawrence (2007), the following theorem is also established

The following statements are equivalent:

- *The pair* (A, B) *is stabilizable.*
- *There exists no left eigenvector of A associated with an eigenvalue having nonnegative real part that is orthogonal to the columns of B;*
- *The matrix* $[\lambda I - A \ B]$ *has full row-rank for all complex* λ *with nonnegative real part.*

So, in our case to address stabilisability, we can see that the matrix *A* (Equation 15) is, by construction, lower triangular, implying that its eigenvalues λ are equal to the elements in the main diagonal. Since $\bar{u}$ is always positive, the modes related to segments for which another downstream segment exists are always stable ($|\lambda| < 1$), while the modes related to segments without any other segment downstream (i.e., at a lane-drop) are marginally stable ($\lambda = 1$). According to the Hautus-test (Williams and Lawrence, 2007), the system is stabilisable if, for each unstable (or marginally stable) mode, relation:

$$rank[(\lambda I - a) \ B] = \bar{H}$$

(25)

is satisfied. This implies that, to guarantee that the pair (A, B) is stabilisable, *B* must have more linearly independent columns than the number of non-stable ($\lambda \geq 1$) modes, that is, for each lane dropping, there must be at least one controlled lane-changing, which is trivially satisfied for the defined network structure.

<u>Detectability</u>

The definition of the Detectability property (Williams and Lawrence, 2007):

The linear state equation (19) *[or the pair* (A, C), *for short] is detectable if there exists an observer gain matrix L for which all eigenvalues of A $-$ LC have strictly negative real part.*

While is the following theorem is essential:

The following statements are equivalent:

- *The pair* (A, C) *is detectable.*
- *There exists no right eigenvector of A associated with an eigenvalue having nonnegative real part that is orthogonal to the rows of C.*
- *The matrix has full-column rank for all complex λ with nonnegative real parts.*

Considering the system of our control strategy, we turn now our attention to the detectability of the pair $(A, C^T Q C)$, which, since $Q > 0$, is equivalent to the detectability of the pair (A, C) (Hespanha, 2009). We proceed thus with the Hautus-test (Williams and Lawrence, 2007) for the pair (A, C), that is, if, for each unstable (or marginally stable) mode, relation:

$$rank \begin{bmatrix} (\lambda I - A) \\ C \end{bmatrix} = \bar{H} \qquad \text{(26)}$$

is satisfied, then the pair (A, C) is detectable. In our case, this is verified in case C has at least a non-zero element in each column corresponding to $\lambda = 1$, which implies controlling the density of each cell that does not have any other cell downstream. This requires the definition of an arbitrary setpoint for the density in this cell, which is, for practical reasons, undesirable. To account for this issue, we propose to place an additional dummy cell immediately downstream of each lane-drop, imposing it, with an appropriate high penalty weight $a_{i,j}$, to have a density equal to zero. Note that, in the described case, the system is also observable.

4. Simulation Results

4.1 Network configuration

In order to test the effectiveness of the aforementioned traffic management strategy, a motorway stretch is selected as a case study. The considered stretch (Figure 6.) is a hypothetical one with a length of 5 km. Basically, it is composed of 3 lanes until its 4 km, where the rightmost lane drops. The stretch is divided into 10 sections of 0.5 km length each. This network's case is a challenge for the evaluation of the proposed traffic control. As for the traffic demand, a hypothetical was used in order to test the proposed strategy near the network's capacity with respect to the no control case.
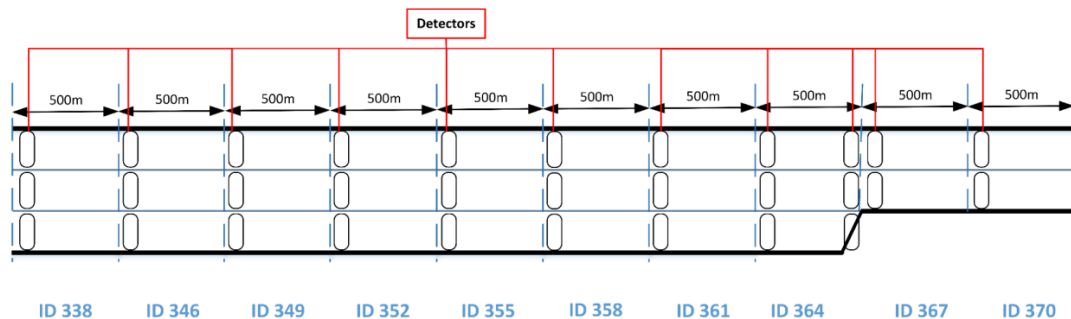
Figure 6: IDs of sections and detectors placed at each lane

The network in the microsimulator contains detectors for each section in order to collect data which are necessary for statistics reasons and the implementation of the proposed real-time strategies.

4.2 Parameters & Control Strategies setup

In the first stage of the calibration, we adjusted some general parameters of the model. These are the simulation step $T = 0.5\ sec$ and the speed limits are *100 km/h* in all sections except the two acceleration areas *(ID 361 & ID 364)* which are *80 km/h*. The warm-up period is considered as 5 minutes and measurement step T^m is 10 seconds. In Table 1. and Table 2.

AIMSUN calibration parameters are presented. The basic task of our calibration was the realistic behavior in the lane-drop area. We achieved realistic lane change in the merge area and reproduction of a realistic capacity drop phenomenon. Note that the calibration was based on (Perraki, 2016) Thesis because of same similarities in the merge areas of the network.

Table 1: Mean, deviation, minimum and maximum values of calibrated key parameters

Parameter	Mean value	Deviation	Min Value	Max value
Max acceleration (m/s²)	2.46	0.20	1.87	3.07
Normal deceleration (m/s²)	2.81	0.20	2.21	3.41
Minimum Headway (sec)	0.88	0.10	0.58	1.18
Min distance vehicle (m)	3.00	0.20	2.20	4.00
Max Desired Speed (km/h)	110.00	10.00	80.00	150.00
Maximum Give-Way time (sec)	12.97	2.64	7.69	18.25

Table 2: Values of manually calibrated parameters

Parameter	Calibrated Value
Reaction time at stop (sec)	1.1
Percentage Overtake (%)	90
Percentage Recover (%)	95
Percentage for staying in overtaking (%)	10
Percentage for imprudent lane-changing (%)	40

Heuristic rules Setup

The Heuristic rules described in Section 2.2.4 replace the default lane-changing model in lane drop area where the Gipps model results are nonrealistic. A lane change decision depends on vehicle's current position and speed, the relative speed with respect to the mainstream vehicles in target lane and the available gap in the target lane. Those variables are compared

to the respective threshold values and in case all the conditions are satisfied the vehicle changes lane. A big number of tests was conducted for the identification of the most appropriate threshold values were conducted while Figure 7. illustrates the applied rules in the acceleration lanes.
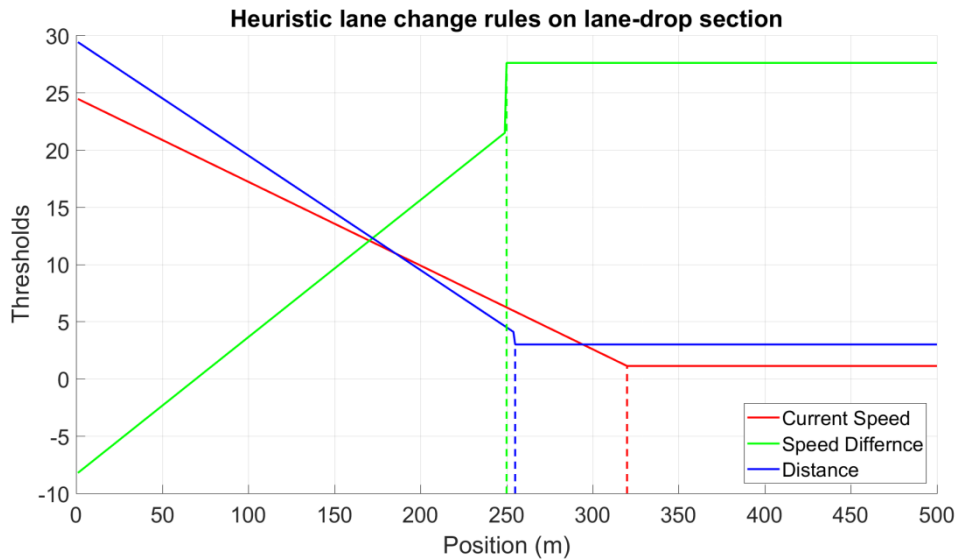
Figure 7: Heuristic lane-changing rules applied in the lane drop

MTFC Setup

The control strategy of MTFC using VSL was described in Section 3.2. The application of the feedback regulator takes place every control period $T^Q (= 1\ min)$ while the real-time density estimations at the bottleneck area are computed every T^Q. The VSL delivered by the PI regulator is rounded to the closest 10 km/h to obtain the corresponded posted VSL. Moreover, the difference between two consecutive posted VSL at the same gantry is limited to 10 km/h and the difference between two consecutive gantries (safety area) at the same control period is limited to 10 km/h.

Table 3. presents the lower and upper bounds of the VSL values for Safety areas (1-4) and the Application area.

Table 3: Max & Min Speed in VSL

Area	Max Speed *(km/h)*	Min Speed *(km/h)*
Safety	100	20
Application	100	20

Figure 8. presents the location of the measurements and each area (Safety 1-4, Application, Acceleration). Note that each area has a length of one segment (0.5 km) except the

Acceleration one which has two segments. The reason for using an extra segment for acceleration is that the two segments are the same that we are going to implement lane-changing control. The extra space is essential for the cars to develop gaps between them and make the lane-changing commands able to execute.

As for the gains of the controller are defined as $K_P = 5 \frac{km^2*lane}{h*veh}$ and $K_I = 5 \frac{km^2*lane}{h*veh}$ after a try-and-error procedure. In addition, the desired set-point $\hat{\rho}$ is different in each case, (so we defined it in the 4.4 and 4.6 sections) for the tracked segments of the section of lane-drop (*ID* 364).
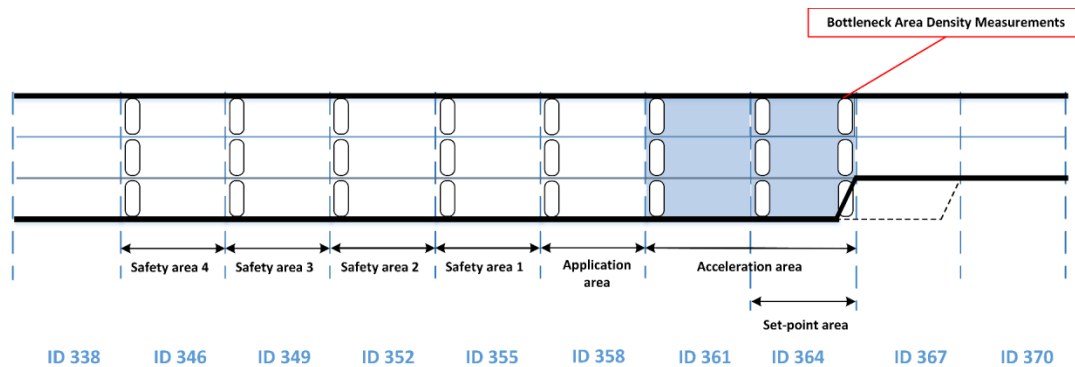
Figure 8: MTFC via VSL areas and measurements in our network

Lane-changing Control Setup

The control period of lane-changing control T^f is 10 seconds. The control area consists of two segments, basically the last two which contain three lanes *(ID 361 and ID 364)*. Figure 9. presents the area we implement the lane-changing control. As it is mentioned in section 3.3.1 we consider only lateral flows from right to left, as a result, we control only two lateral flows in each section. In addition, the external flow *d* mentioned in Figure 9. is considered in the start of the first section we control, while the desired set-point $\hat{\rho}_{ij}$ defined in section 3.3.2 targets the section *(ID 367)* after the lane-drop.
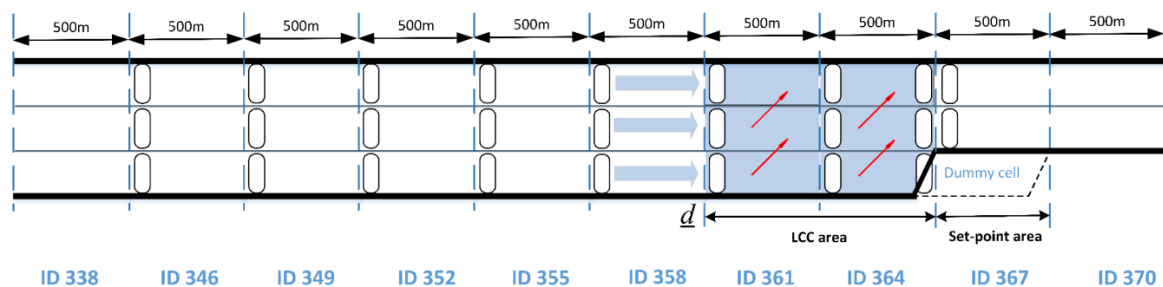
Figure 9: Lane-changing and Set-point areas

4.3 No control case

No-control is the base case that will be used to quantify any efficiency improvements arising from the use of control actions. The concept is to test the aforementioned strategies (Section 3.) while the demand is for some minutes near the bottleneck's capacity and even overcome it. Also, we consider that the number of cars at the beginning of the simulation is similar to the number at the end of it, meaning that any congestion as a result of high demand has been eliminated during the last minutes of the simulation, even in the no-control case. The capacity for the two lanes downstream of the lane-drop area is around $4200\ veh/h$. The traffic demand that was used as an input to the microscopic simulator AIMSUN is displayed in Figure 10. The demand is being raised in steps reaching overcapacity values for a couple of minutes until the 25th minute where we reduce significantly the traffic flow.
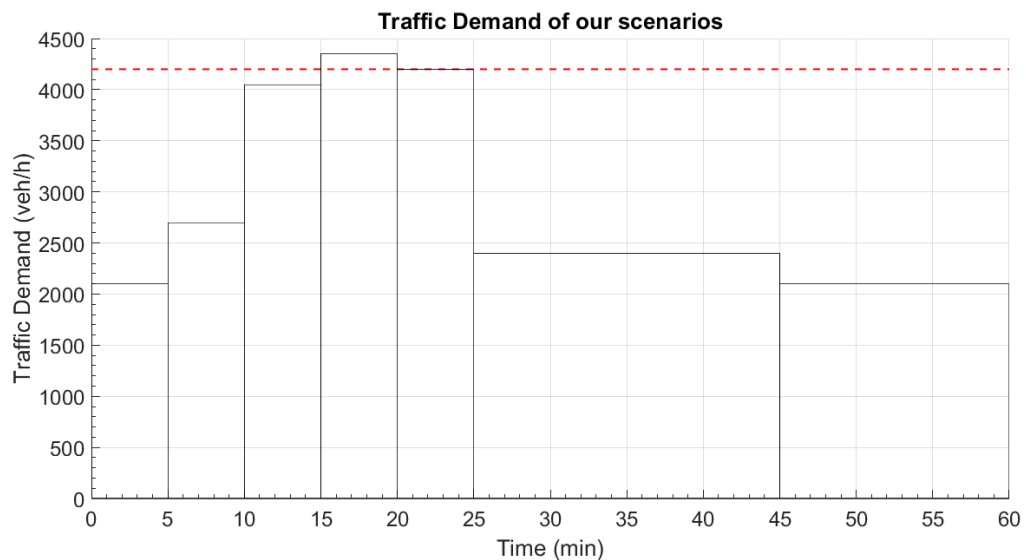
Figure 10: Traffic Demand used in AIMSUN (black lines) and the Capacity of bottleneck (red line)

In the microscopic simulator AIMSUN, we reproduced a set of 10 replications for our experiment and the acquired average Total Travel Time (TTT) in the 1-hour simulation is $223.3\ veh \cdot h$ with a standard deviation of $13.9\ veh \cdot h$. In the next figures, the no-control case is presented via the replication with the closest TTT to the average value.

In the Fundamental diagram (Figure 11.) it is obvious that as a result of the congestion, high-densities are obtained and the flow is lower than the capacity. Therefore, the traffic system has passed from the uncongested to the congested zone.
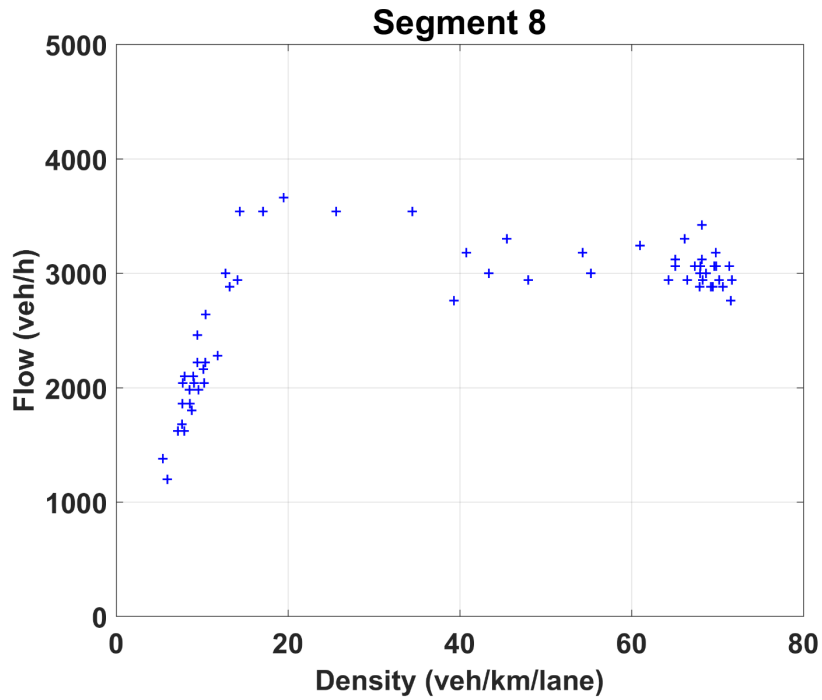
Figure 11: Fundamental diagram (aggregated) at lane-drop Section (ID 364), No control

Figure 12. represent the comparison of the density for each lane at the lane-drop location (*ID* 364). The lane 2 and 3 acquire high-density values approximate at the same time that the lane 1 reaches the highest values of density for this section. We notice that the congestion on the lanes is not homogeneous.
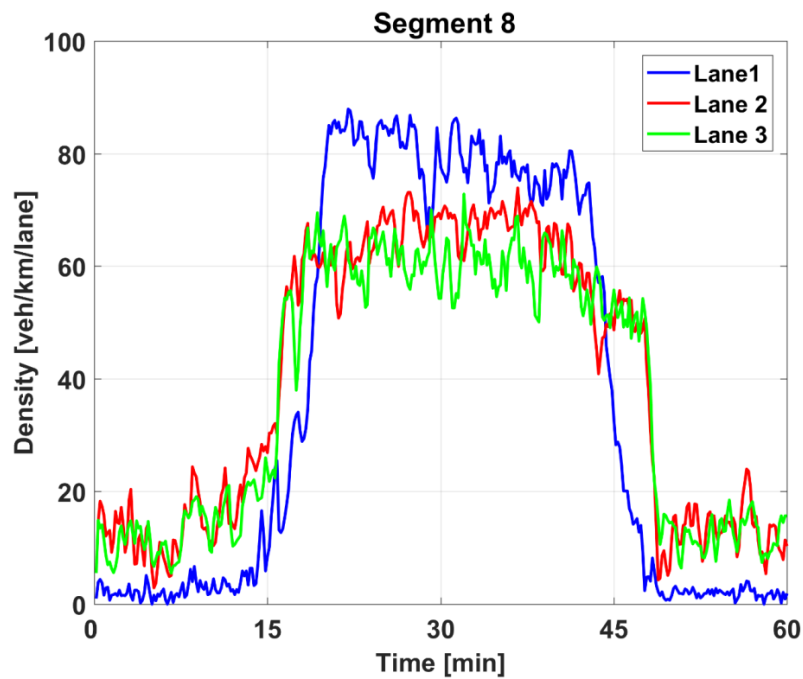
Figure 12: Density comparison in lane-drop Section (ID 364), lane 1 (blue), lane 2 (red) and lane 3 (green), No-control
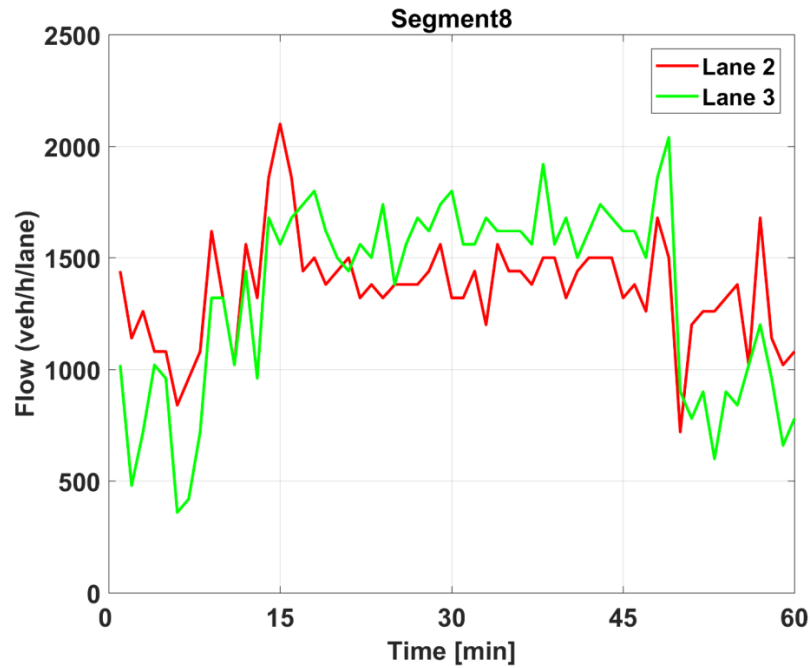
Figure 13: Flow comparison in lane 2 (red) and lane 3 (green) at lane-drop Section (ID 364), No control

Another interesting diagram is the one with the flows of the lane 2 and 3 at the bottleneck (Figure 13.) where lane 2 reaches the capacity around the 15th minute and then the flow is reduced significantly. Lane 3 behaves in a similar way with a couple of minutes delay but never reaches its capacity. The reduction of flow in this high demand period is a result of the capacity drop phenomenon if we consider the increase of density (Figure 11.) these moments.

The density of three sections before and two after the lane-drop *(ID 358, 361, 364, 367, 370)* are presented in the Figure A.3. (see Figure 6. for network description). The congestion spill back covering 3 sections as a result of the merging zone of section *ID 364* we investigate and the high demand (Figure A.4.) arriving the merge-zone.

The speed measurements through the stretch are presented in the Figure 14. A speed drop appears first at the lane drop area ($4.0\ km$) around the 18th minute of the simulation. The speed remains low at this area for about 25 minutes. Congestion is spilling back covering an area of about 2.5 km.
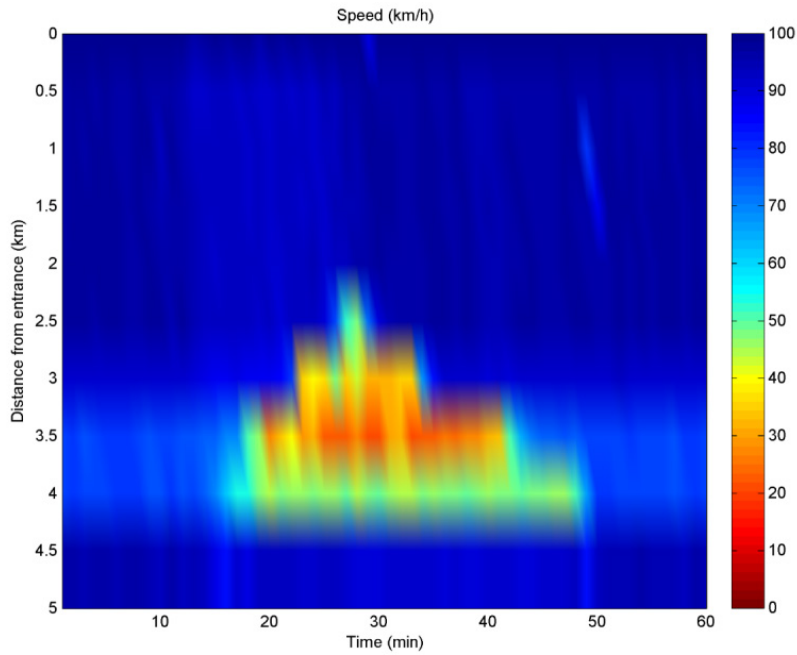
Figure 14: Speed-Distance-Time 3D Diagram for network, No control

4.4 VSL case

The MTFC strategy via using VSL presented in the section 3.2 aims to establish optimal traffic conditions (maximum throughput) for any appearing demand. VSL decisions are applied per section, as if they were displayed on a gantry located at the beginning of the section. Density measurements at the lane-drop area (ID 364) are compared against the selected critical density value $\hat{\rho}$ which was defined as 25 veh/km. This value is the optimal one, considering the no-control Fundamental diagram (Figure 11.) and plenty of tests we conducted.

In the microscopic simulator AIMSUN, we reproduced a set of 10 replications for our experiment and the acquired average TTT in the 1-hour simulation is 199.9 $veh \cdot h$ an improvement of 10.47% compared to the no-control case while the standard deviation is 16.7$veh \cdot h$. In the next figures, the VSL case is presented via the replication with the closest TTT to the average value.

The speed measurements through the stretch are presented in Figure 15. It is observed that the Application Area (between 2.5 and 3.0 km) (see Figure 8. for VSL areas) has the lower speeds of the network while the Safety areas (between 0.5 and 2.5 km) are the second lower. It is interesting that in the acceleration areas (between 3.0 and 4.0 km) the cars are accelerating, so the speed is rising. In contrast to the no-control case (Figure 14.), a controlled congestion is created further upstream of the lane-drop area, thus the bottleneck reached its maximum capacity because of the higher speeds (Figure 15.) achieved after the lane-drop in

36

section ID 367 (between 4 and 4.5 km). In addition, as for the safety areas (between 0.5 and 2.5 km), it is interesting to notice that speed is higher in the more upstream Safety areas.
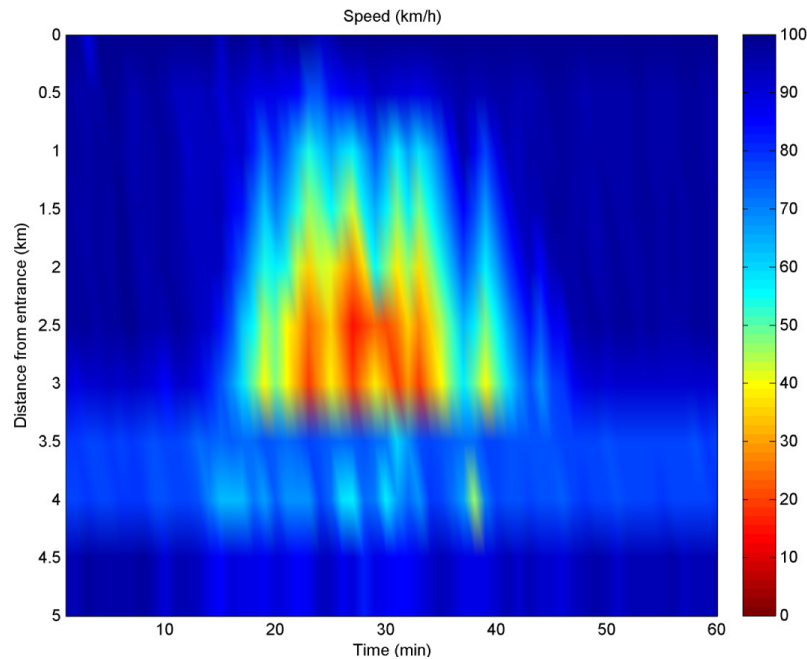
Figure 15: Speed-Distance-Time 3D Diagram for network, VSL

Figure 16. presents flow, density, speed over time and aggregated fundamental diagram at lane-drop Section *ID 364.* (see Figure 8.). As for the Density-time diagram, it displays the response of the system regarding the constant set-point. The real-time measurements are used from the VSL controller (Section 3.2.2) in order to maintain the density around the desired value. In Application Area (*ID* 358) (see Figure 8. for VSL areas) VSL decisions are applied and presented in Figure 17. Considering these last two figures (Figure 16, Figure 17) we can explain the overshooting issues in some specific times. Basically, this fact originates either from the saturated system or the big slope of the raising demand where the controller needs a couple of minutes to reduce the density value.
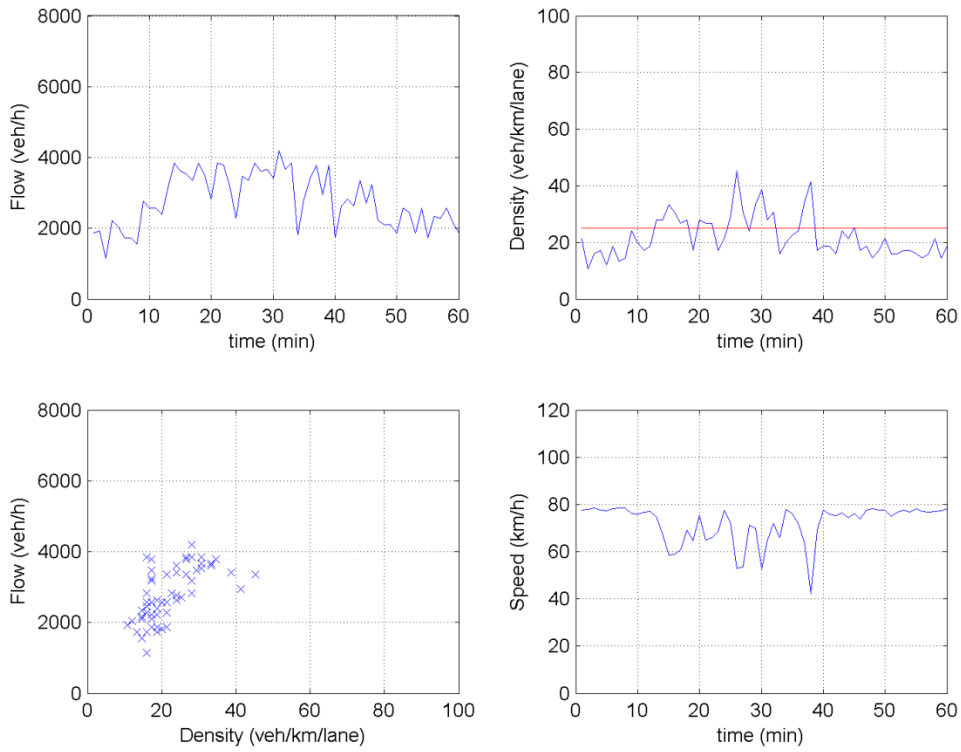
Figure 16: Flow, Density, Speed-Time & Flow-Density at lane-drop Section (ID 367), Set-point (red), VSL
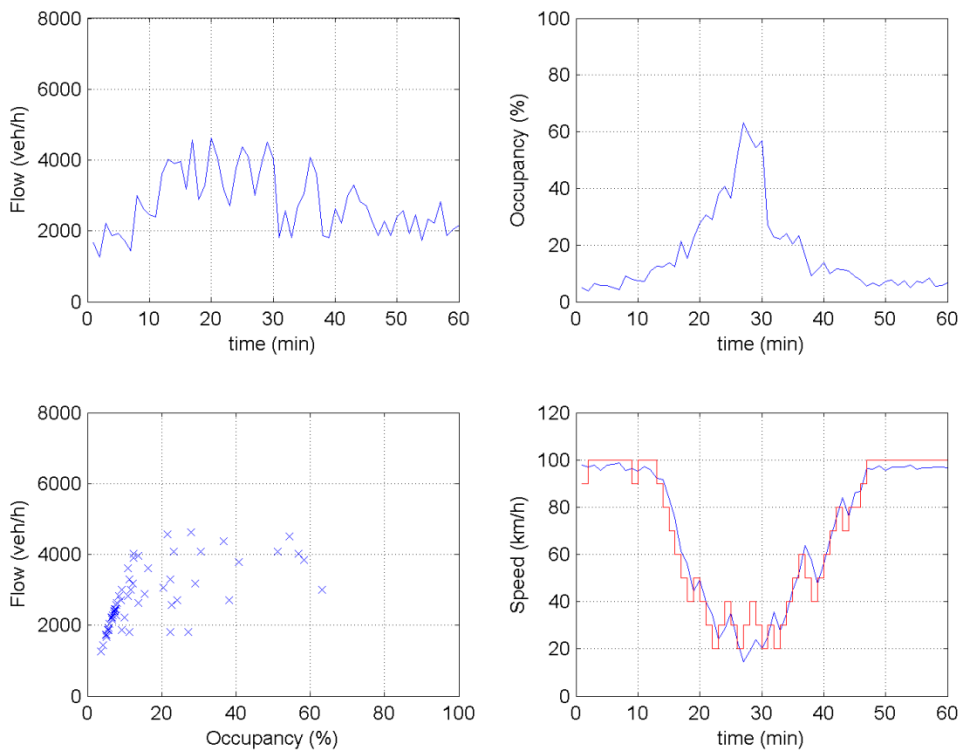
Figure 17: Flow, Density, Speed-Time & Flow-Density at the Application area (ID 358), VSL decisions (red), VSL

4.5 Lane-changing case

For the LCC case, we conducted simulations for various penetration rates of VACS $(20\%, 40\%, 60\%, 80\% \; and \; 100\%)$, to study the effect of lane-changing advice in the traffic system. The desired set-point $\hat{\rho}_{ij}$ in the Section after the lane-drop (see Figure 9. for set-point area) for the Lane-changing controller is defined for each lane $(1 - 2 - 3)$ as $(0 - 28 - 33 \; veh/km)$. The selection of these critical densities is based on the Fundamental diagram Figure 11. of No-Control case and various tests we conducted, where we end up that this set-point is optimal. The results after the reproduction of a set of 10 replications of 1-hour in AIMSUN are presented in Table 4., where, for all the tested (for all penetration) rates, the TTT is improved with respect to the no-control case. Obviously, when higher penetration is available the improvement of obtained TTT is more worthwhile. It is observed that for rates bigger than 60% the reducing of TTT is insignificant (see Figure 18. for a graphic representation of the results), because these penetrations are already high to improve the traffic conditions, the congestion is pretty much cleared. As for the Standard Deviation (S.D.) values are slightly increased in the lower rates $(20\% \, \& \, 40\%)$ compared to the no-control case, which is normal as we control a small fraction of cars. As the penetration rate is increasing the S.D. is decreasing significantly with respect to the no-control value. In the next figures, the LCC cases for each rate are presented via the replication with the closest TTT to the average value of each case.
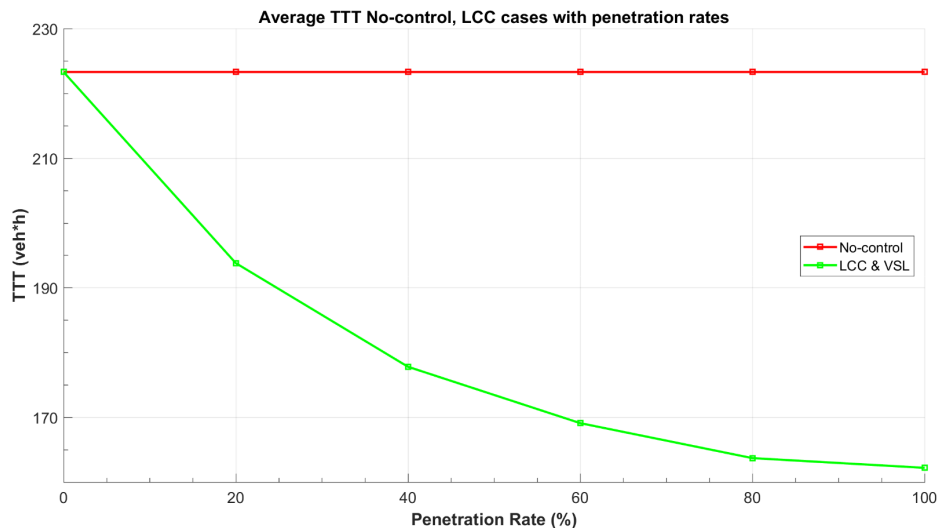

Figure 18: Average Total Travel Time of Lane-Change for different Penetration rates and No-control case

Table 4: No-control, LCC Average Results (TTT, TTT improvement, S.D.) with penetration rates

		No-Control	Penetration Rate (%)	LCC[1]
Results	TTT (veh·h)	-	20	193.8
	TTT improvement (%)	-		13.2%
	S.D. (veh·h)	-		16.2
	TTT (veh·h)	-	40	177.8
	TTT improvement (%)	-		20.4%
	S.D. (veh·h)	-		20.0
	TTT(veh·h)	-	60	169.1
	TTT improvement (%)	-		24.3%
	S.D. (veh·h)	-		12.2
	TTT (veh·h)	-	80	163.8
	TTT improvement (%)	-		26.65%
	S.D. (veh·h)	-		8.3
	TTT(veh·h)	223,3	100	162.3
	TTT improvement (%)	-		27.36%
	S.D. (veh·h)	13,9		3.8
[1] Desired set-point for LCC (0-28-33 veh/km)				

Comparing the Fundamental diagrams of No-control and LCC for all penetrations rates (Figure 19.) we observe that in LCC cases the flow reaches higher values which is a direct outcome of the more suitable lane assignment of the cars. Furthermore, as the penetration rate of connected vehicles is reinforced the FD diagrams present even fewer spots in the congested zone (for densities bigger than the critical values), wherein the last two rates (80%, 100%) the flow reaches the capacity and maintains.
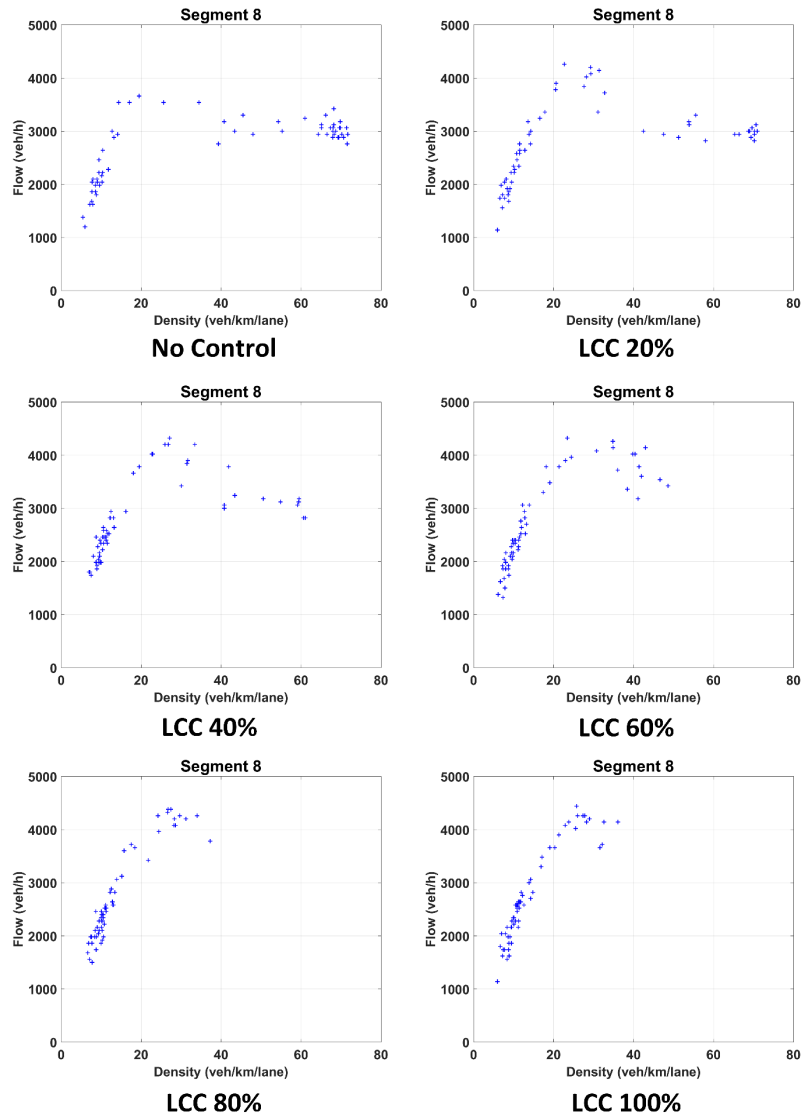
Figure 19: Compare Fundamental Diagrams at ID 364, LCC cases

Looking at speed contour plots, (Figure 20.) it is worthwhile to mention that speed in the network is significantly higher in LCC cases, even in the low penetration rate of 20%, with respect to the no-control scenario. As the rate is becoming higher the speeds are even higher, but the improvement is insignificant in 100% case compared to 80% as shown and in their TTT values. It is important to notice that the increased speeds in the LCC cases before the lane-drop (before 4th km) are linked with higher flows in the area and consequently less congestion. Additionally, the higher speeds at the Section after the lane-drop (between 4.0 and 4.5 km) indicates that LLC strategies fully exploit the capacity of each and every lane, thus increasing the overall capacity.
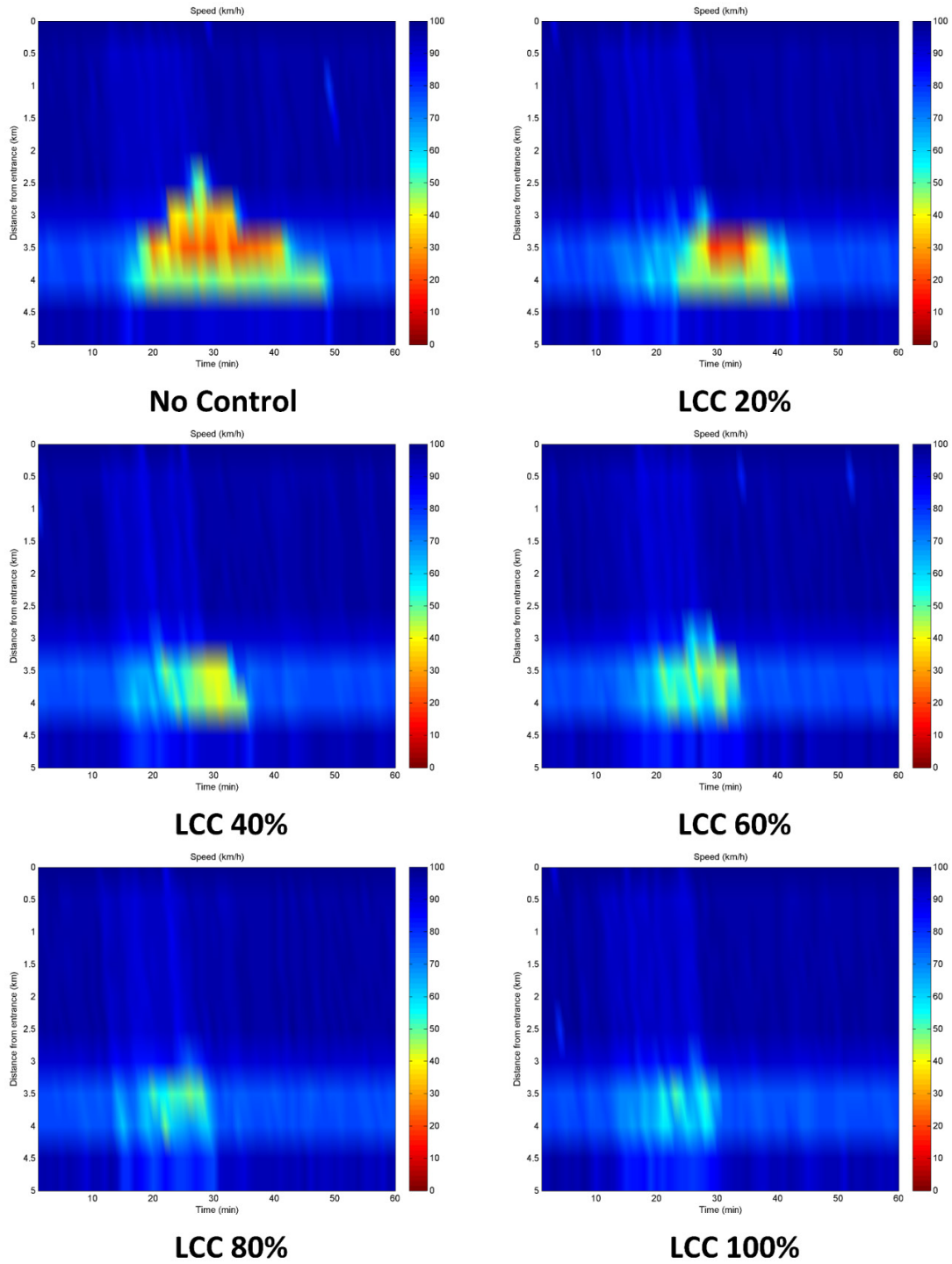
Figure 20: Compare 3D Speed diagrams, LCC cases

Figure 21. and Figure 22. present the comparison between lanes in LCC 80% case of lane-drop Section *ID 364* (see Figure 9.) for flow and density accordingly. Looking at the flow trajectories higher values are observed with respect to the No-control case, like in the speed plots. We observe that 80% of connected vehicles is sufficient to achieve a distribution among the lanes. Considering the density diagram, lane 2 & 3 are pretty much homogenized and they do not reach very high values compared to the No-control case. Also, lane 1 displays low

density values which is the object, as the controller mentioned in section 3.3.2 manages to move connected vehicles to adjacent lanes before reach the lane-drop location. The density between the high demand period ($15^{th}, 25^{th}$ min) (see Figure 10. for demand) is slightly increased for lane 1 and further for other lanes which is the reason of flow fluctuation these times.
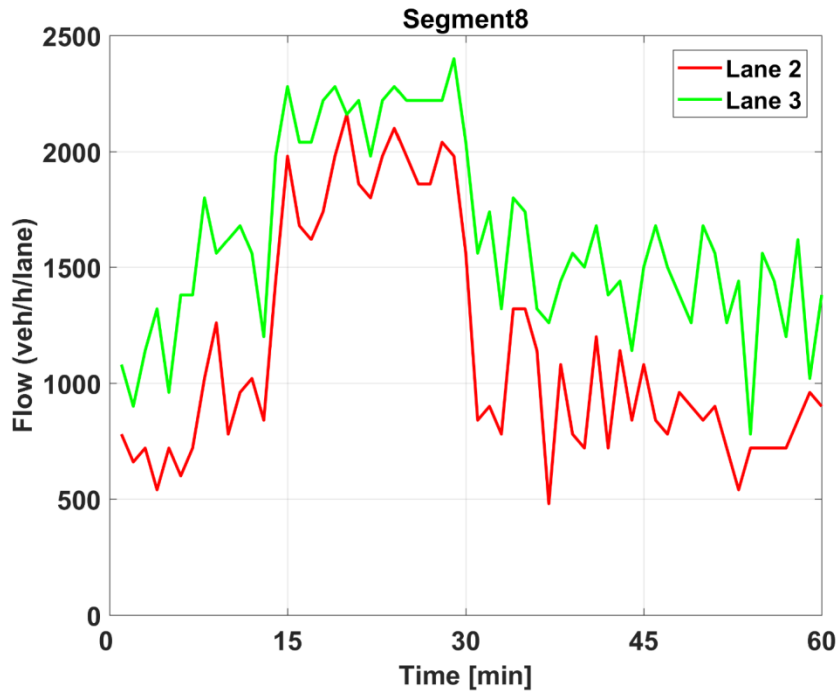
Figure 21: Flow comparison in lane 2 (red) and lane 3 (green) at lane-drop Section (ID 364), LCC 80%
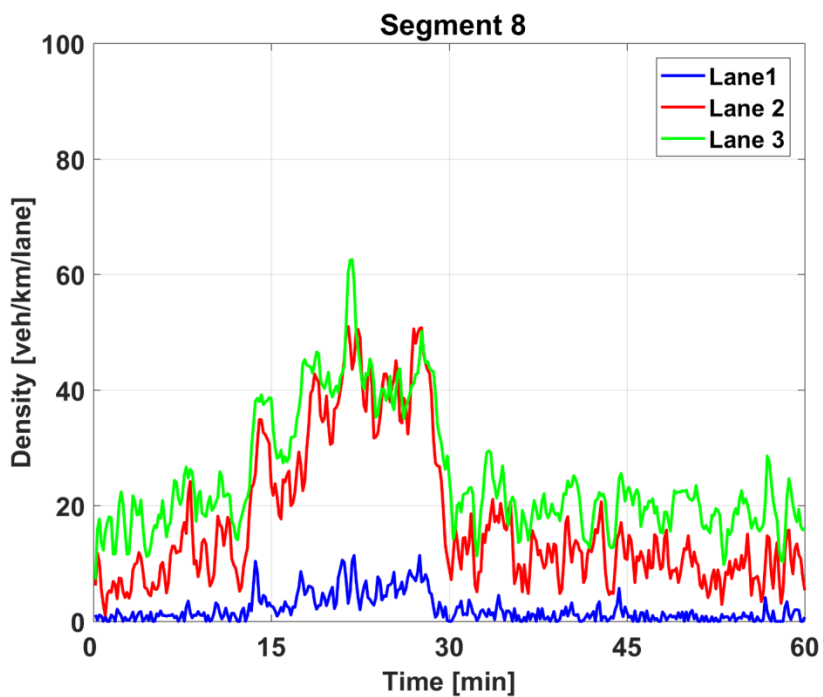
Figure 22: Density comparison in lane-drop Section (ID 364), lane 1 (blue), lane 2 (red) and lane 3 (green), LCC 80%

43

4.6 VSL & Lane-changing case

For the LCC & VSL case, we conducted simulations for the same penetration rates of LCC as before. The desired set-point $\hat{\rho}_{ij}$ (see Figure 9. for LCC set-point area) for the Lane-changing controller is defined for each lane $(1 - 2 - 3)$ as $(0 - 28 - 33\ veh/km)$ for all rates. The selection of these critical densities is based on the Fundamental diagram Figure 11. of No-control and various tests we conducted, where we end up that this set-point is optimal.

The optimal set-point for the MTFC controller is selected using the information Fundamental diagrams of the single LCC cases (Figure 19.) provided us and defined as $35\ veh/h$ for each tracked lane (see Figure 8. for VSL set-point area) for all LCC rates. The VSL set-point values in the case with LCC are higher than the single VSL case because LCC case achieves a higher critical density at the FD diagram offering better traffic conditions to implement MTFC than in the No-control case.

The results after the reproduction on a 1-hour set of 10 replications in AIMSUN are presented in Table 5., where, for all the tested rates, TTT is improved with respect to the no-control case. Also, we include the results of single VSL case and LCC cases. Obviously, when higher penetration is available the improvement of obtained TTT is more worthwhile. It is noted that for rates bigger than 60% the LCC & VSL scenario reduce the TTT is insignificantly (see Figure 23. for a graphic representation of the results), because these penetrations are already high to improve the traffic conditions, the congestion is pretty much cleared. Comparing the cases of LCC and LCC & VSL is obvious for the second one (Table 5.) as lower the penetration rate is, further improvement is observed, while in higher penetration rates there is lack of improvement.
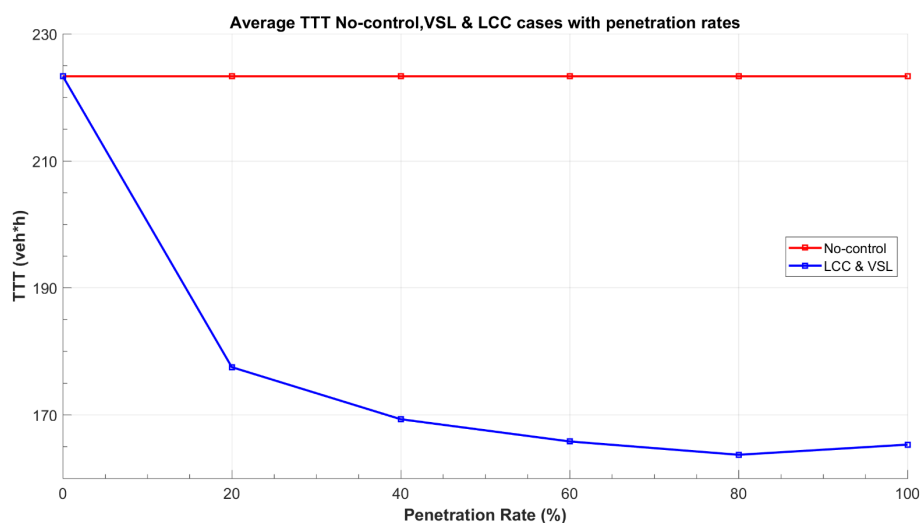
Figure 23: Average Total Travel Time of Lane-Change for different Penetration rates with VSL and No-control case

Table 5: No-control, LCC, LCC & VSL Average Results (TTT, TTT improvement, S.D.) with penetration rates

		No-Control	VSL$_3$	Penetration Rate (%)	LCC$_1$	VSL$_2$ & LCC$_1$
Results	TTT (veh·h)	-	-	20	193.8	177.5
	TTT improvement (%)	-	-		13.2%	20.5%
	S.D. (veh·h)	-	-		16.2	17.1
	TTT (veh·h)	-	-	40	177.8	169.3
	TTT improvement (%)	-	-		20.4%	24.2%
	S.D. (veh·h)	-	-		20.0	10.6
	TTT(veh·h)	-	-	60	169.1	165.8
	TTT improvement (%)	-	-		24.3%	25.75%
	S.D. (veh·h)	-	-		12.2	7.5
	TTT (veh·h)	-	-	80	163.8	163.7
	TTT improvement (%)	-	-		26.65%	26.68%
	S.D. (veh·h)	-	-		8.3	4.7
	TTT(veh·h)	223,3	199,9	100	162.3	165.3
	TTT improvement (%)	-	10,5%		27.36%	25.98%
	S.D. (veh·h)	13,9	16,7		3.8	7.2

$_1$ Desired set-point for LCC (0-28-33 veh/km)
$_2$ Desired set-point for VSL (35 veh/km)
$_3$ Desired set-point for VSL (25 veh/km/)

In the next figures, the LCC for each rate and VSL cases are presented via the replication with the closest TTT to the average value of each case.

Comparing the Fundamental diagrams of No-control and LCC & VSL for all penetrations rates (Figure 24.) we observe that in the LCC & VSL cases the flow reaches higher values which is a direct outcome of the more suitable lane assignment of the vehicles. Furthermore, as the penetration rate of connected vehicles is reinforced the FD diagrams present even fewer spots in the congested zone, wherein the last two rates (80%, 100%) the flow reaches the capacity and maintains. Comparing Fundamental diagrams of LCC and LCC & VSL cases (Figure 19, Figure 24), we reach to similar outcomes with the Table 5. results. Specifically, the 20, 40 and 60% rates are received a respective improvement, but the higher ones don't succeed a significant result.
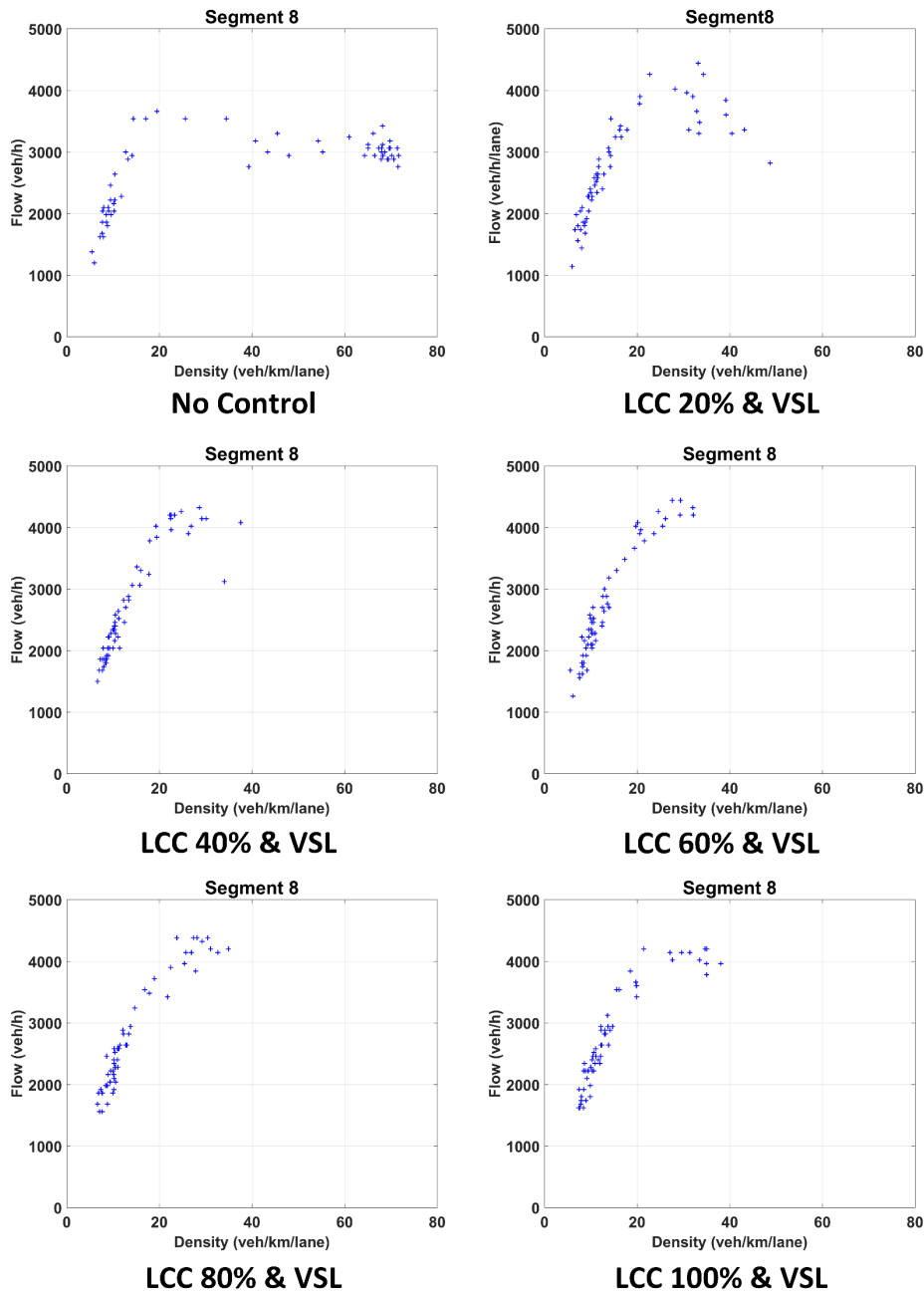
Figure 24: Compare Fundamental Diagrams at ID 364, LCC & VSL cases

As for the speeds in the network (Figure 25.) the speed in the network is significantly higher in LCC & VSL cases with respect to No-control case. The acceleration Sections *ID* 361 & 364 (*between* 3.0 *and* 4.0 km) reach higher speeds compared to the MTFC area (between 2.5 to 3.0 km) which copes with a desirable controlled congestion. Comparing with the LCC case, in LCC & VSL cases there are improvements for low rates of connected vehicles (20,40 & 60%), while the others have similar results as the LCC case in the accordingly penetrations (Figure 20.). The bigger penetrations cannot reach better results because congestion is almost eliminated and MTFC strategy cannon further improve. It is obvious from the speed contour plots (Figure 25.) of 80 & 100%, speeds in the MTFC area

46

(from 2.5 to 3.0 km) do not reflect a desirable controlled congestion. In addition, LCC in 80% rate, provoked better flow distribution and consequently higher capacity in the lane-drop area, with lower density compared to the No-control case. This density was not enough for the desirable density VSL set-point, as shown in Figure 26.
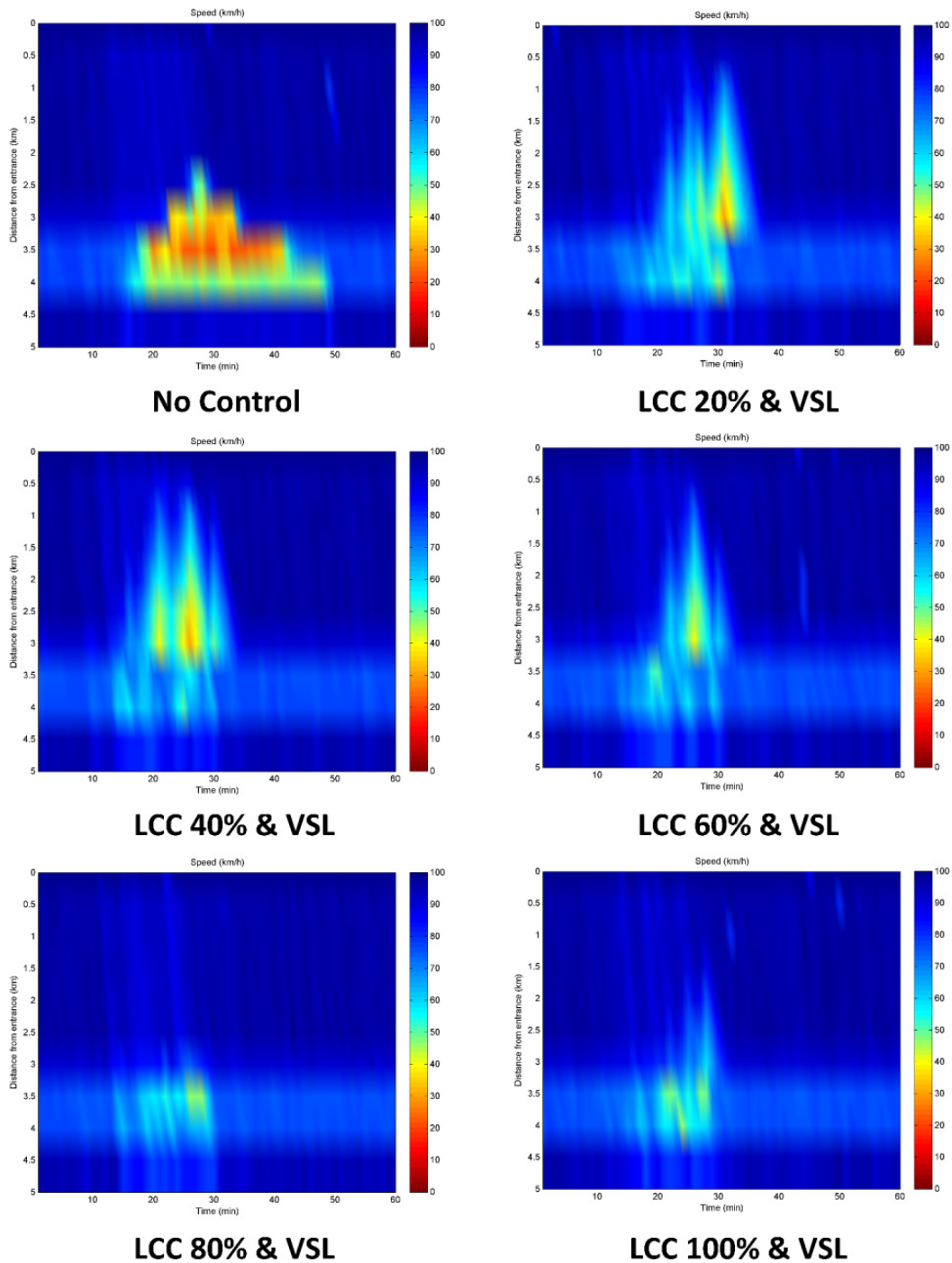
Figure 25: Compare 3D Speed diagrams, LCC & VSL cases
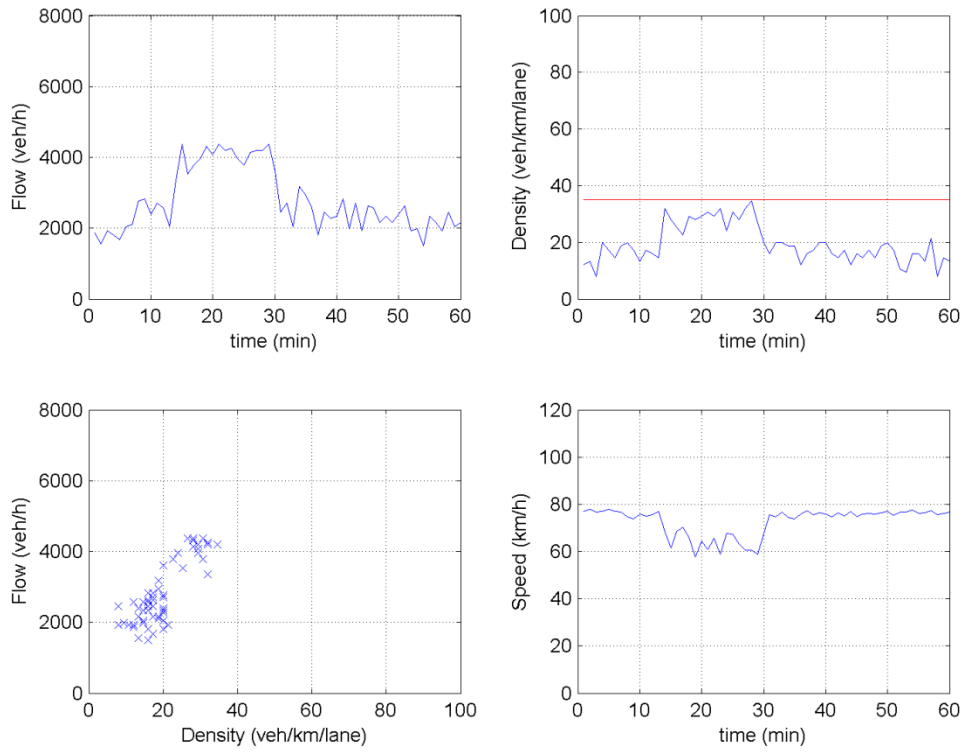
Figure 26: Flow, Density, Speed-Time & Flow-Density at lane-drop Section (ID 367), Set-point (red), LCC 80% & VSL

5. Conclusions

The objective of this thesis was the investigation of the integrated use of two feedback control strategies on a hypothetical motorway stretch featuring a lane-drop bottleneck. The case study site is a hypothetical stretch with a length of $5\ km$ which is composed of 3 lanes until its 4 km, where the rightmost lane drops. The dynamic scenario of the simulation was based on a hypothetical demand in order to test the proposed strategy near the network's capacity. To this end, a calibration of AIMSUN microscopic simulator for a realistic behaviour in lane-drop area was carried out in the first part of this work. Considering the determinate stretch, calibration parameters and traffic demand, in No-control scenario the average TTT was 223.3 $veh \cdot h$. In the second part the application of an MTFC strategy using VSLs proposed by Papamichail et al. (2017) on the calibrated model was tested. A Proportional–Integral (PI) feedback regulator is employed, keeping the bottleneck density close to the selected set-point that maximises the bottleneck throughput. The MTFC approach resulted (Figure 27.) in an improvement of traffic congestion in the case study network (average TTT=199.9 $veh \cdot h$) with an improvement of 10.47% compared to No-control case.
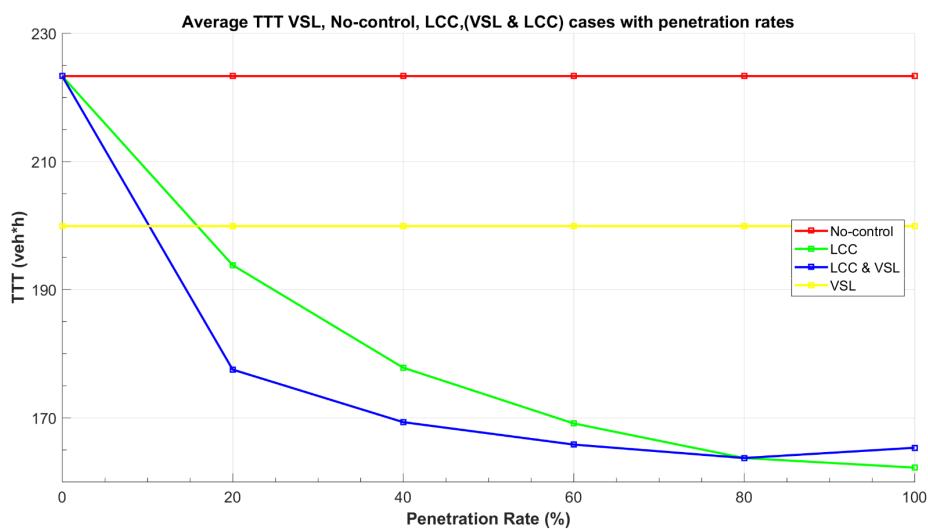
Figure 27: Average Total Travel Time of VSL, Lane-Change for different Penetration rates, VSL with Lane-Change and No-control case

Afterwards, the application of a different control strategy that delivers appropriate lane-changing actions was investigated on the calibrated model. LCC is a promising new strategy proposed by Roncoli et al. (2016). This control strategy aims at the distribution of traffic flow among the lanes in the immediate proximity of a bottleneck, so as to exploit the capacity of each and every lane, thus increasing the overall (cross-lane) capacity. For all the tested penetration rates, LCC strategy obtained significant improvements in our case study (Figure 27.). Specifically, an improvement (compared to No-control case) of 13.20% on TTT was observed in the lower penetration rate, while the higher penetration rate achieved an 27.36% reduction on TTT.

At the end, a combination of the aforementioned strategies was investigated in our calibrated model. The advantages of each strategy are combined to improve the traffic congestion. The results (Figure 27.) are significant, mainly for lower penetrations compared to single LCC case and of course, No-control case. Specifically, an improvement (compared to the No-control case) of 20.50% on TTT was observed in the lower penetration rate, while the higher penetration rate achieved a 25.98% reduction on TTT.

Appendix

In this Appendix the graphs for all cases are presented. In the microscopic simulator AIMSUN, we reproduced a set of 10 replications (471, 472, 473, 474, 475, 476, 477, 478, 479, 480) for each case. In the next figures, each case is presented via the replication with the closest TTT to the average value. More specifically:

- Figure A. → No-control case (Replication 471)
- Figure B. → VSL case (Replication 472)
- Figure C. → LCC 20% case (Replication 472)
- Figure D. → LCC 40% case (Replication 473)
- Figure E. → LCC 60% case (Replication 475)
- Figure F. → LCC 80% case (Replication 474)
- Figure G. → LCC 100% case (Replication 472)
- Figure H. → LCC 20% & VSL case (Replication 472)
- Figure I. → LCC 40% & VSL case (Replication 479)
- Figure J. → LCC 60% & VSL case (Replication 477)
- Figure K. → LCC 80% & VSL case (Replication 474)
- Figure L. → LCC 100% & VSL case (Replication 476)

Figure A.1: Aggregated Flow at lane-drop Section (ID 364), No control
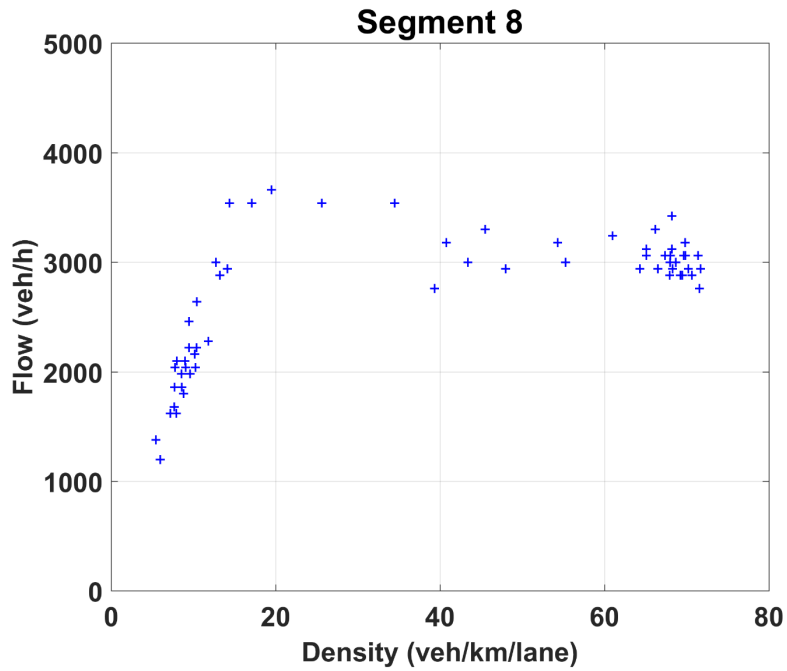
Figure A.2: Fundamental diagram (aggregated) at lane-drop Section (ID 364), No control
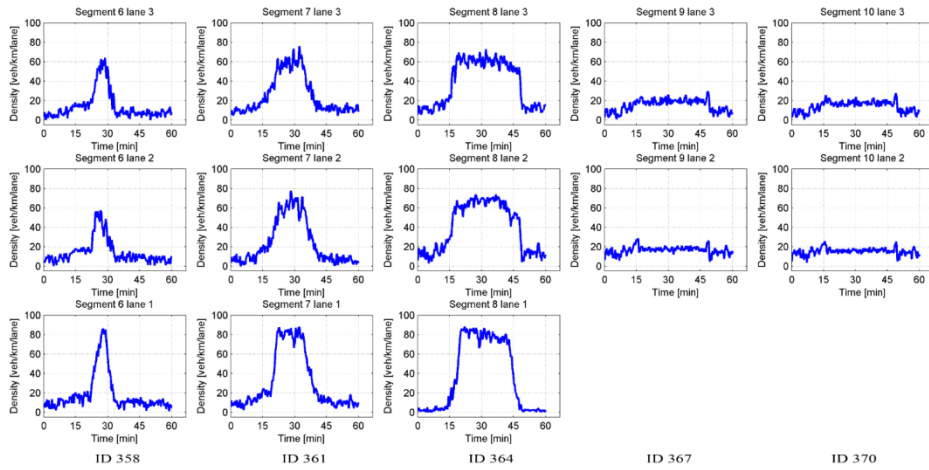
Figure A.3: Density-Time diagram of each lane from Section ID 358 until ID 370, No control
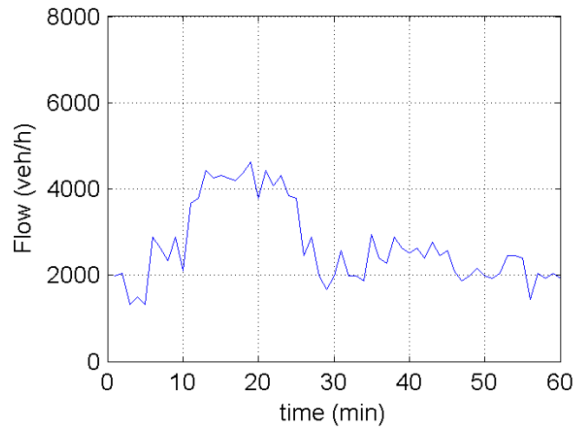
Figure A.4: Demand entering the network (ID 338)

VSL case Diagrams (Replication 472)
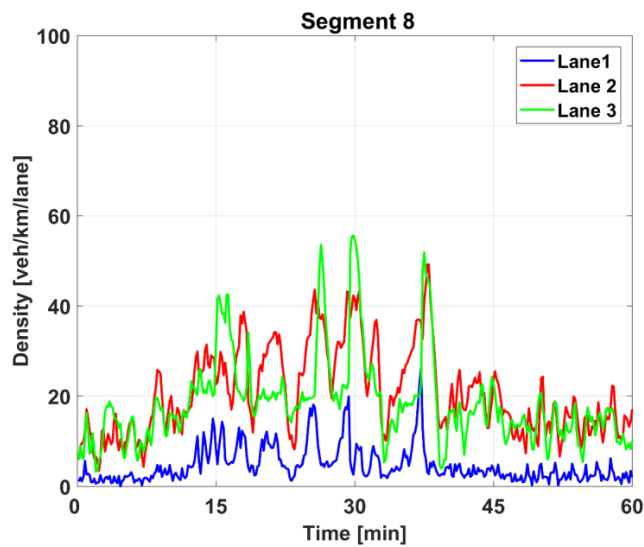
Figure B.1: Density comparison in lane-drop Section (ID 364), lane 1 (blue), lane 2 (red) and lane 3 (green), VSL
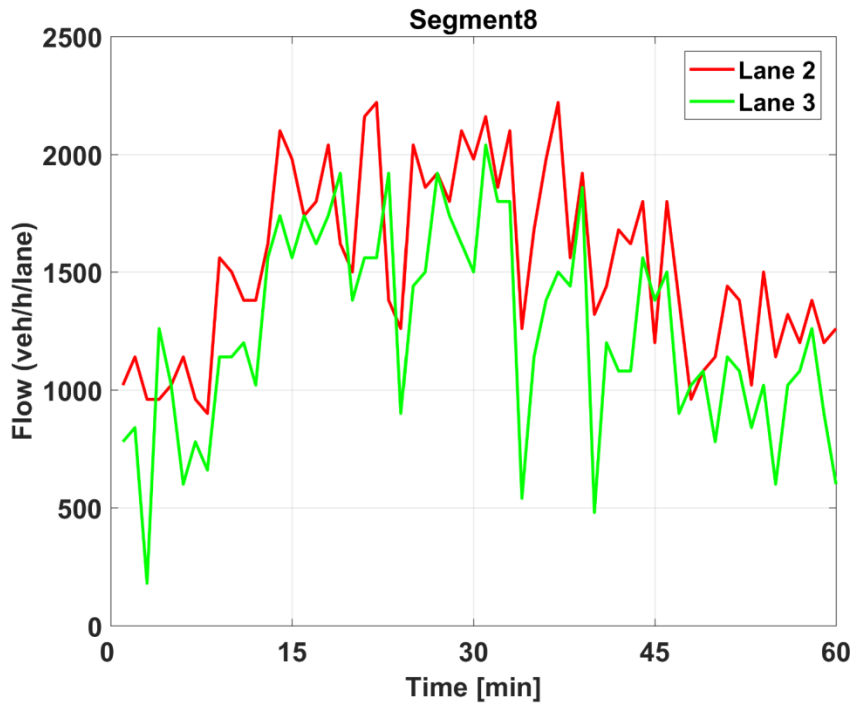
**Figure B.2: Flow comparison in lane 2 (red) and lane 3 (green) at lane-drop Section (ID 364), VSL**
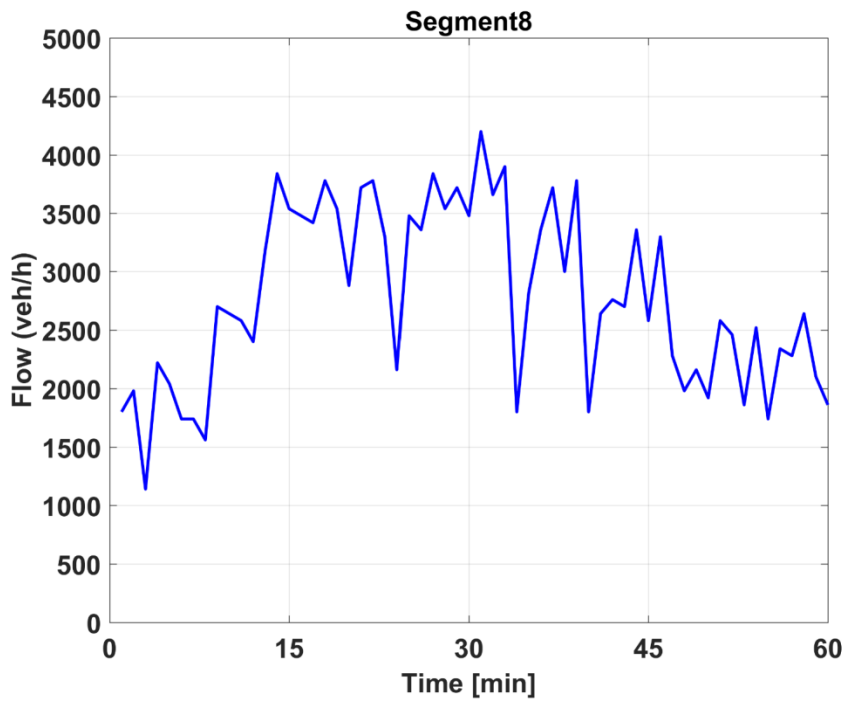
Figure B.3: Aggregated Flow at lane-drop Section (ID 364), VSL
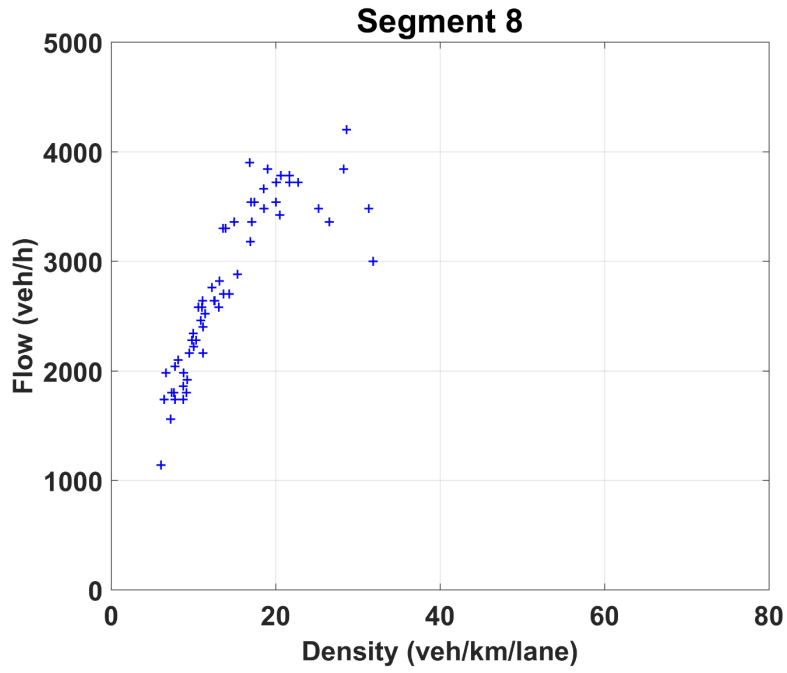
Figure B.4: Fundamental diagram (aggregated) at lane-drop Section (ID 364), VSL
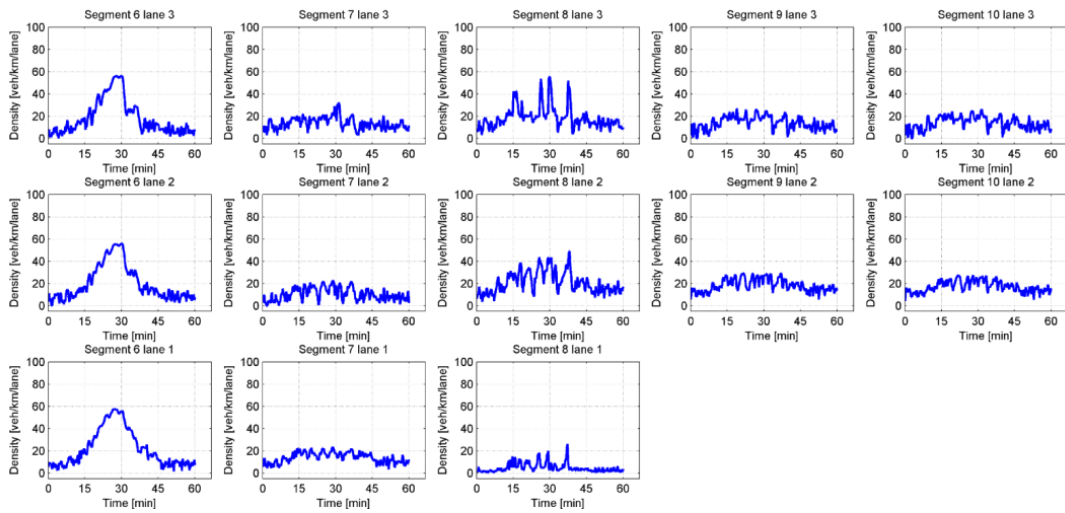
**Figure B.5: Density-Time diagram of each lane from Section ID 358 until ID 370, VSL**

55
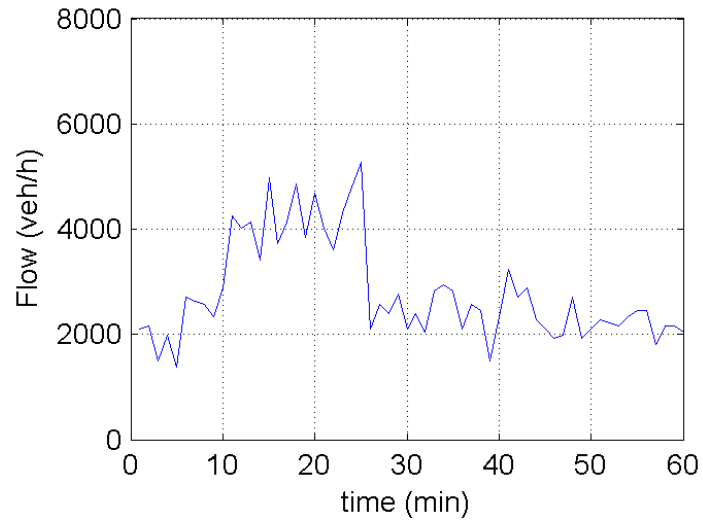
Figure B.6: Demand entering the network (ID 338)
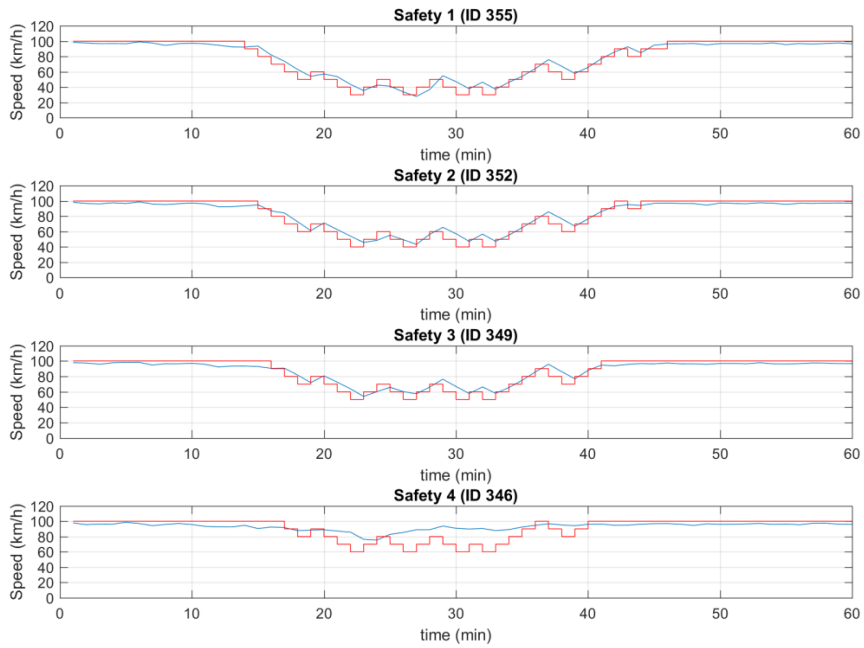
**Figure B.7: Speed (blue) and VSL decisions (red) in Safety areas**
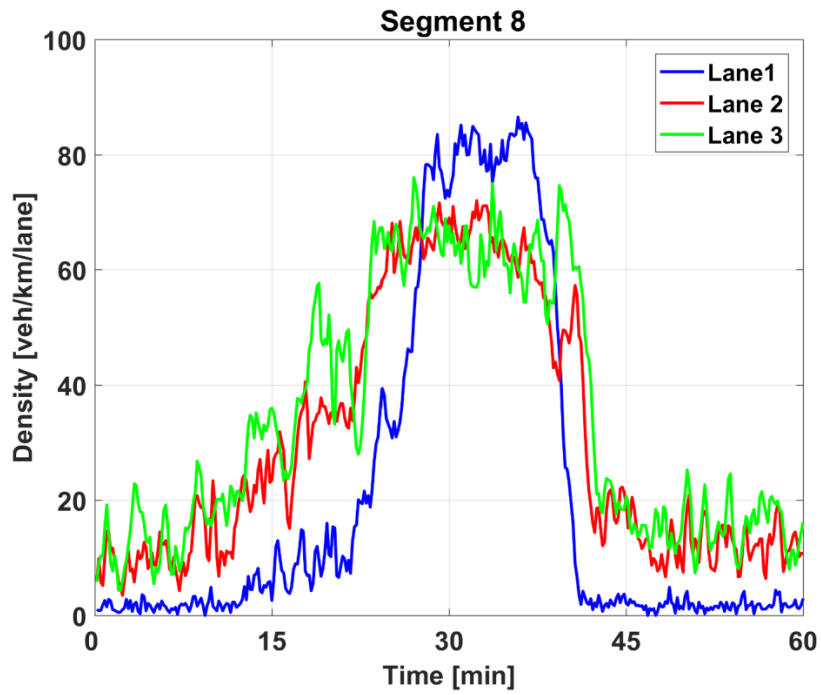
Figure C.1: Density comparison in lane-drop Section (ID 364), lane 1 (blue), lane 2 (red) and lane 3 (green), LCC 20%
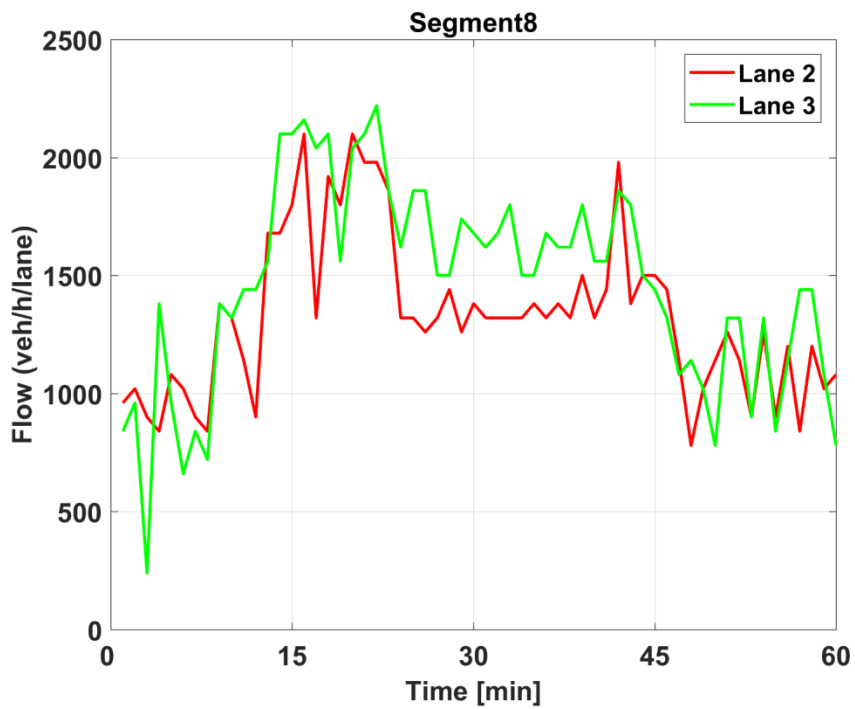

**Figure C.2: Flow comparison in lane 2 (red) and lane 3 (green) at lane-drop Section (ID 364), LCC 20%**
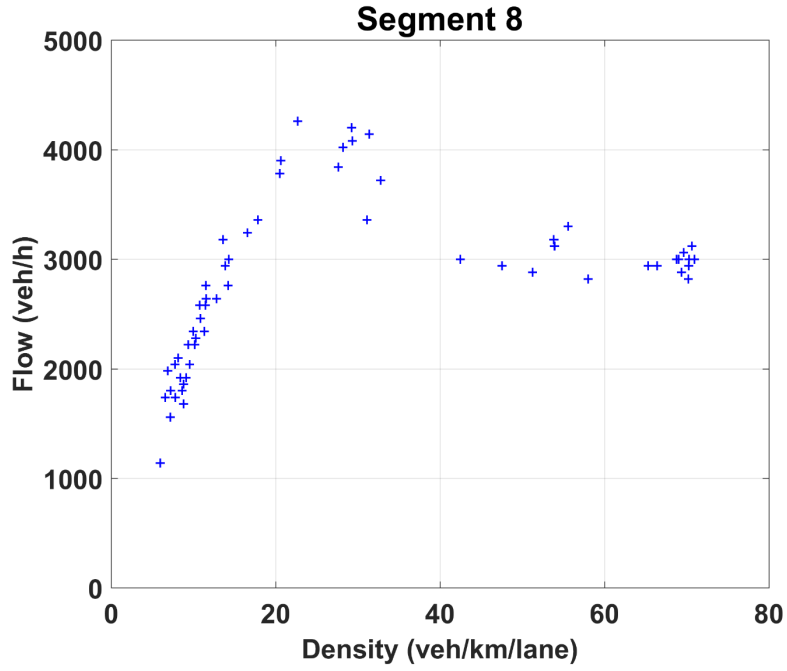
Figure C.3: Fundamental diagram (aggregated) at lane-drop Section (ID 364), LCC 20%
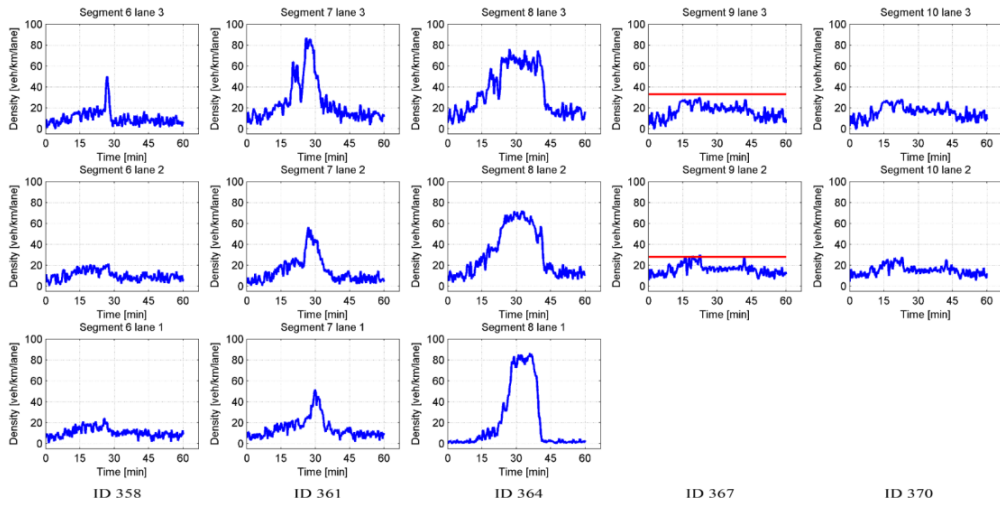
Figure C.4: Density-Time diagram of each lane from Section ID 358 until ID 370, Set-point (red), LCC 20%

58
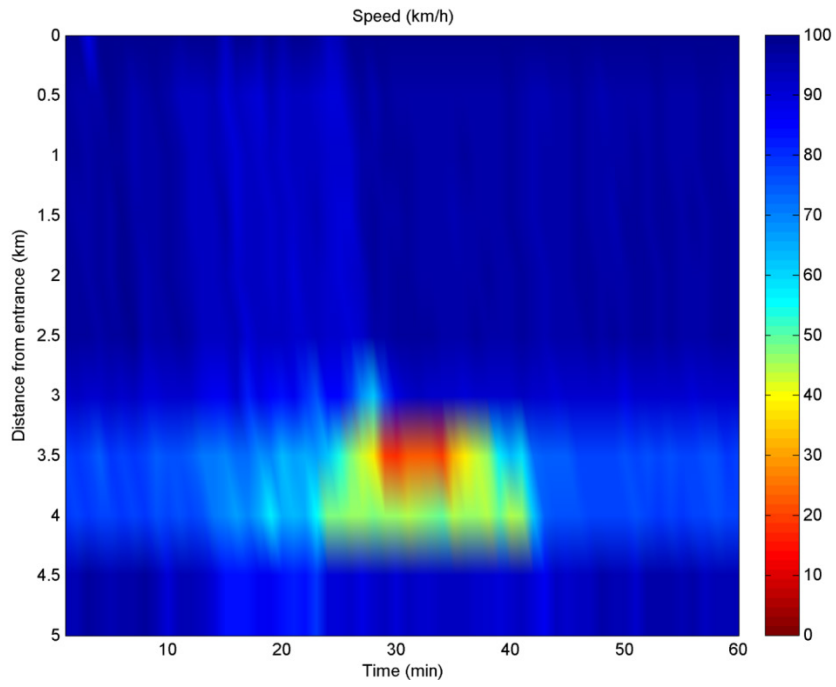
Figure C.5: Speed-Distance-Time 3D Diagram for network, LCC 20%
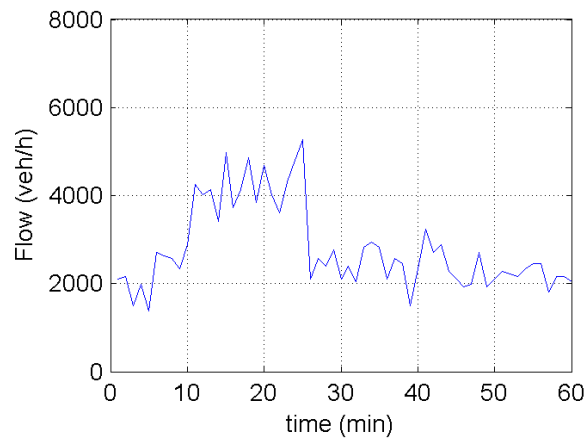
Figure C.6: Demand entering the network (ID 338)

LCC 40% Penetration Case (Replication 473)
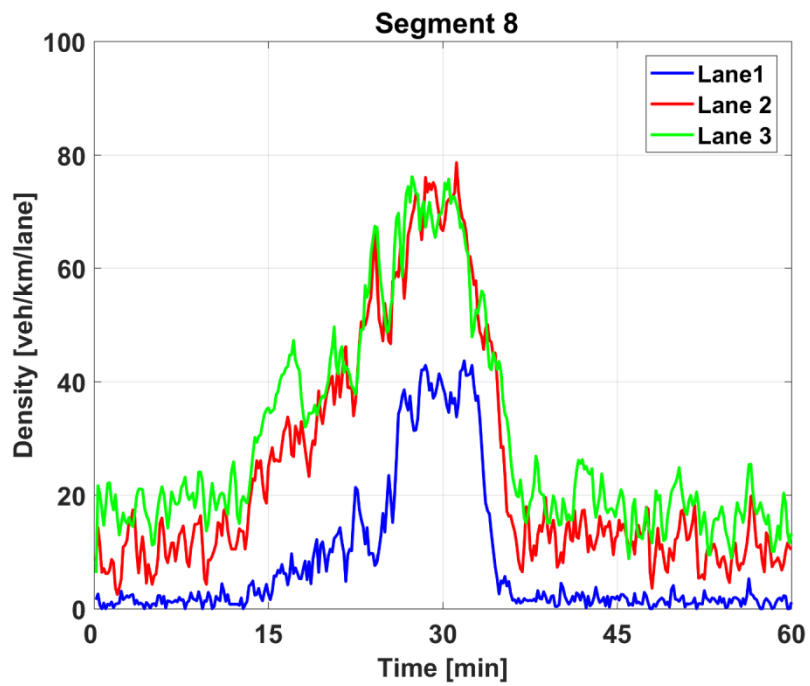
Figure D.1: Density comparison in lane-drop Section (ID 364), lane 1 (blue), lane 2 (red) and lane 3 (green), LCC 40%
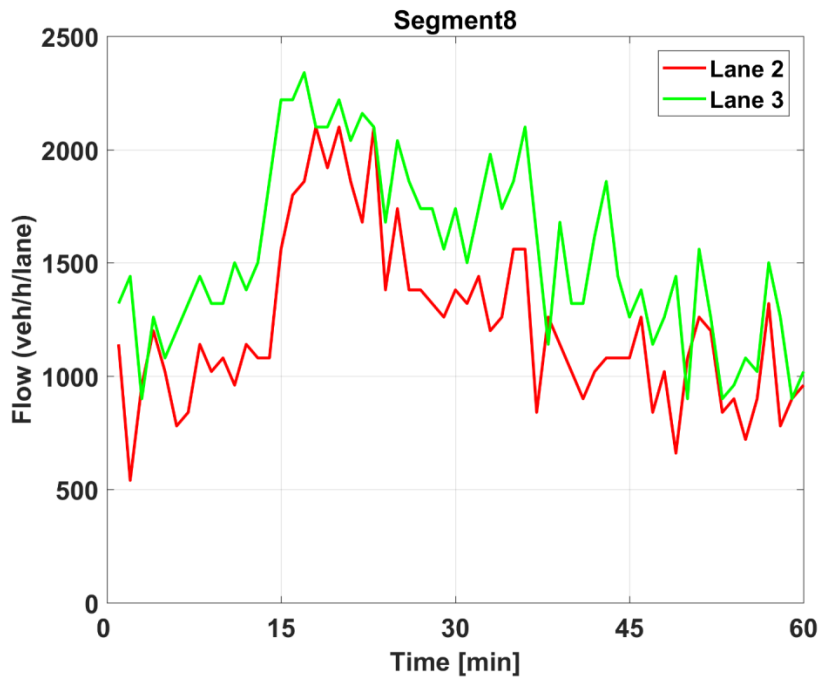
Figure D.2: Flow comparison in lane 2 (red) and lane 3 (green) at lane-drop Section (ID 364), LCC 40%
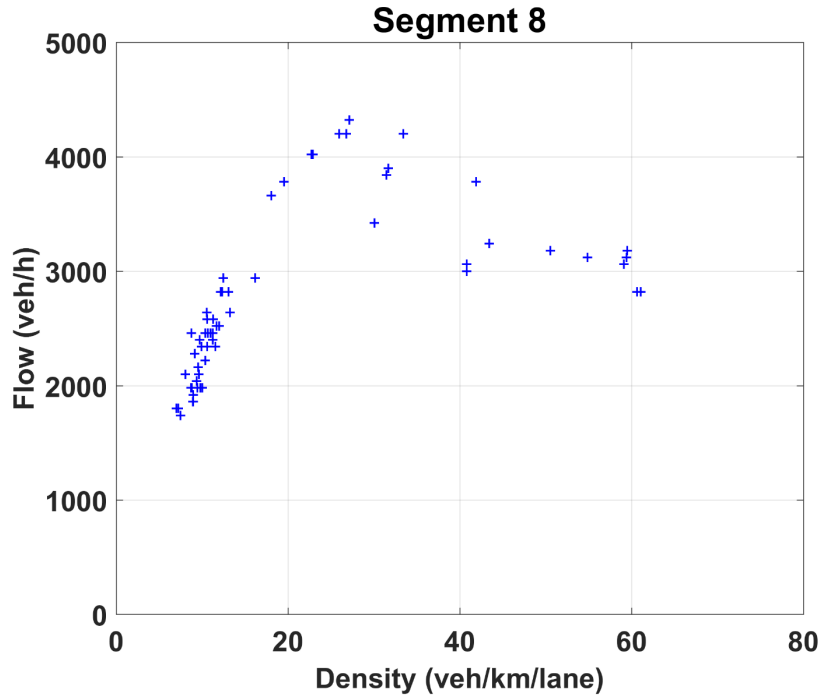
**Figure D.3: Fundamental diagram (aggregated) at lane-drop Section (ID 364), LCC 40%**
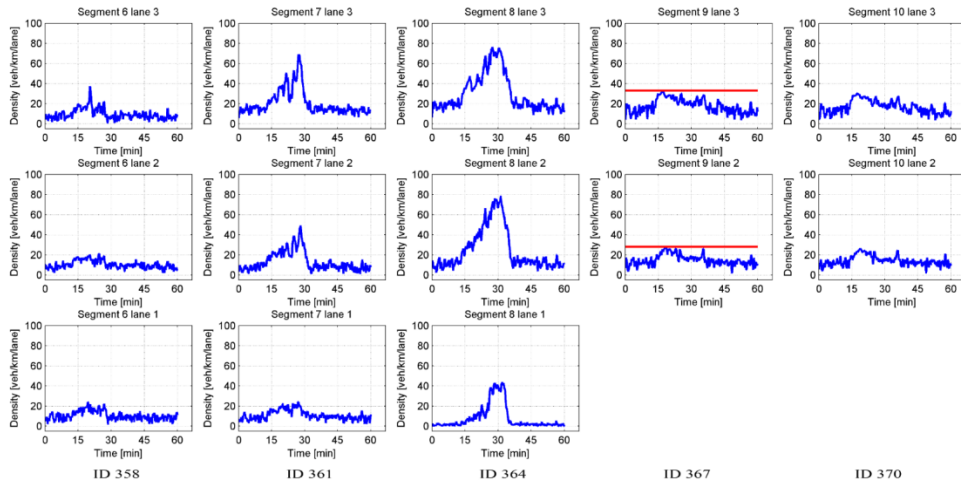
**Figure D.4: Density-Time diagram of each lane from Section ID 358 until ID 370, Set-point (red), LCC 40%**
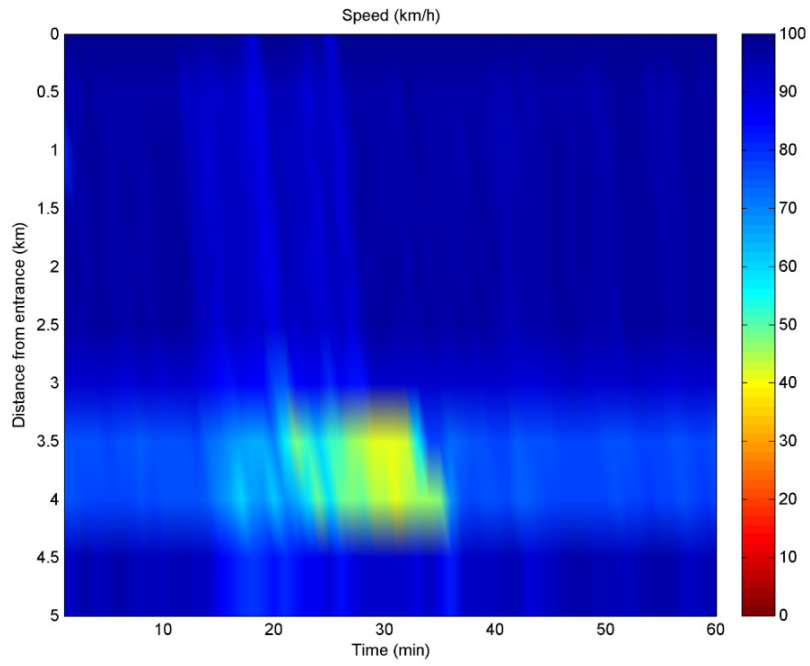
Figure D.5: Speed-Distance-Time 3D Diagram for network, LCC 20%
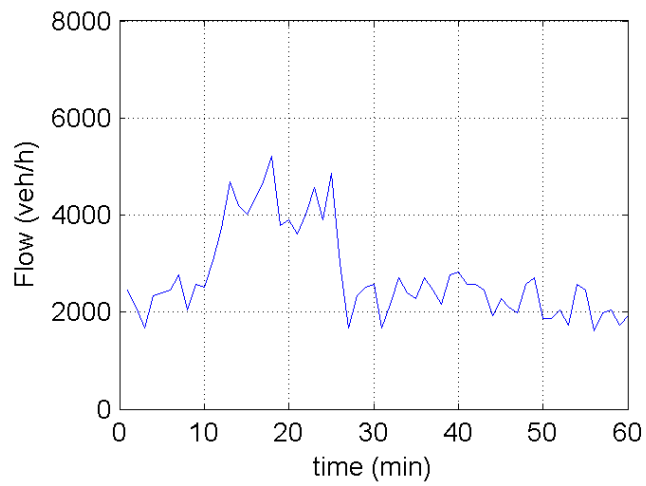
**Figure D.6: Demand entering the network (ID 338)**
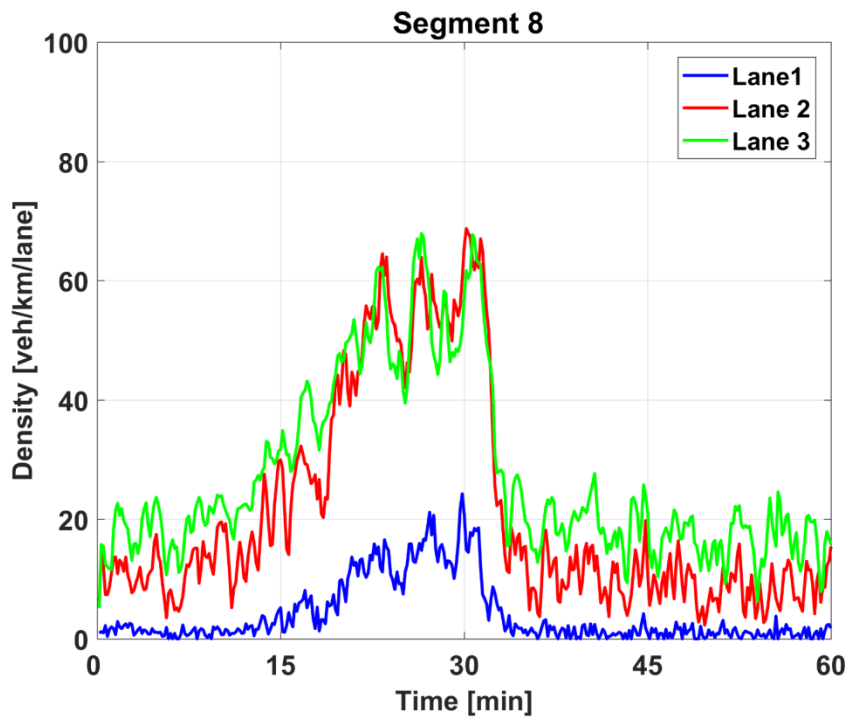
Figure E.1: Density comparison in lane-drop Section (ID 364), lane 1 (blue), lane 2 (red) and lane 3 (green), LCC 60%
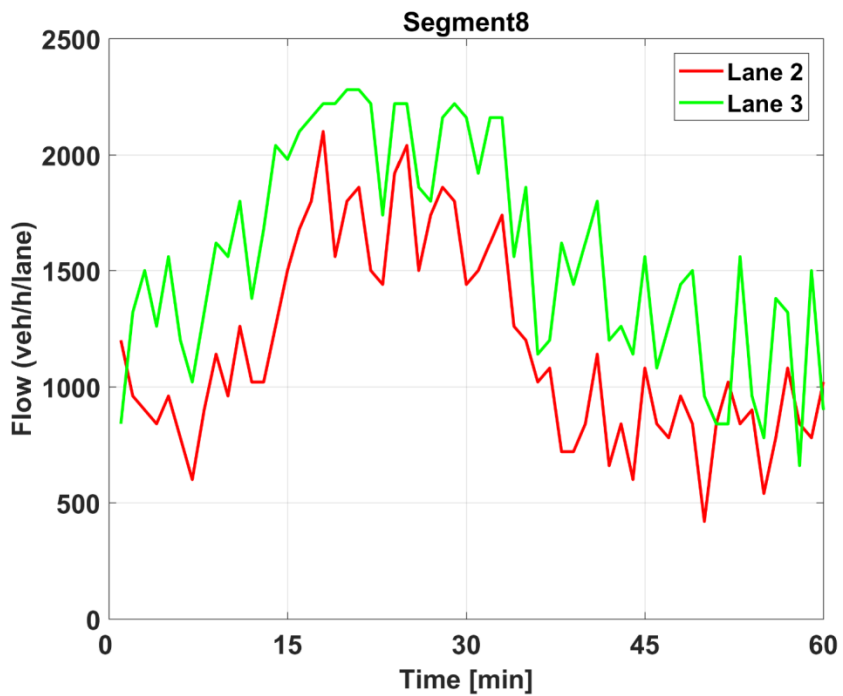
Figure E.2: Flow comparison in lane 2 (red) and lane 3 (green) at lane-drop Section (ID 364), LCC 60%
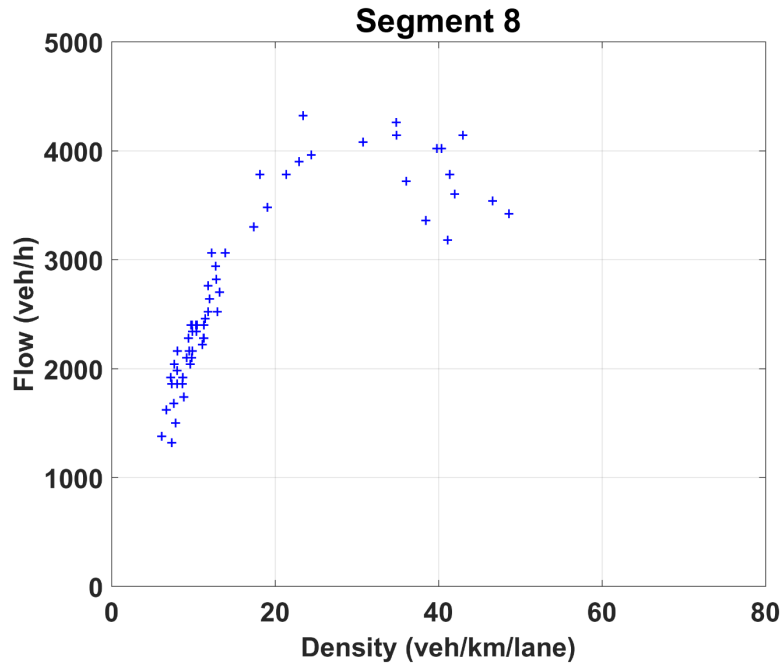
Figure E.3: Fundamental diagram (aggregated) at lane-drop Section (ID 364), LCC 60%
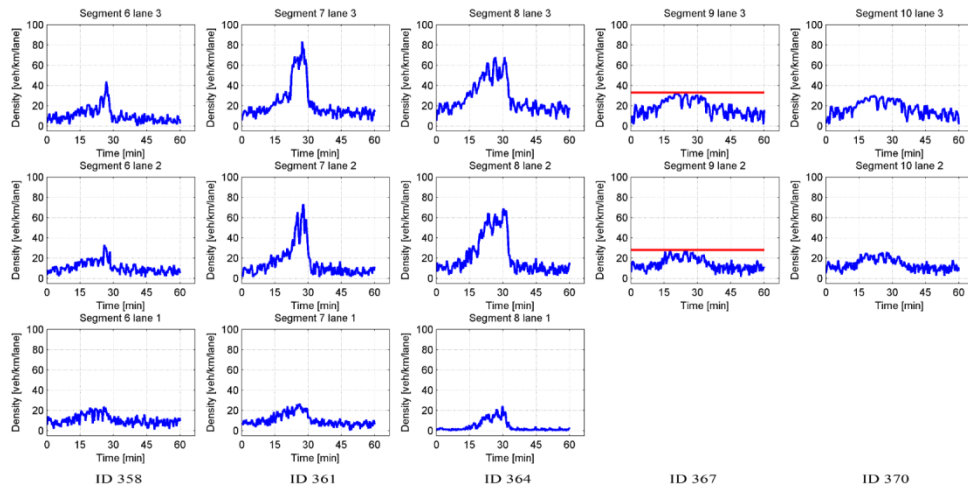
Figure E.4: Density-Time diagram of each lane from Section ID 358 until ID 370, Set-point (red), LCC 60%
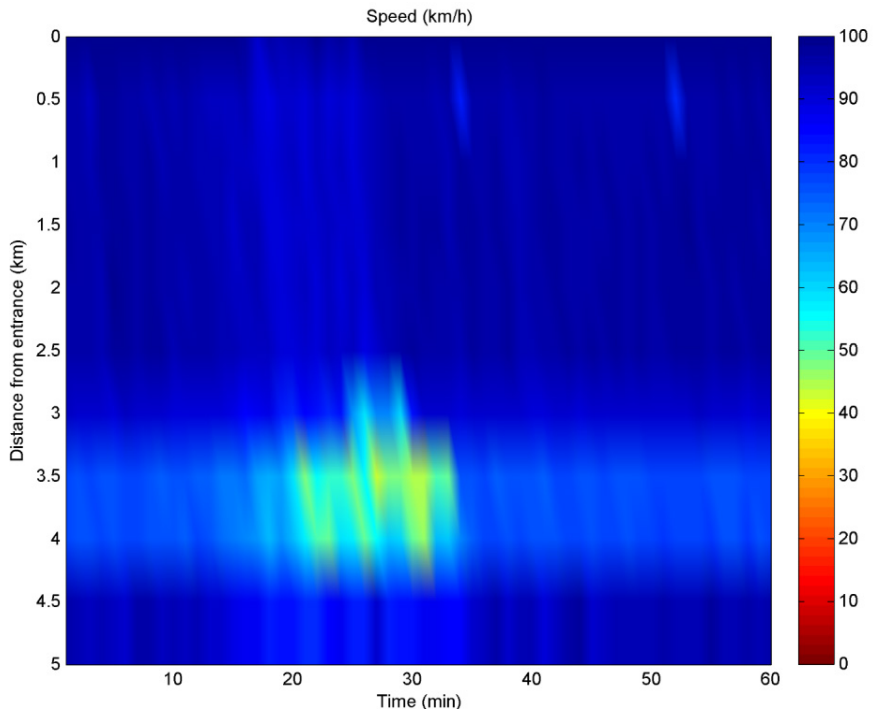
Figure E.5: Speed-Distance-Time 3D Diagram for network, LCC 60%
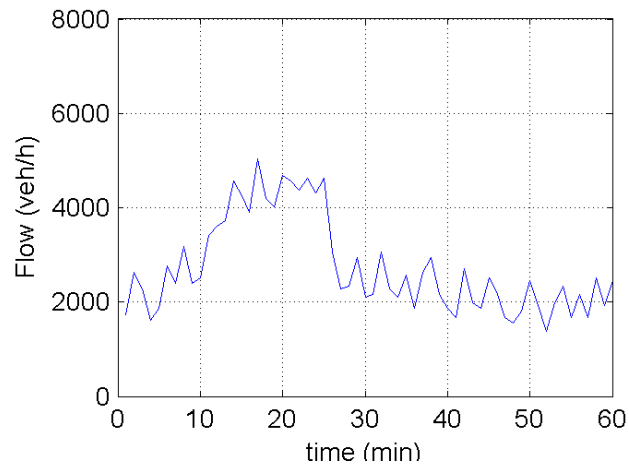
Figure E.6: Demand entering the network (ID 338)

65

LCC 80% Penetration Case (Replication 474)
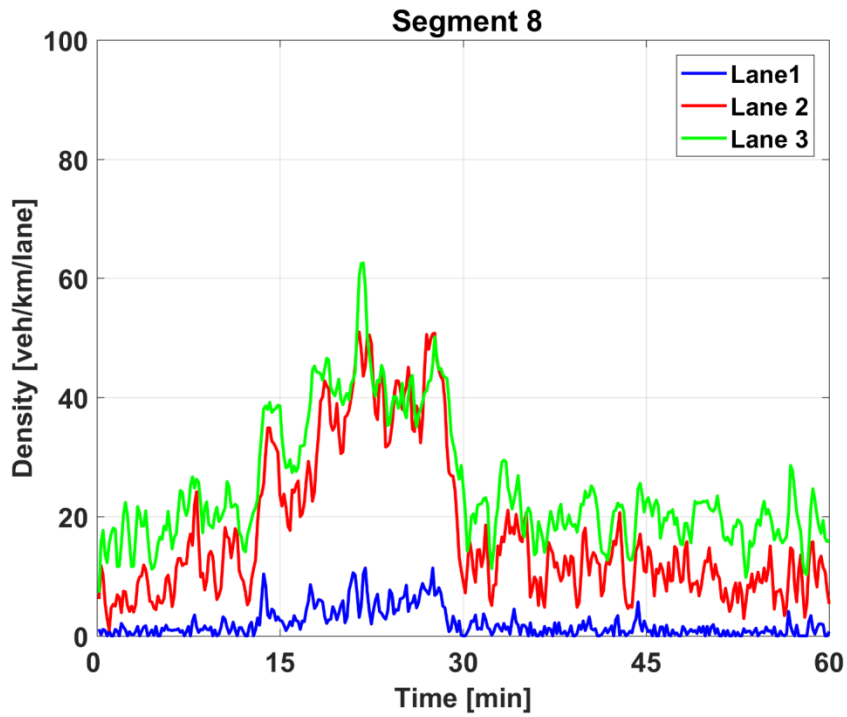
Figure F.1: Density comparison in lane-drop Section (ID 364), lane 1 (blue), lane 2 (red) and lane 3 (green), LCC 80%
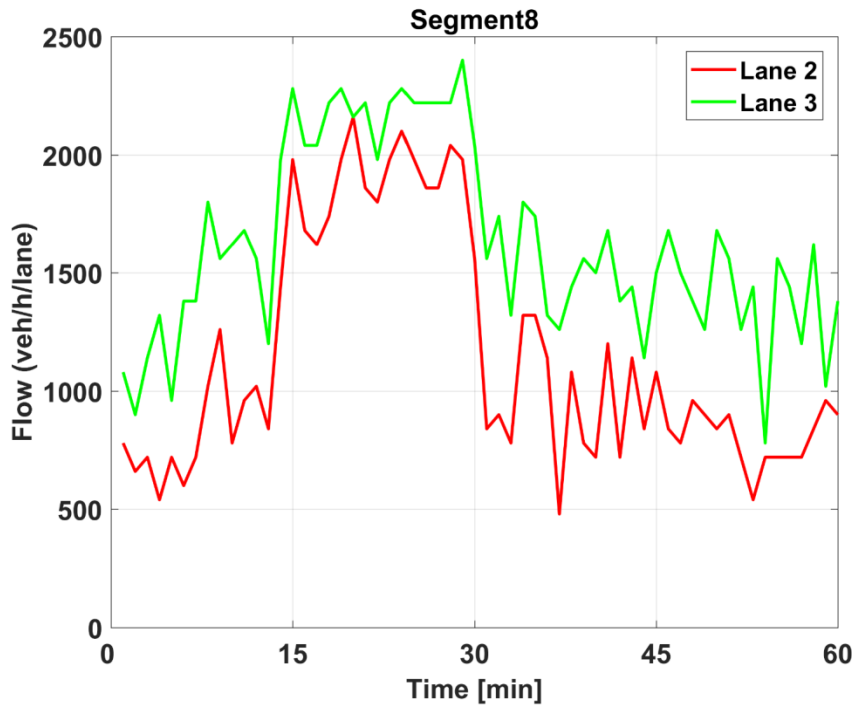

Figure F.2: Flow comparison in lane 2 (red) and lane 3 (green) at lane-drop Section (ID 364), LCC 80%
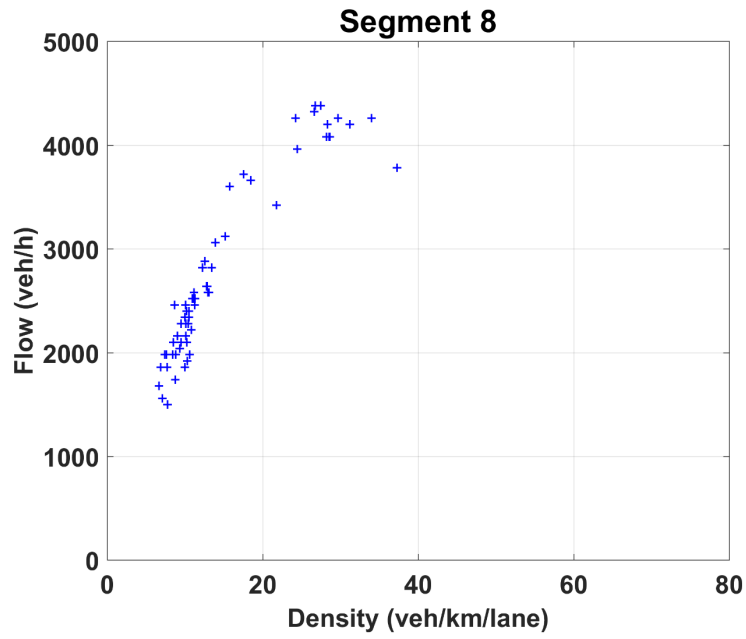
Figure F.3: Fundamental diagram (aggregated) at lane-drop Section (ID 364), LCC 80%
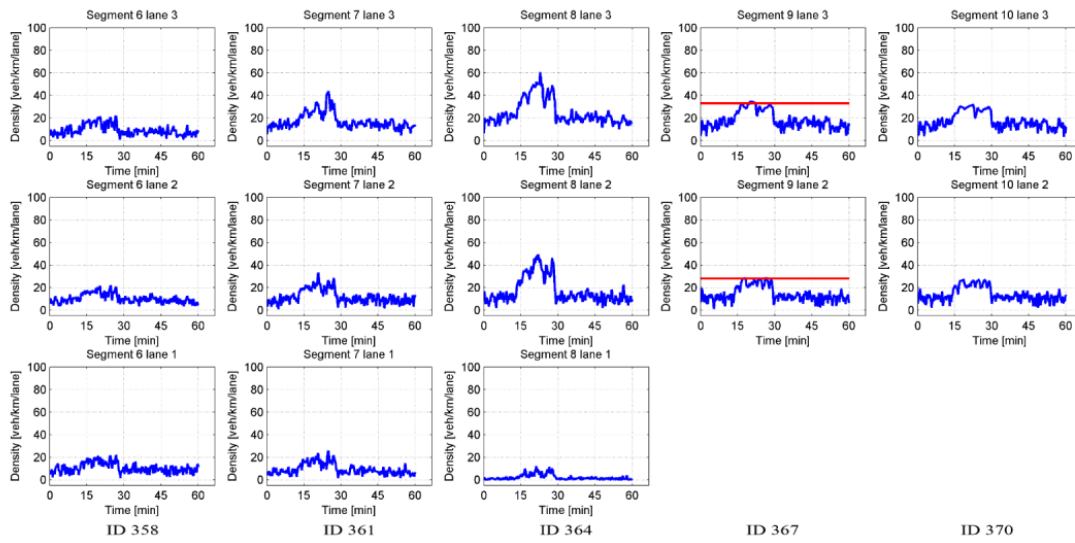
Figure F.4: Density-Time diagram of each lane from Section ID 358 until ID 370, Set-point (red), LCC 80%
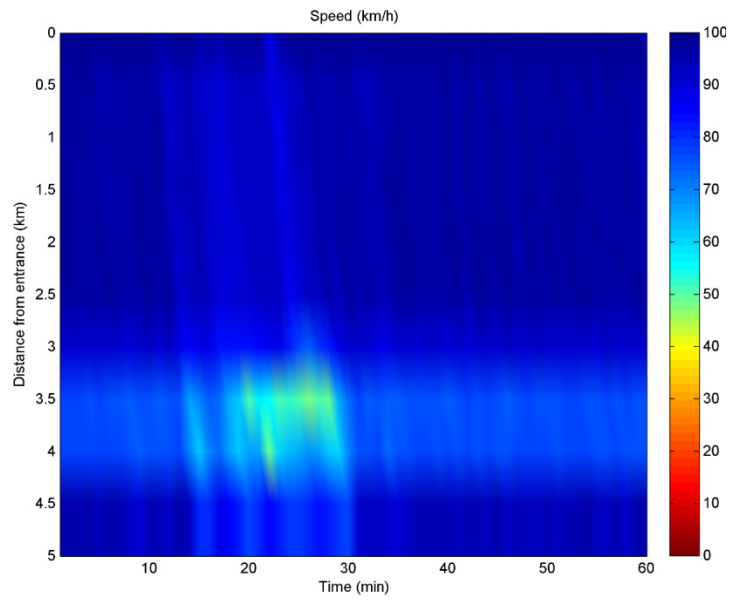
Figure F.5: Speed-Distance-Time 3D Diagram for the network, LCC 80%
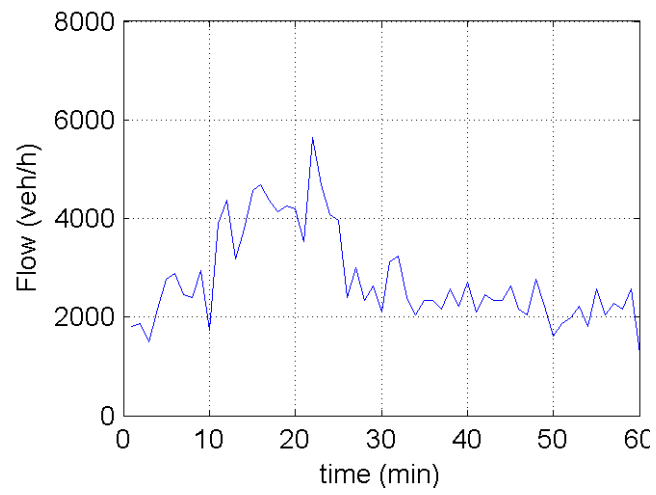
Figure F.6: Demand entering the network (ID 338)
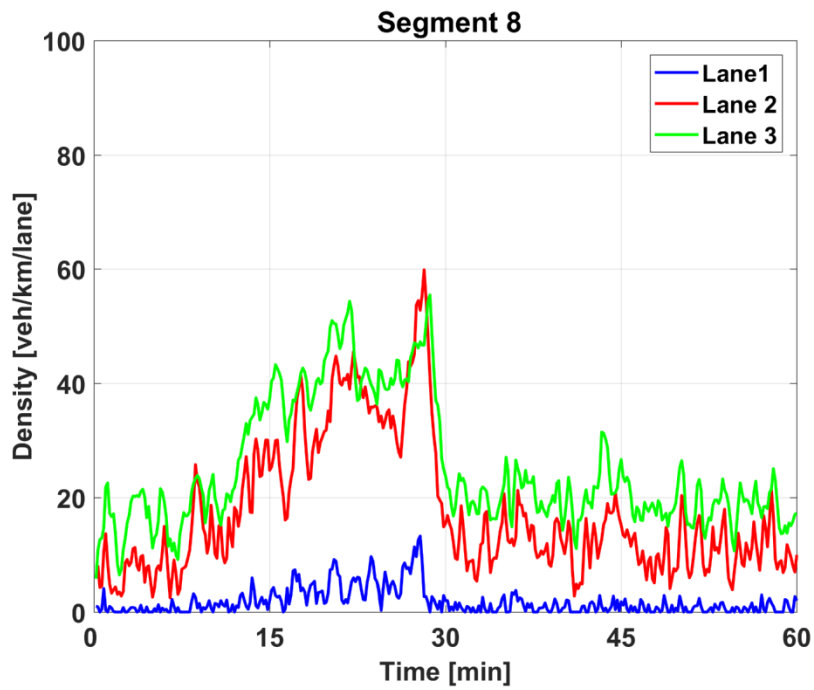
Figure G.1: Density comparison in lane-drop Section (ID 364), lane 1 (blue), lane 2 (red) and lane 3 (green), LCC 100%
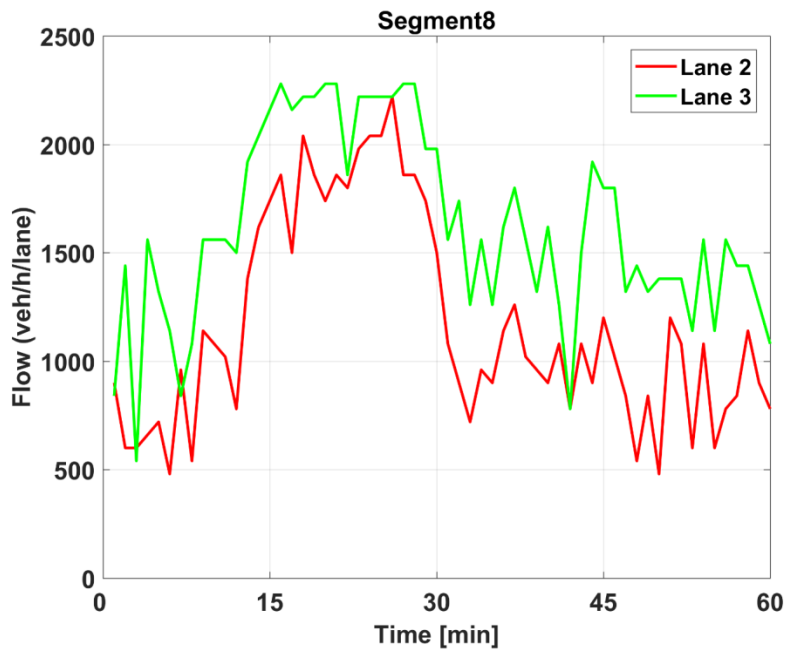
**Figure G.2: Flow comparison in lane 2 (red) and lane 3 (green) at lane-drop Section (ID 364), LCC 100%**
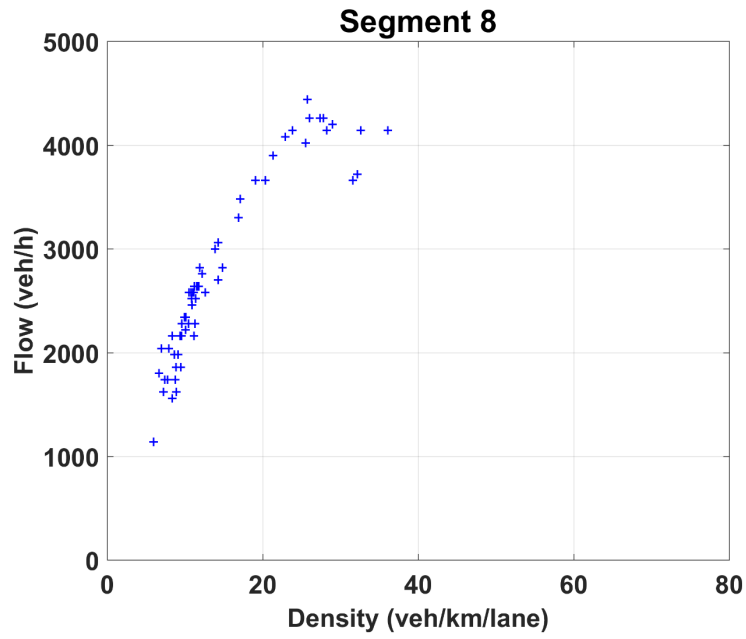
**Figure G.3: Fundamental diagram (aggregated) at lane-drop Section (ID 364), LCC 100%**
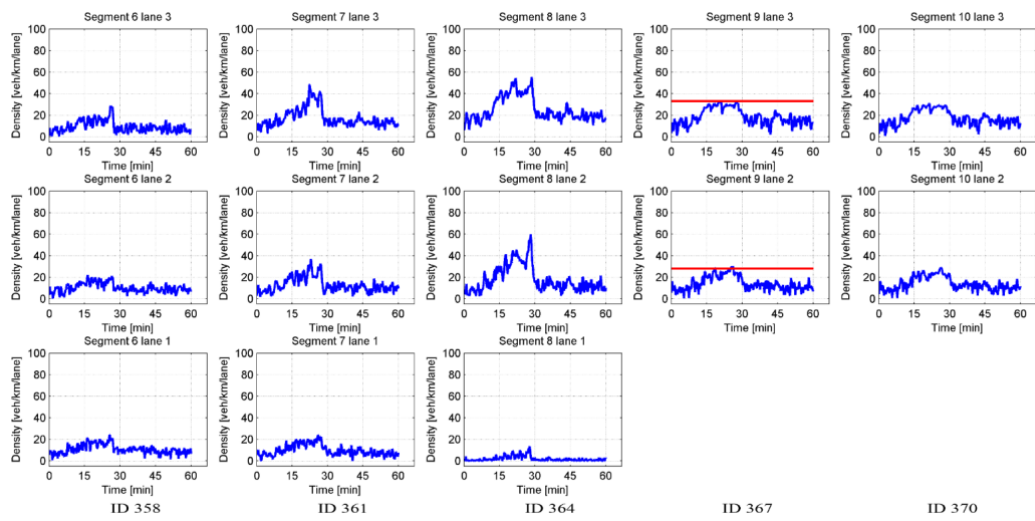
**Figure G.4: Density-Time diagram of each lane from Section ID 358 until ID 370, Set-point (red), LCC 100%**
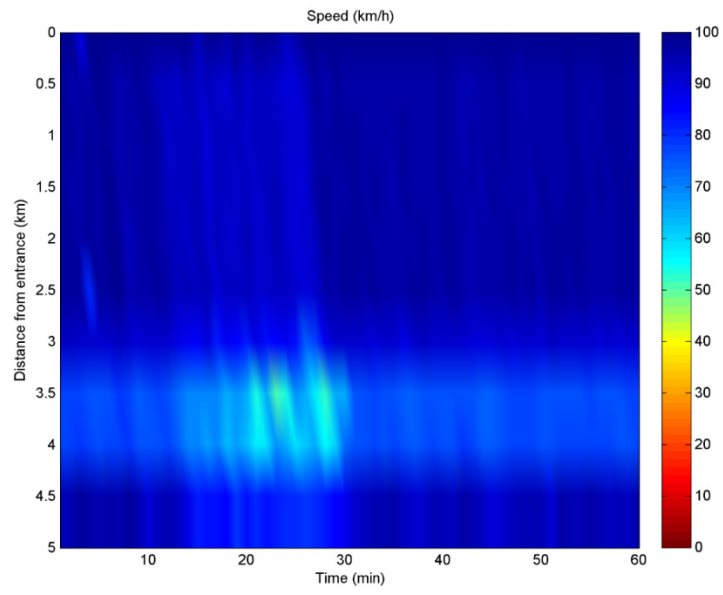
Figure G.5: Speed-Distance-Time 3D Diagram for network, LCC 100%
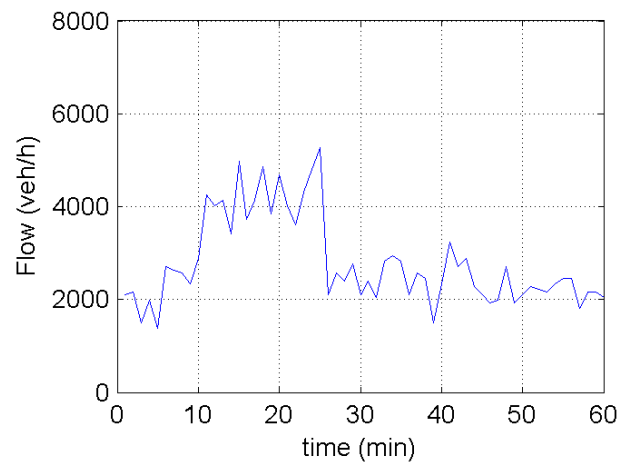
Figure G.6: Demand entering the network (ID 338)

LCC 20% & VSL Case (Replication 472)
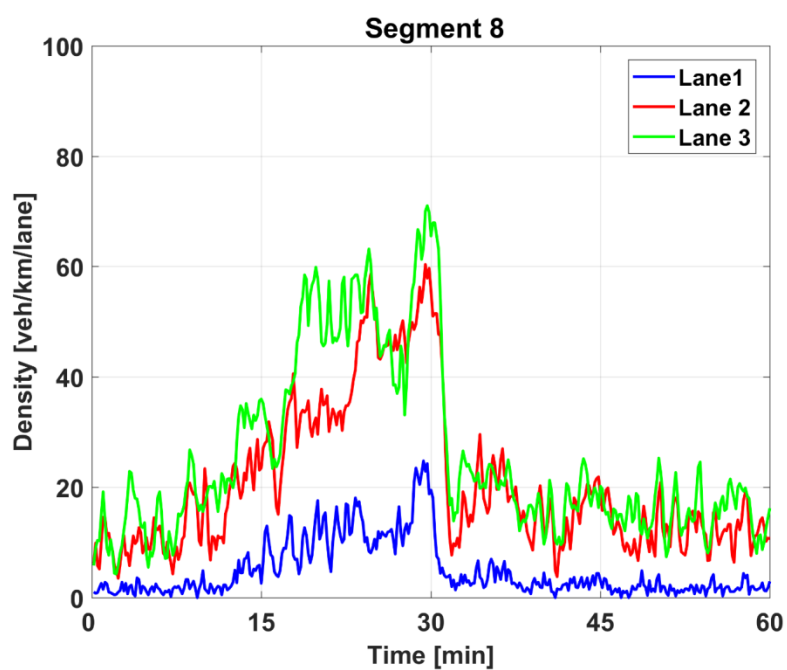
Figure H.1: Density comparison in lane-drop Section (ID 364), lane 1 (blue), lane 2 (red) and lane 3 (green), LCC 20% & VSL
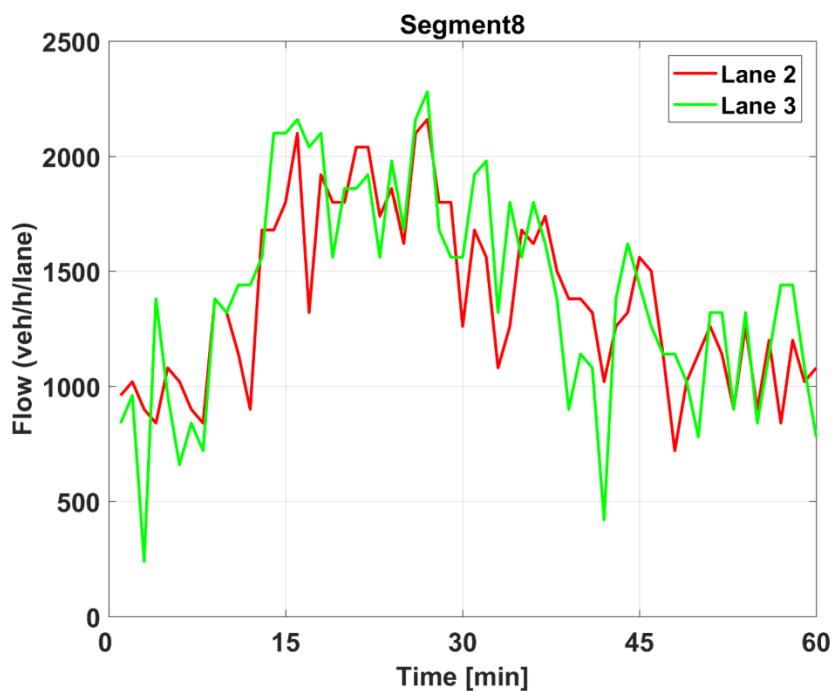
Figure H.2: Flow comparison in lane 2 (red) and lane 3 (green) at lane-drop Section (ID 364), LCC 20% & VSL

72
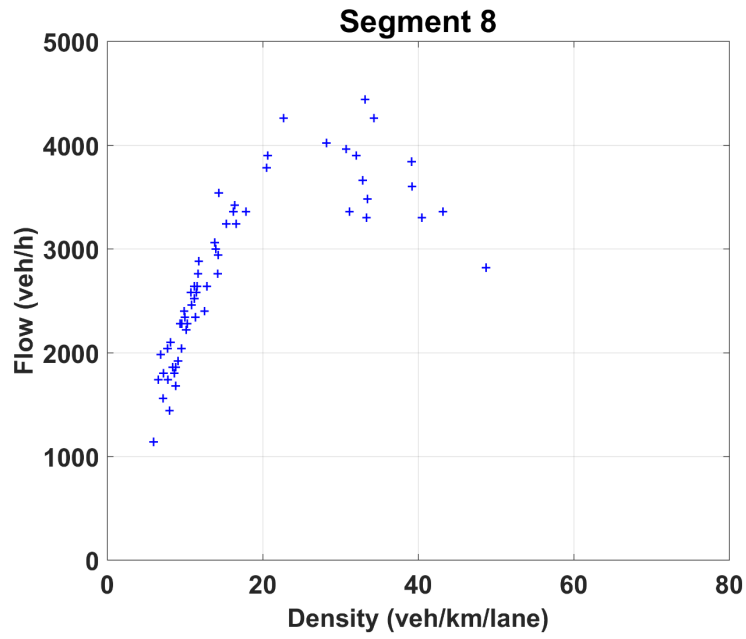
Figure H.3: Fundamental diagram (aggregated) at lane-drop Section (ID 364), LCC 20% & VSL
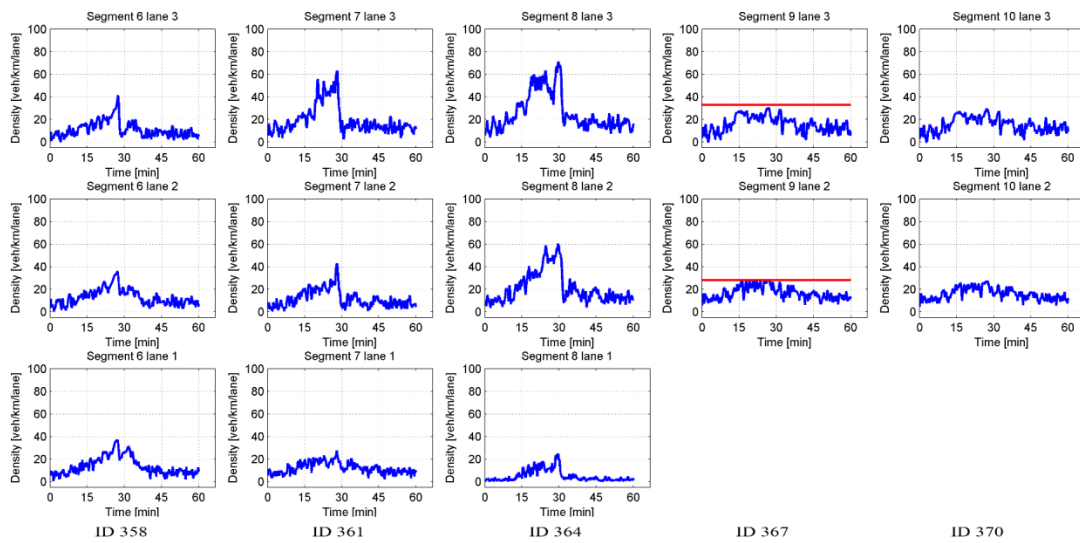
Figure H.4: Density-Time diagram of each lane from Section ID 358 until ID 370, LCC Set-point (red), LCC 20% & VSL

73
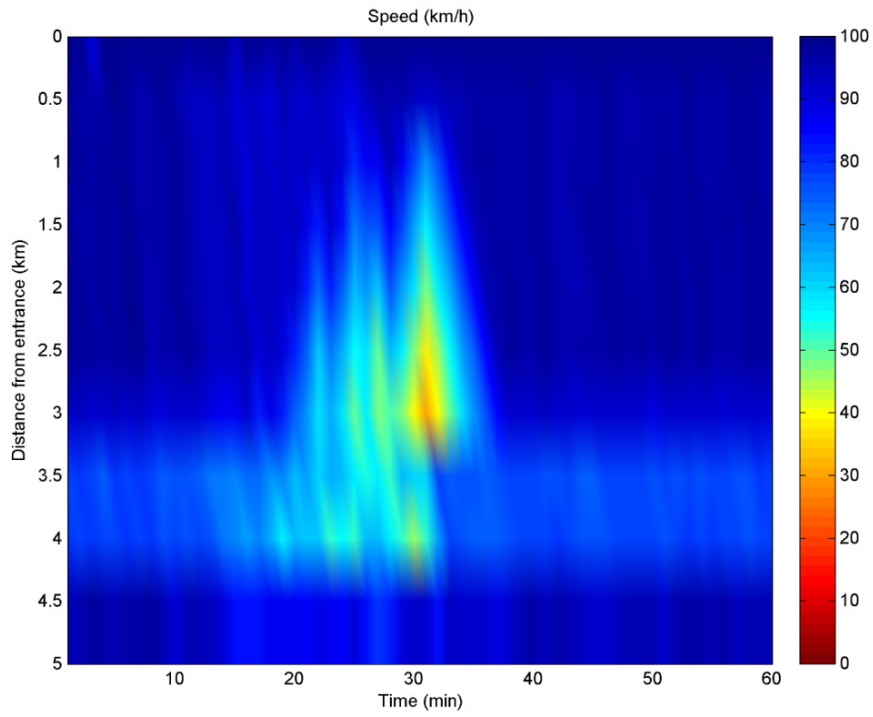
Figure H.5: Speed-Distance-Time 3D Diagram for network, LCC 20% & VSL
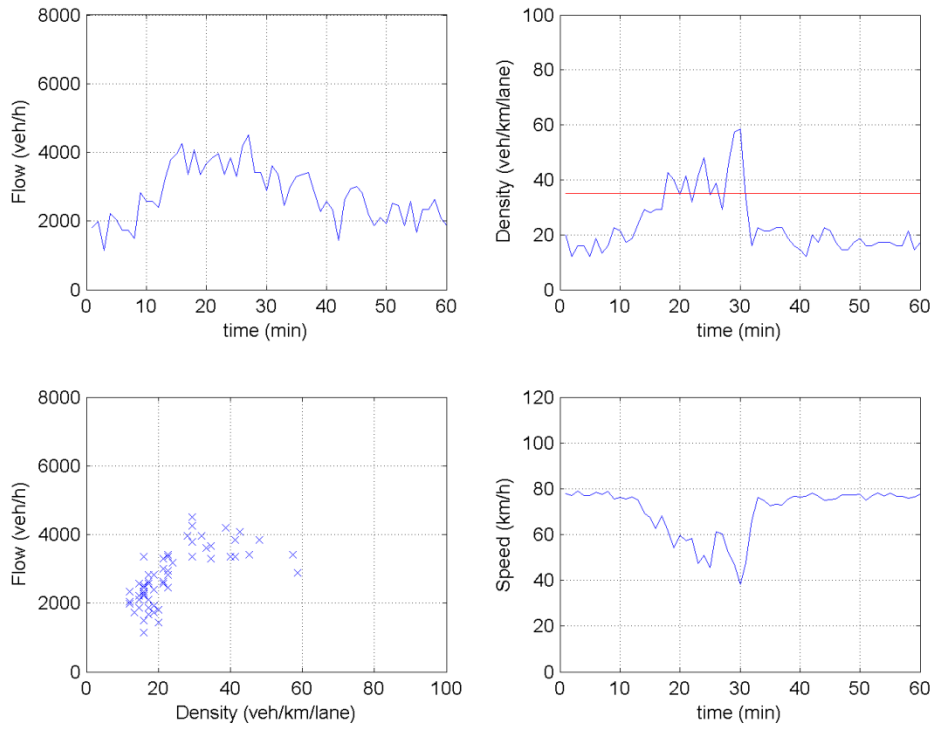
Figure H.6: Flow, Density, Speed-Time & Flow-Density at lane-drop Section (ID 367), Set-point (red), LCC 20% & VSL
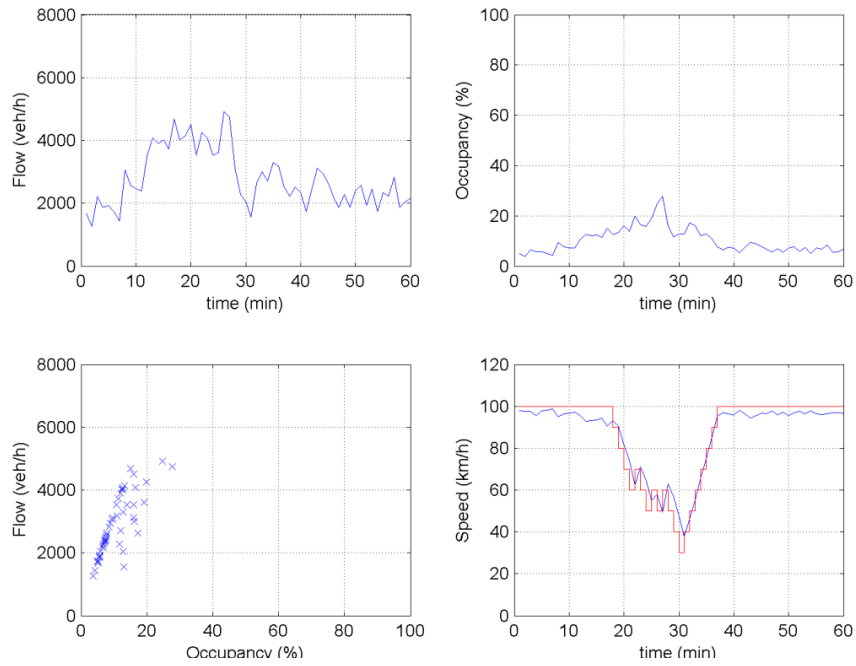
Figure H.7: Flow, Density, Speed-Time & Flow-Density at the Application area (ID 358), VSL decisions (red), LCC 20% &VSL
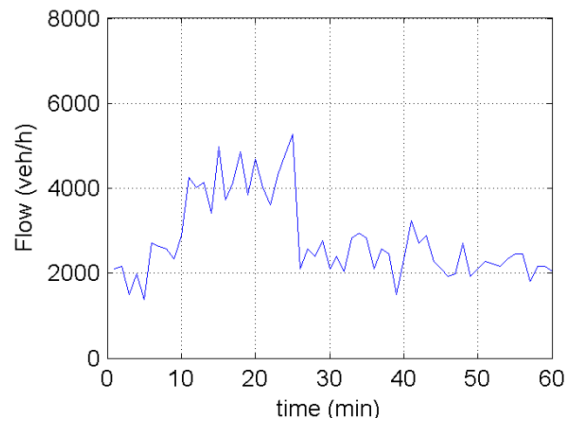

Figure H.8: Demand entering the network (ID 338)
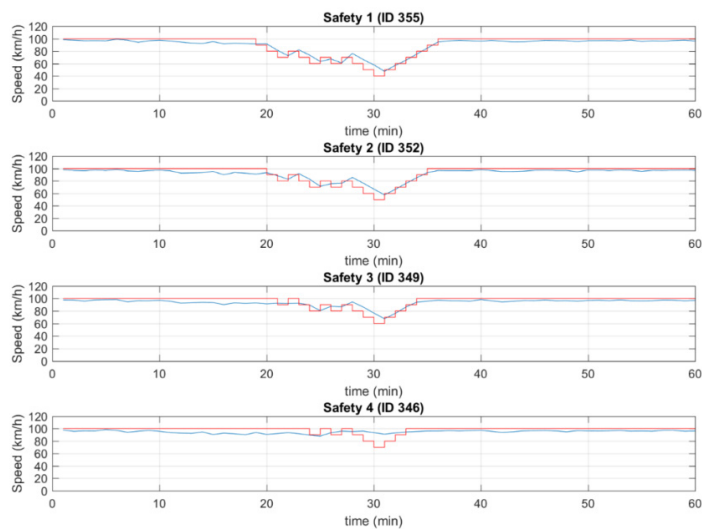
Figure H.9: Speed (blue) and VSL decisions (red) in Safety areas, LCC 20% & VSL
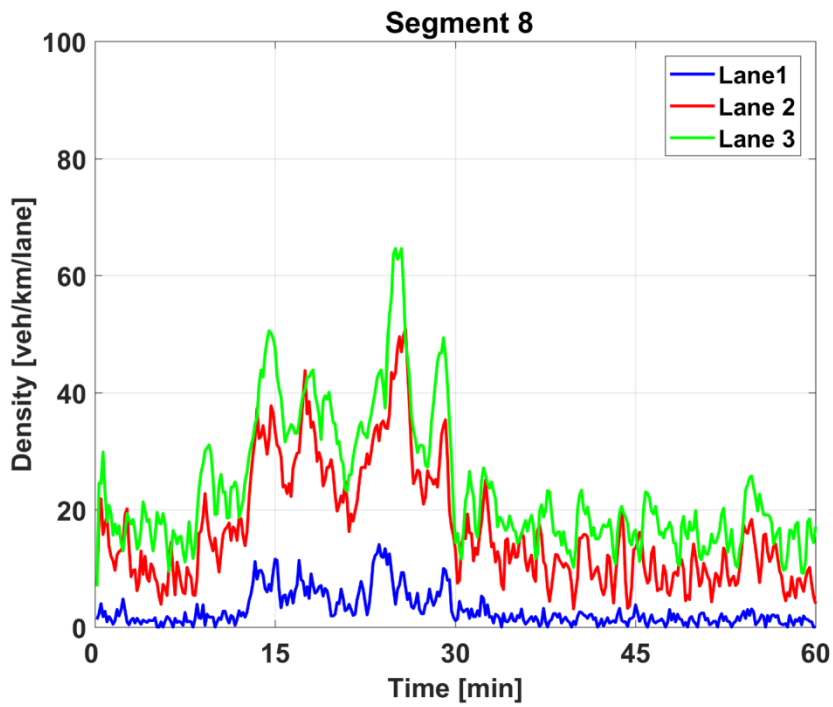
Figure I.1: Density comparison in lane-drop Section (ID 364), lane 1 (blue), lane 2 (red) and lane 3 (green), LCC 40% & VSL
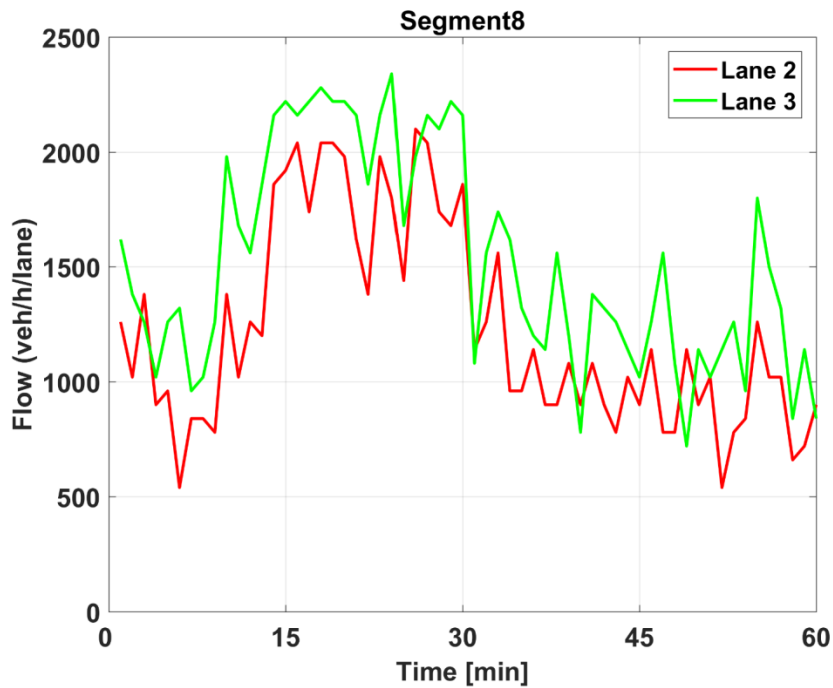

Figure I.2: Flow comparison in lane 2 (red) and lane 3 (green) at lane-drop Section (ID 364), LCC 40% & VSL
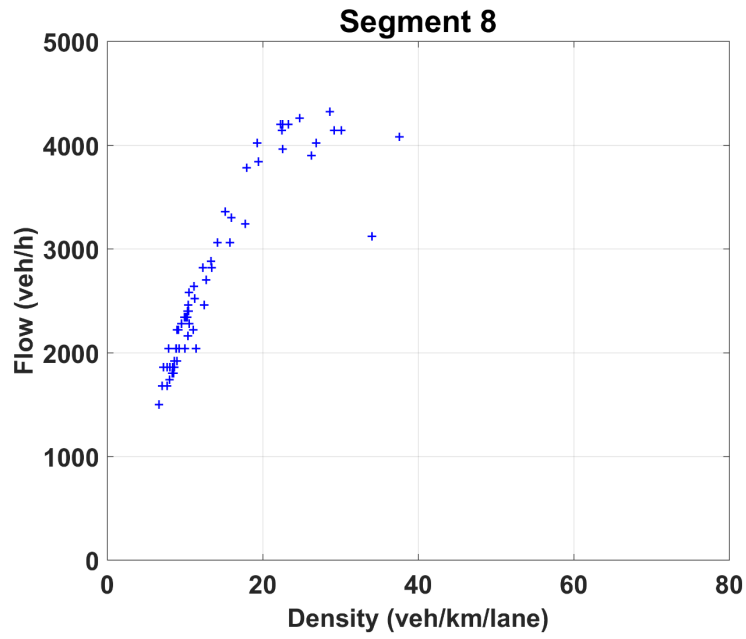
Figure I.3: Fundamental diagram (aggregated) at lane-drop Section (ID 364), LCC 40% & VSL
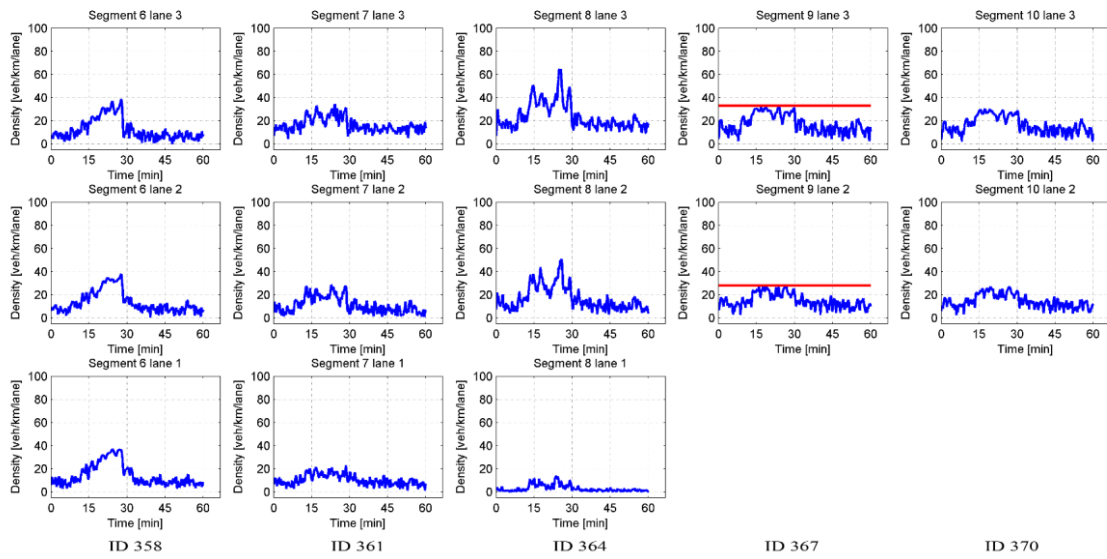

Figure I.4: Density-Time diagram of each lane from Section ID 358 until ID 370, LCC 40% & VSL
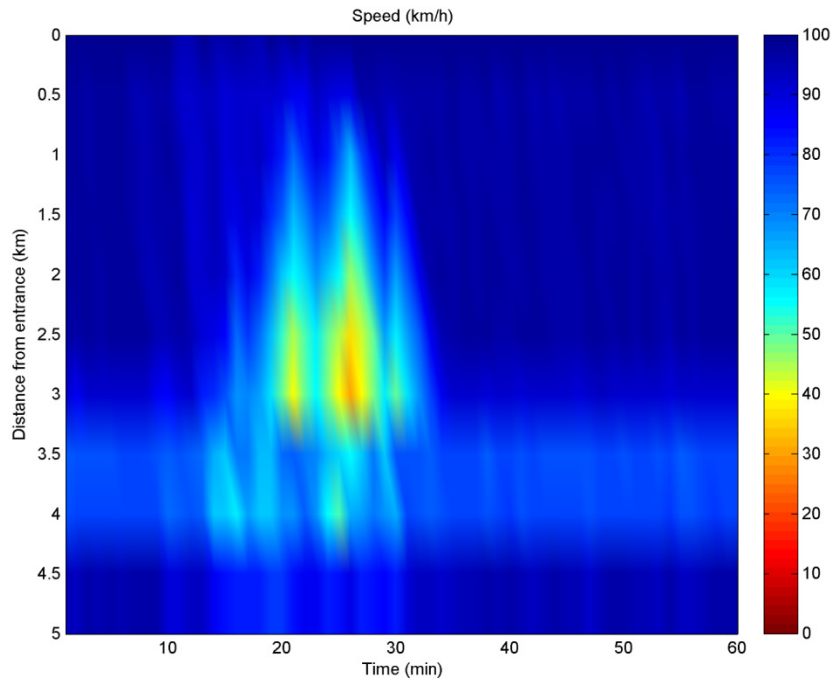
Figure I.5: Speed-Distance-Time 3D Diagram for network, LCC 40% & VSL
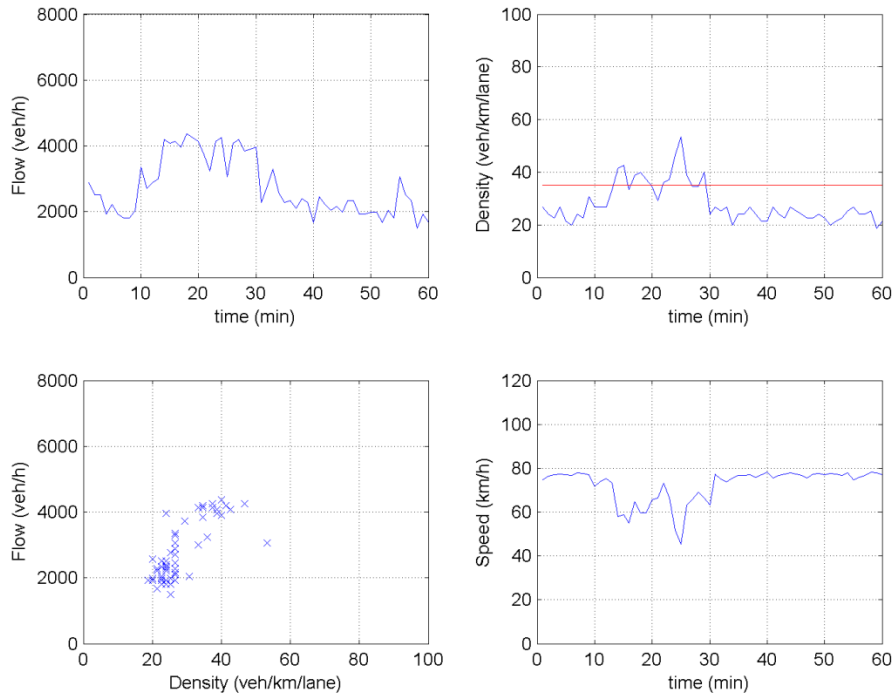

Figure I.6: Flow, Density, Speed-Time & Flow-Density at lane-drop Section (ID 367), VSL Set-point (red), LCC 40% & VSL

78
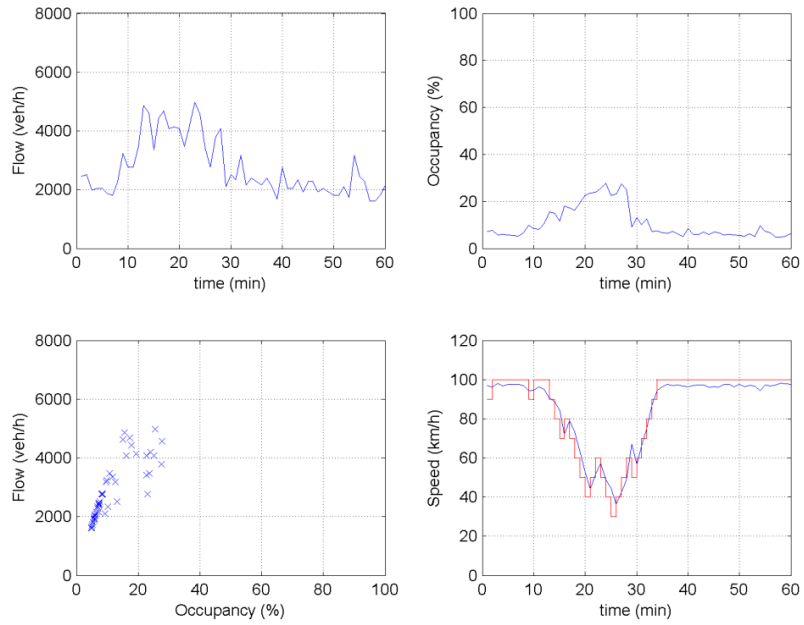
Figure I.7: Flow, Density, Speed-Time & Flow-Density at the Application area (ID 358), VSL decisions (red), LCC 40% & VSL
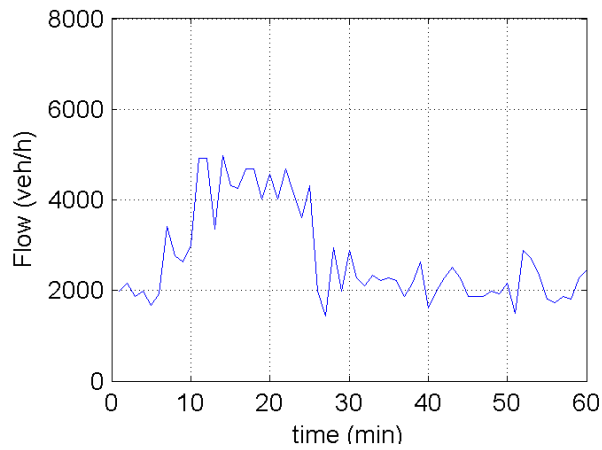
Figure I.8: Demand entering the network (ID 338)
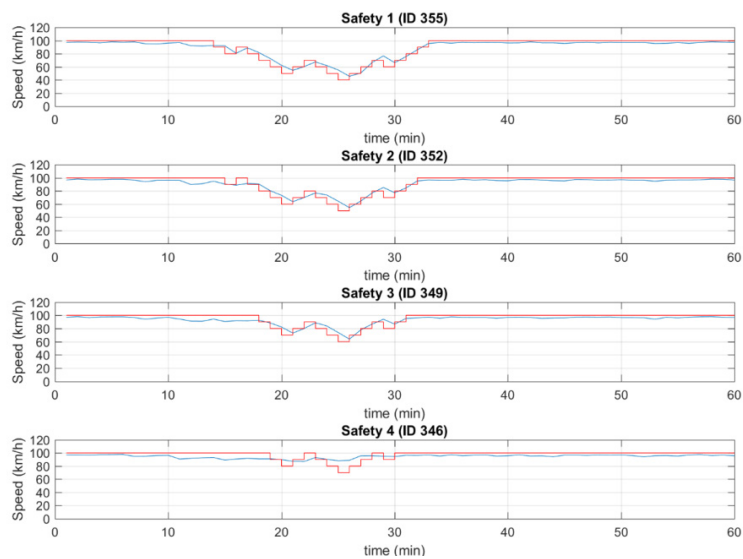
Figure I.9: Speed (blue) and VSL decisions (red) in Safety areas, LCC 40% & VSL

79
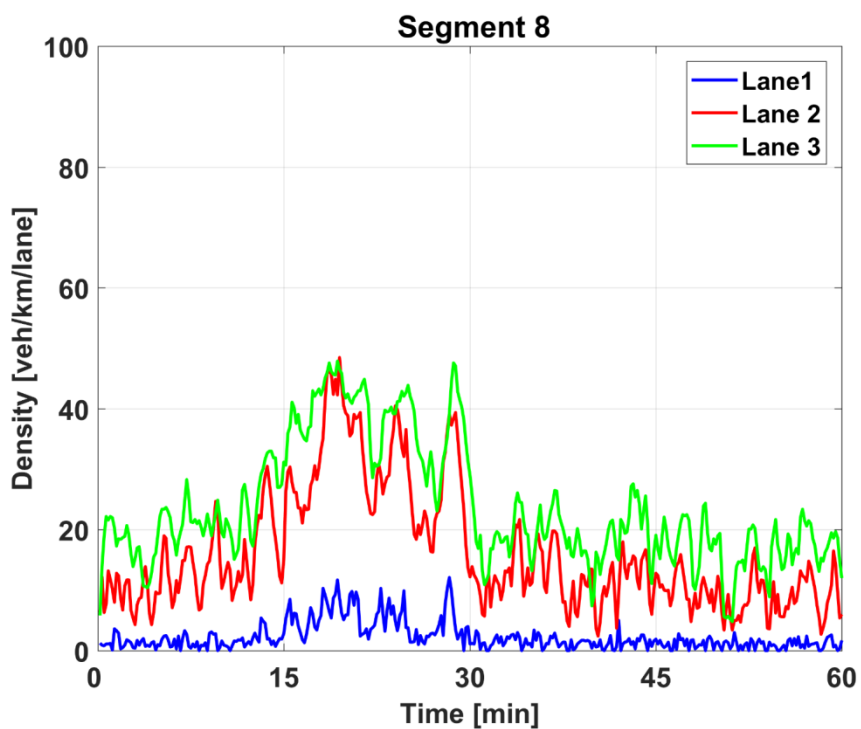
Figure J.1: Density comparison in lane-drop Section (ID 364), lane 1 (blue), lane 2 (red) and lane 3 (green), LCC 60% & VSL
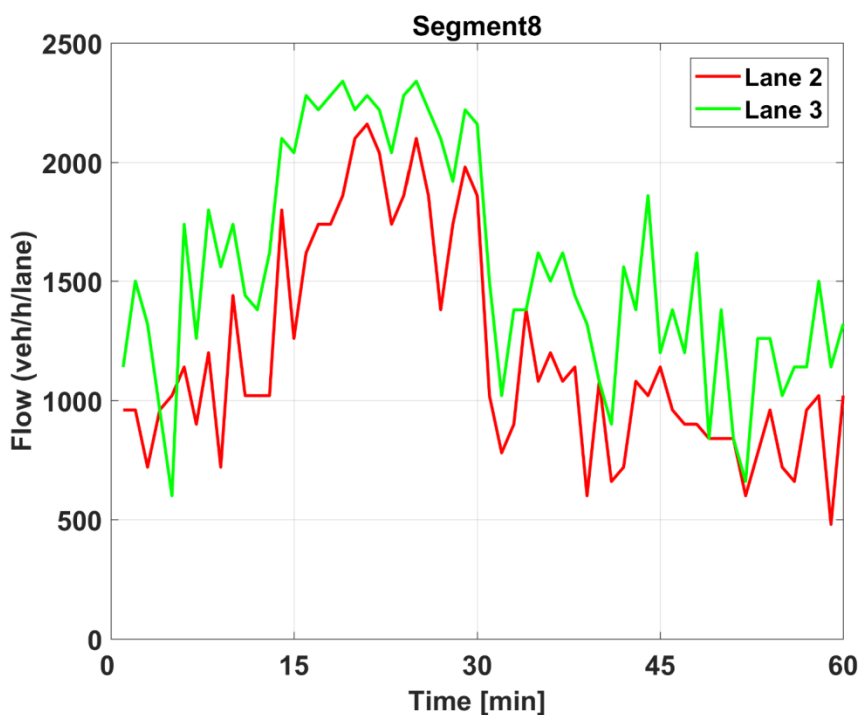
Figure J.2: Flow comparison in lane 2 (red) and lane 3 (green) at lane-drop Section (ID 364), LCC 60% & VSL
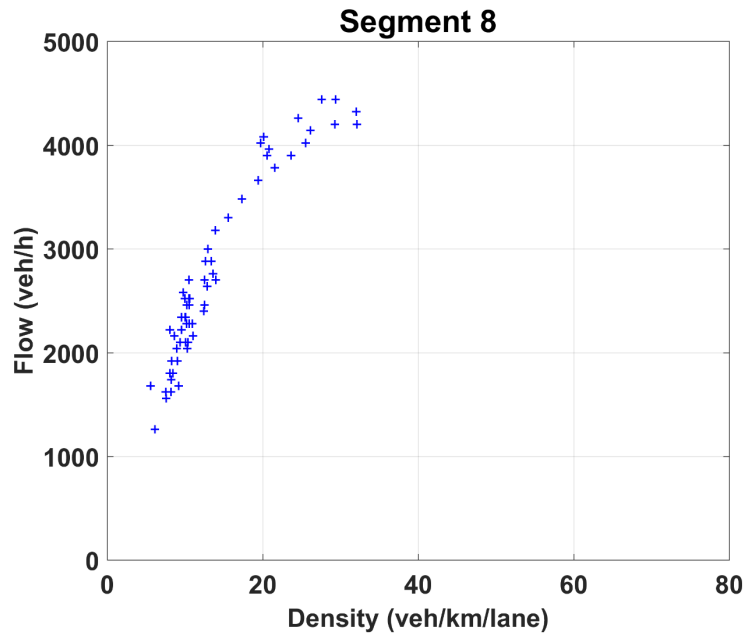
Figure J.3: Fundamental diagram (aggregated) at lane-drop Section (ID 364), LCC 60% & VSL
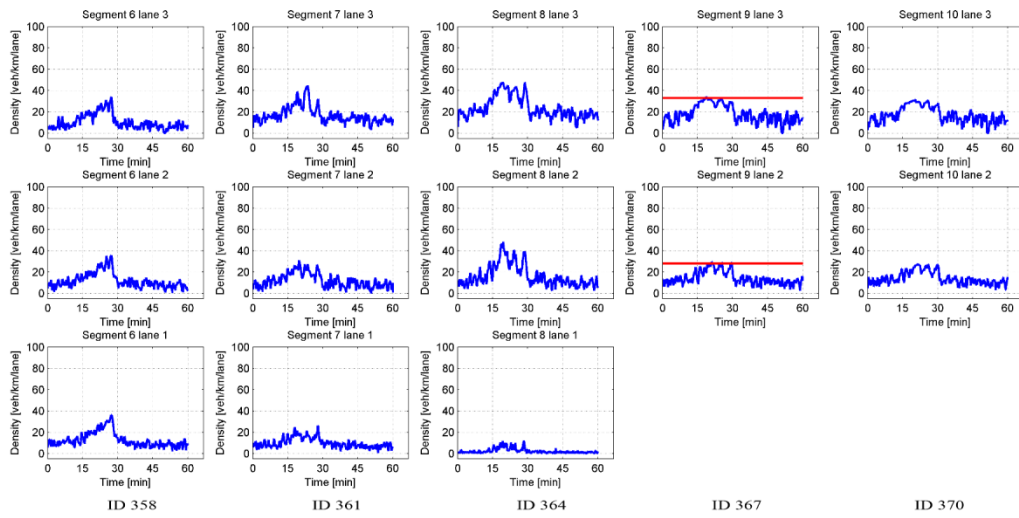
Figure J.4: Density-Time diagram of each lane from Section ID 358 until ID 370, LCC Set-point (red), LCC 60% & VSL

81
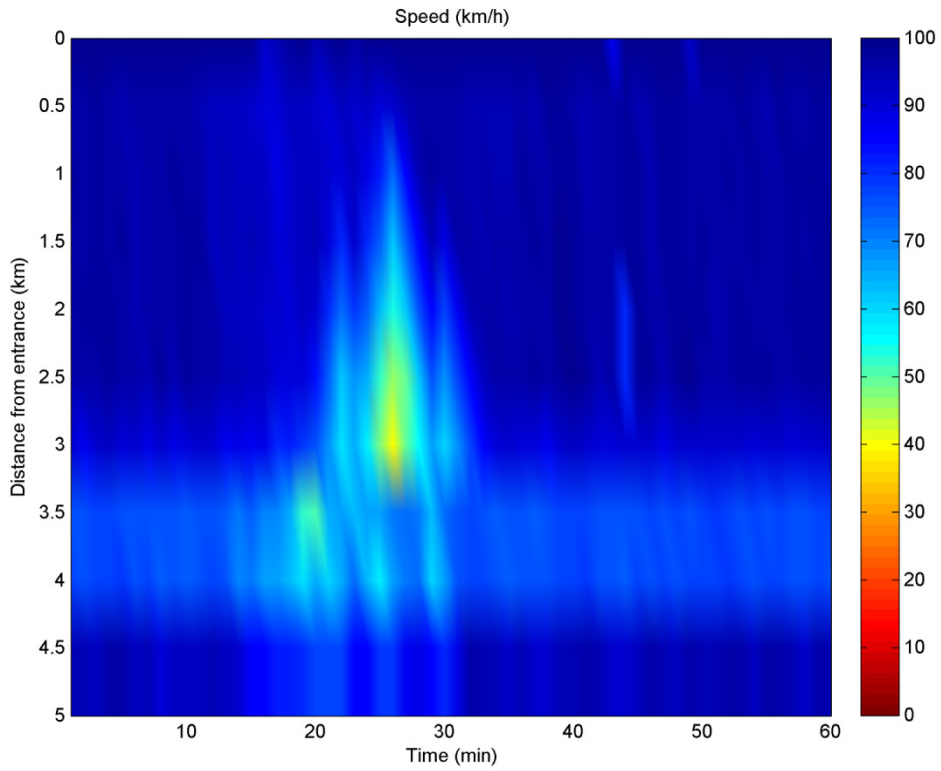
Figure J.5: Speed-Distance-Time 3D Diagram for network, LCC 60% & VSL
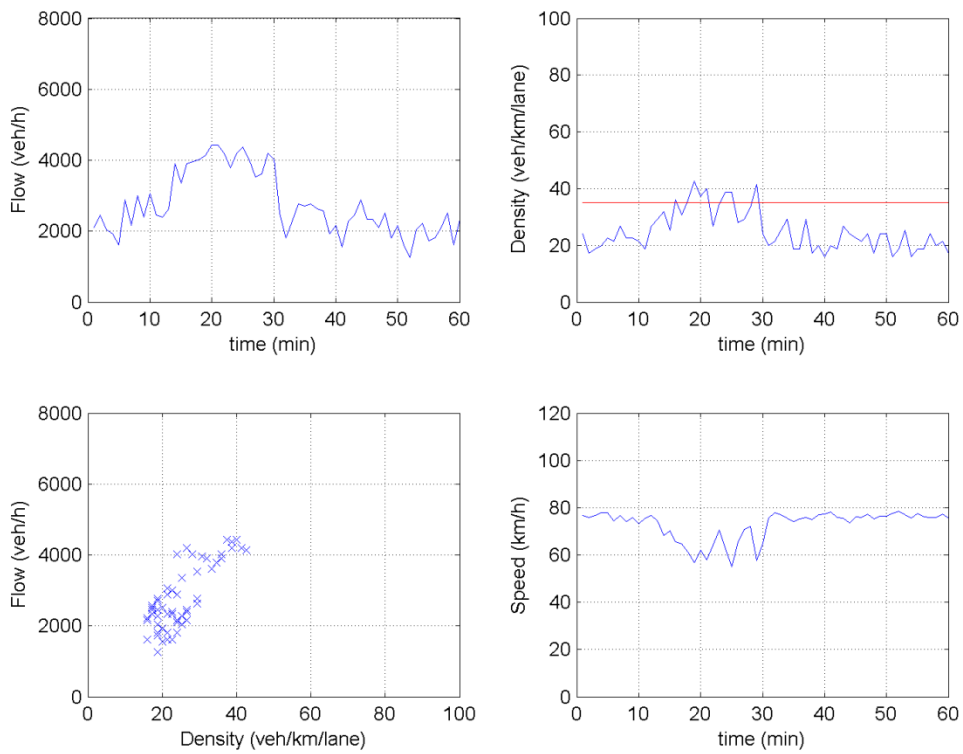
**Figure J.6: Flow, Density, Speed-Time & Flow-Density at lane-drop Section (ID 367), VSL Set-point (red), LCC 60% & VSL**
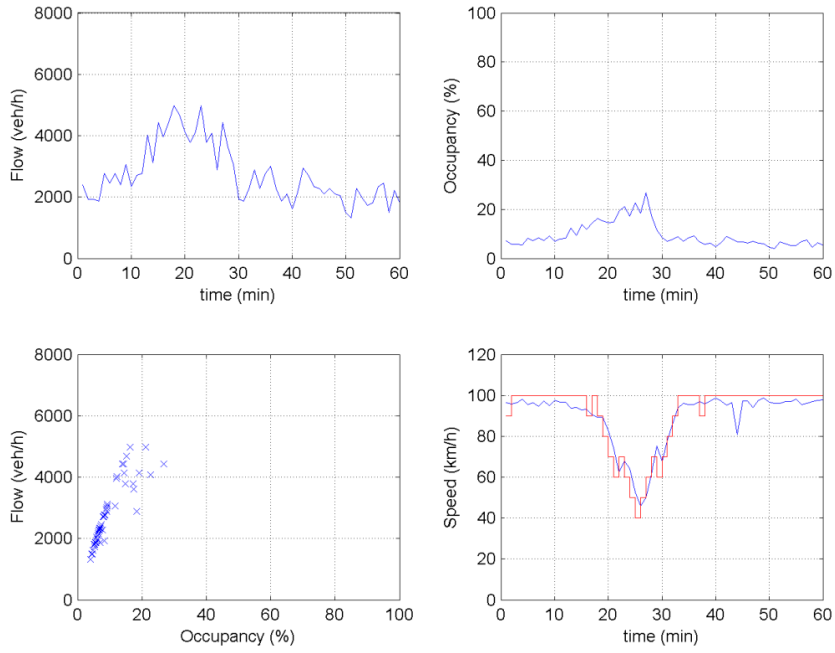
Figure J.7: Flow, Density, Speed-Time & Flow-Density at the Application area (ID 358), LCC 60% & VSL
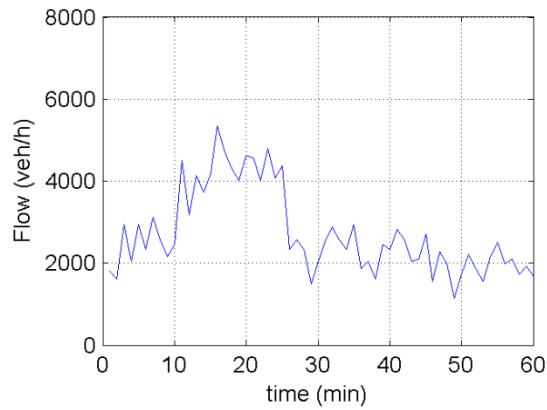

**Figure J.8: Demand entering the network (ID 338)**
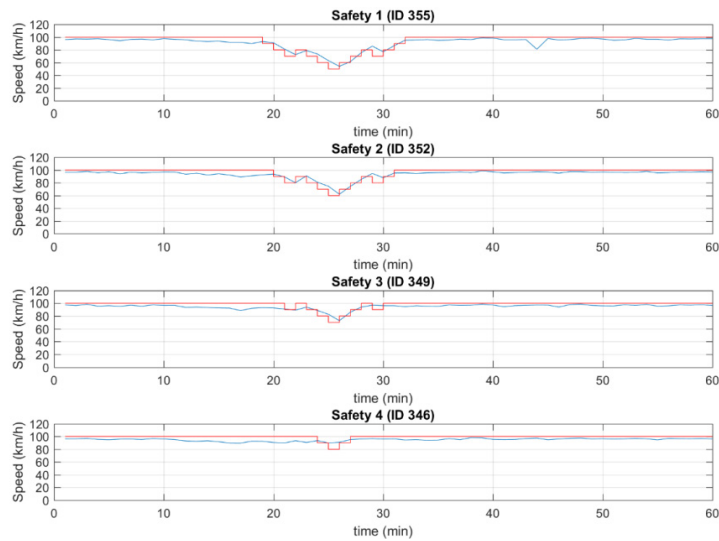
Figure J.9: Speed (blue) and VSL decisions (red) in Safety areas LCC 60% & VSL

83

LCC 80% & VSL Case (Replication 474)
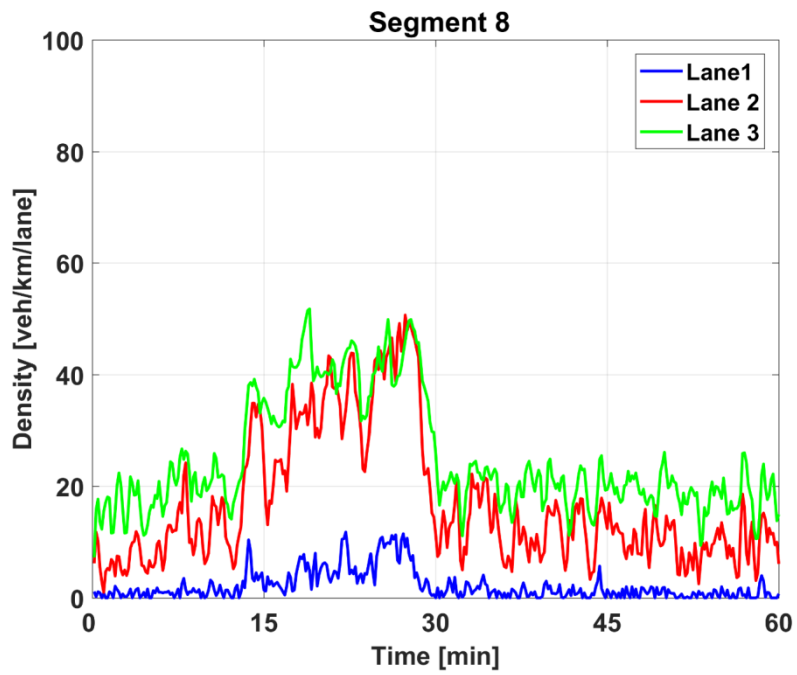
Figure K.1: Density comparison in lane-drop Section (ID 364), lane 1 (blue), lane 2 (red) and lane 3 (green), LCC 80% & VSL
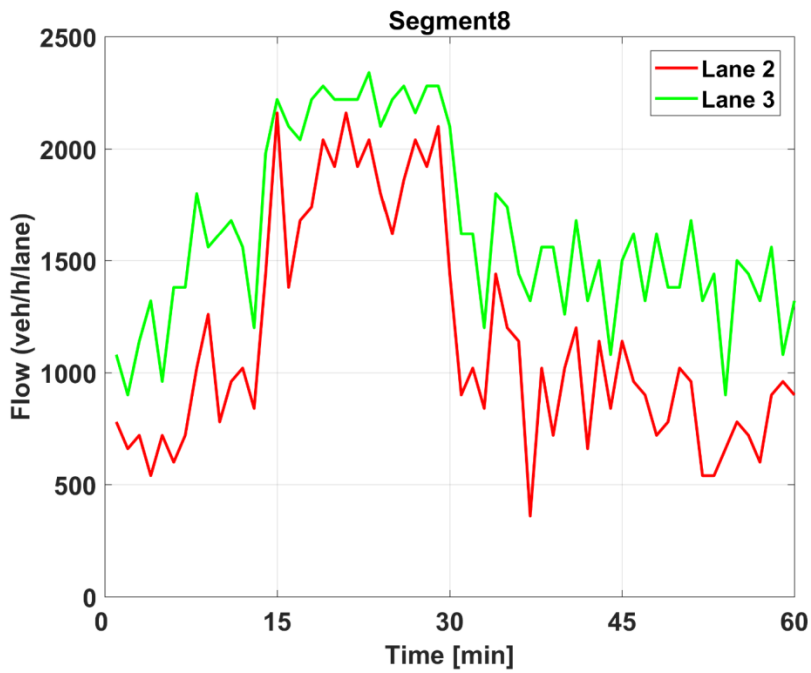

Figure K.2: Flow comparison in lane 2 (red) and lane 3 (green) at lane-drop Section (ID 364), LCC 80% & VSL

84
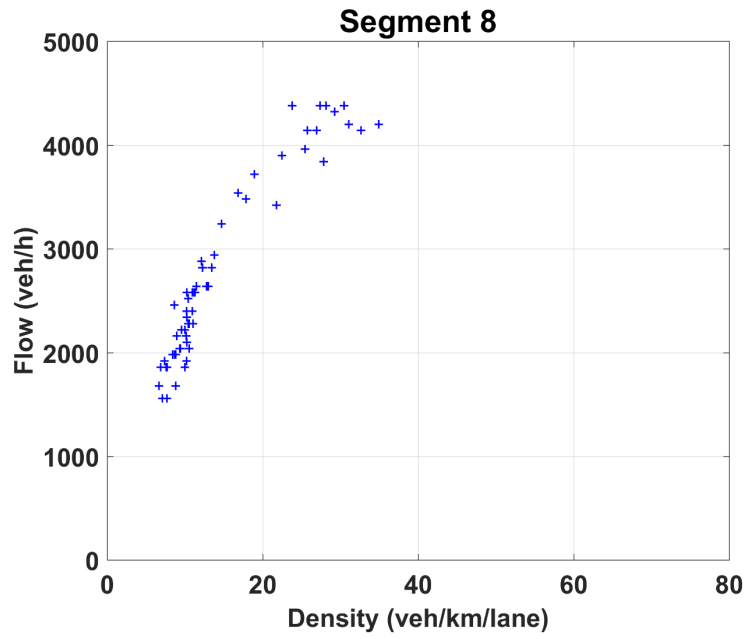
Figure K.3: Fundamental diagram (aggregated) at lane-drop Section (ID 364), LCC 80% & VSL
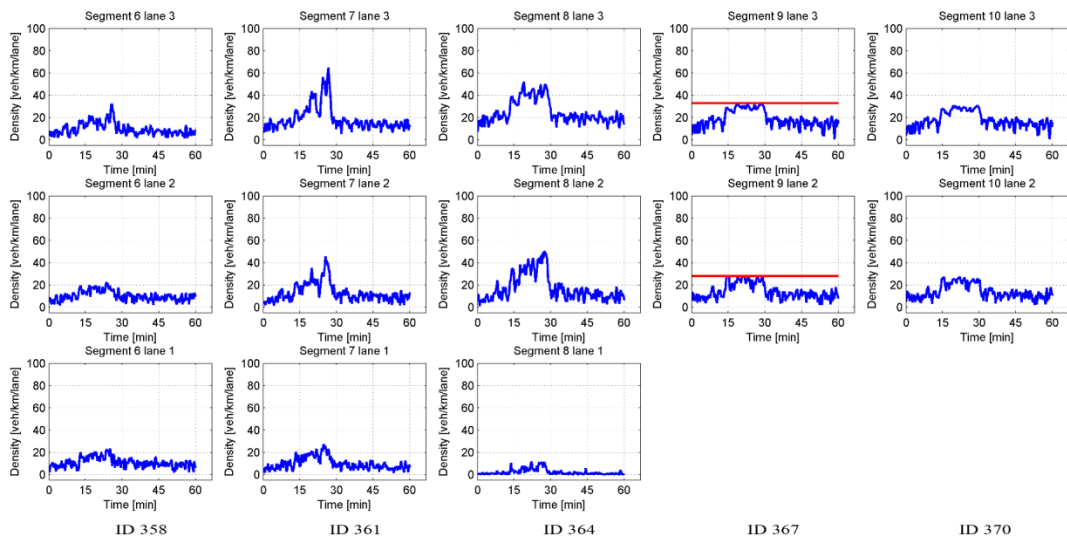

Figure K.4: Density-Time diagram of each lane from Section ID 358 until ID 370, LCC Set-point (red), LCC 80% & VSL
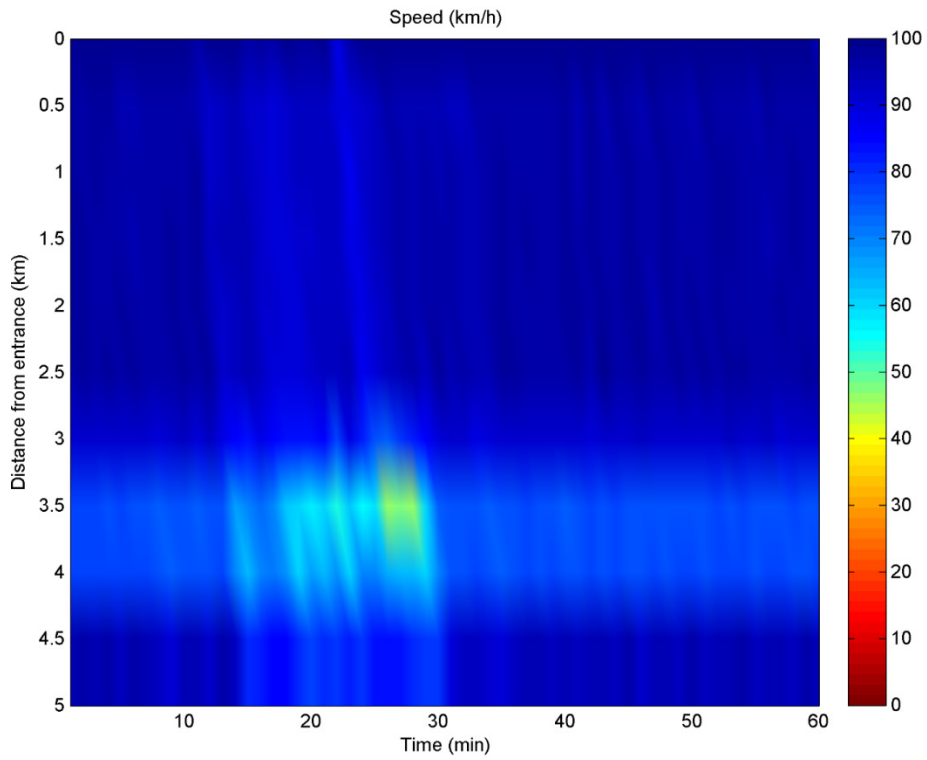
**Figure K.5: Speed-Distance-Time 3D Diagram for network, LCC 80% & VSL**
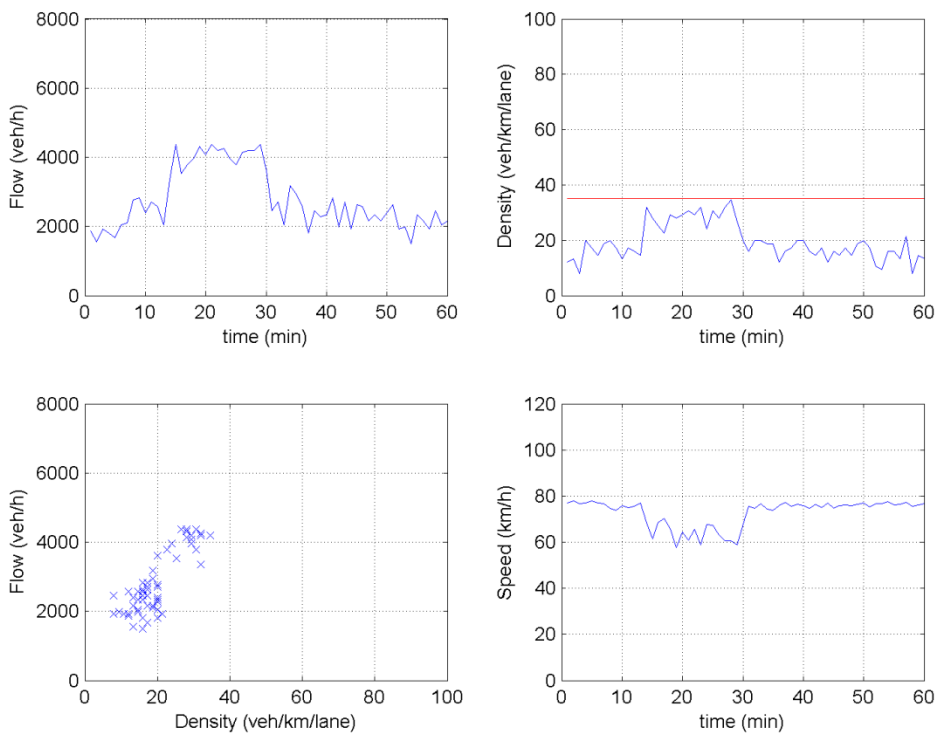
**Figure K.6: Flow, Density, Speed-Time & Flow-Density at lane-drop Section (ID 367), VSL Set-point (red), LCC 80% & VSL**
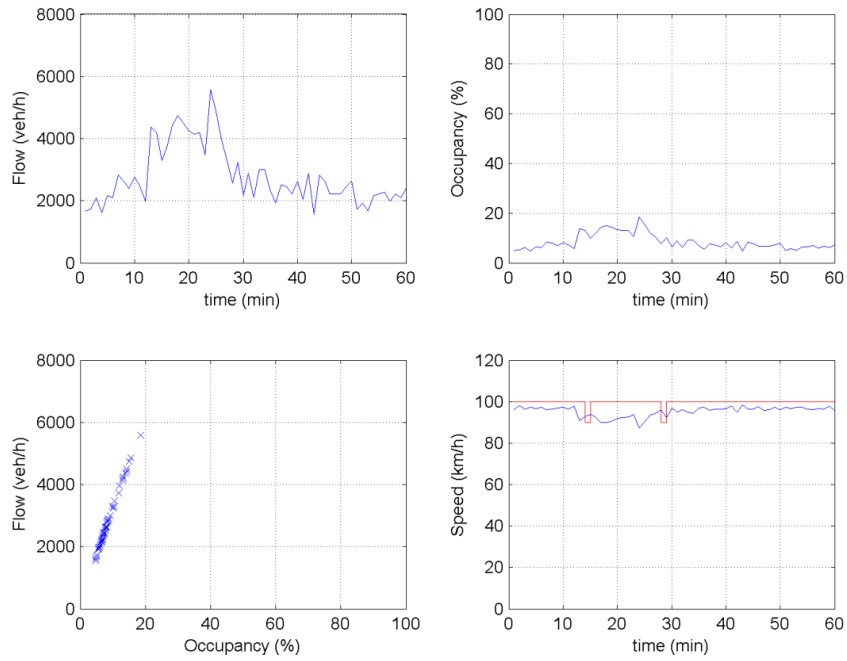
Figure K.7: Flow, Density, Speed-Time & Flow-Density at the Application area (ID 358), VSL decisions (red), VSL decisions (red), LCC 80% & VSL
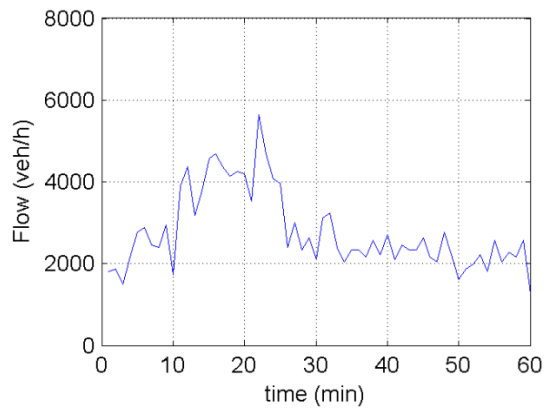

Figure K.8: Demand entering the network (ID 338)
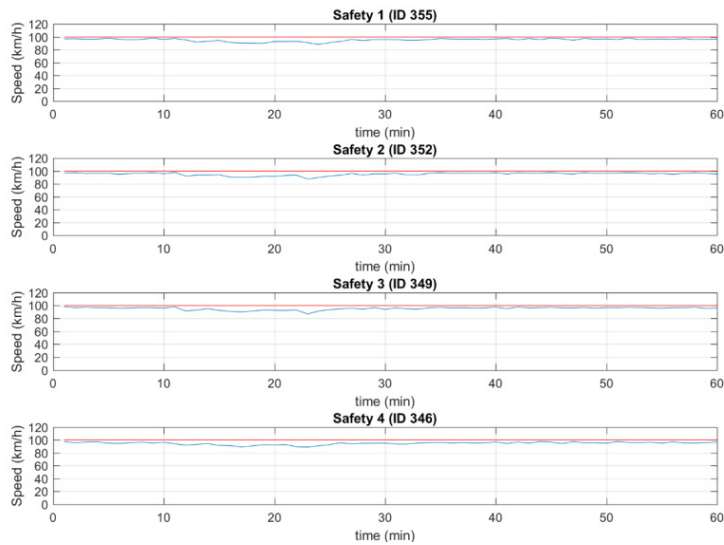
Figure K.9: Speed (blue) and VSL decisions (red) in Safety areas, LCC 80% & VSL

87
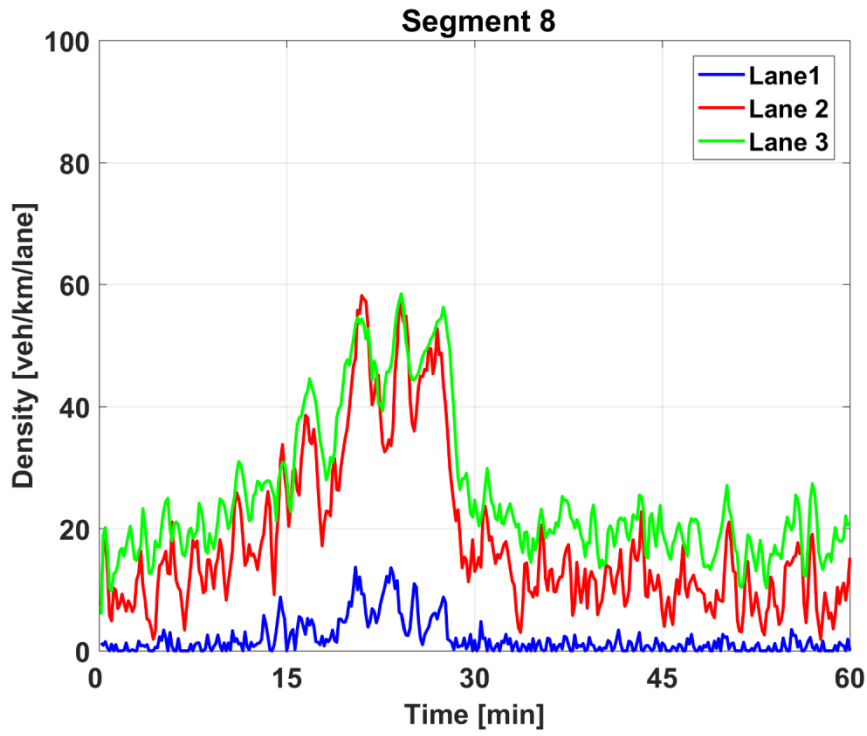
Figure L.1: Density comparison in lane-drop Section (ID 364), lane 1 (blue), lane 2 (red) and lane 3 (green), LCC 100% & VSL
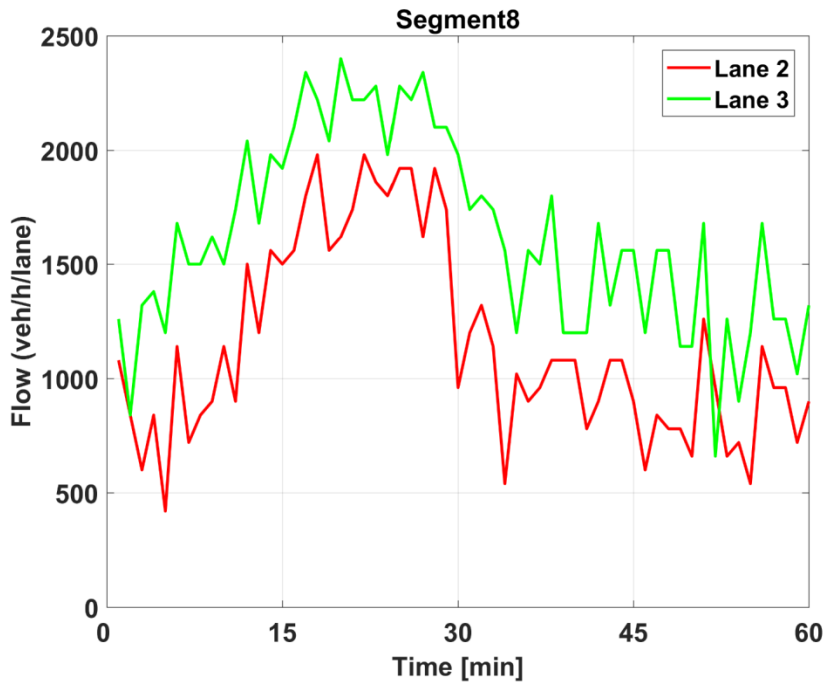
Figure L.2: Flow comparison in lane 2 (red) and lane 3 (green) at lane-drop Section (ID 364), LCC 100% & VSL
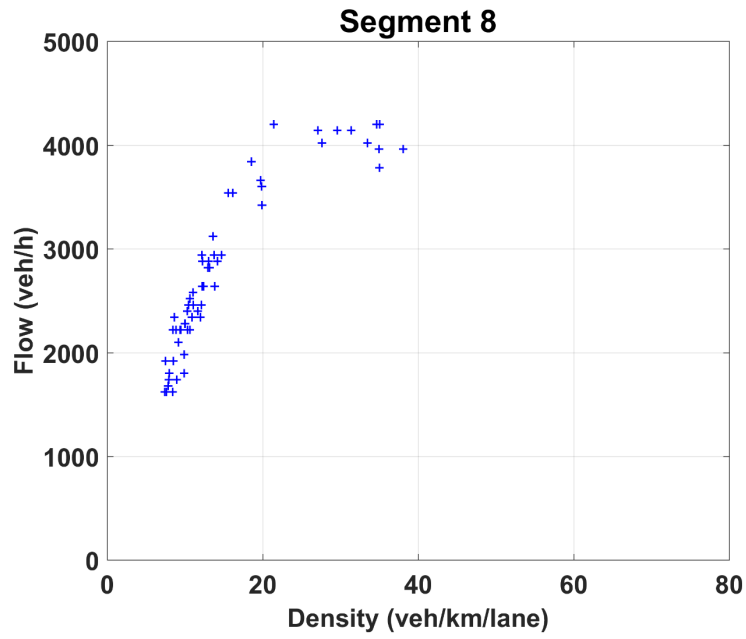
Figure L.3: Fundamental diagram (aggregated) at lane-drop Section (ID 364), LCC 100% & VSL
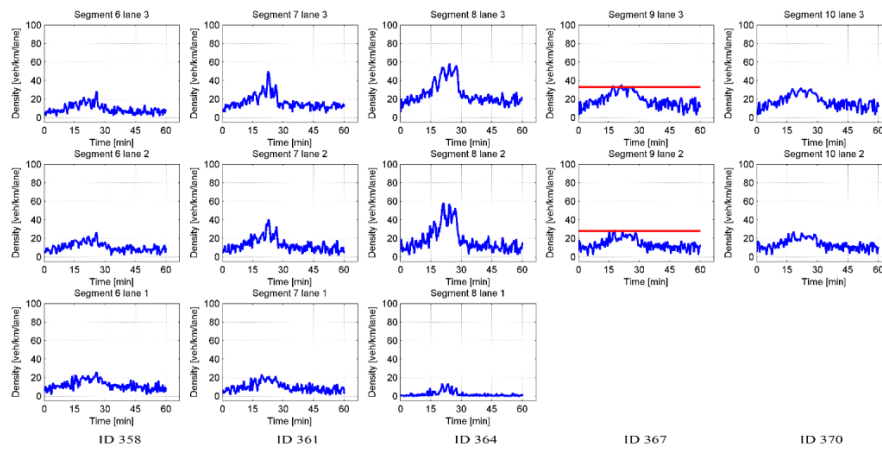
Figure L.4: Density-Time diagram of each lane from Section ID 358 until ID 370, LCC 100% & VSL

89
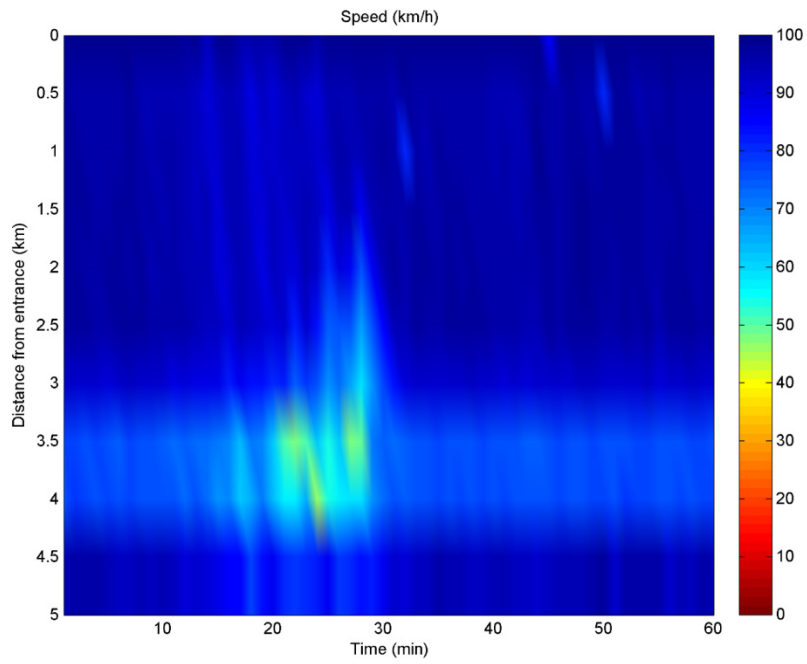
Figure L.5: Speed-Distance-Time 3D Diagram for network, LCC 100% & VSL
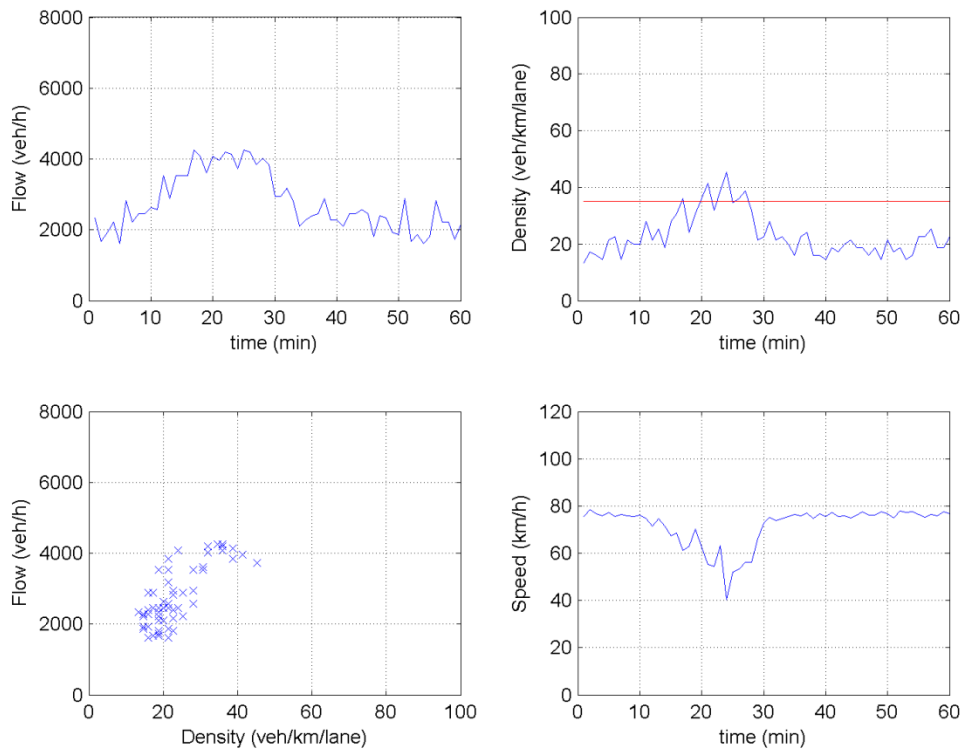
Figure L.6: Flow, Density, Speed-Time & Flow-Density at lane-drop Section (ID 367), VSL Set-point (red), LCC 100% & VSL
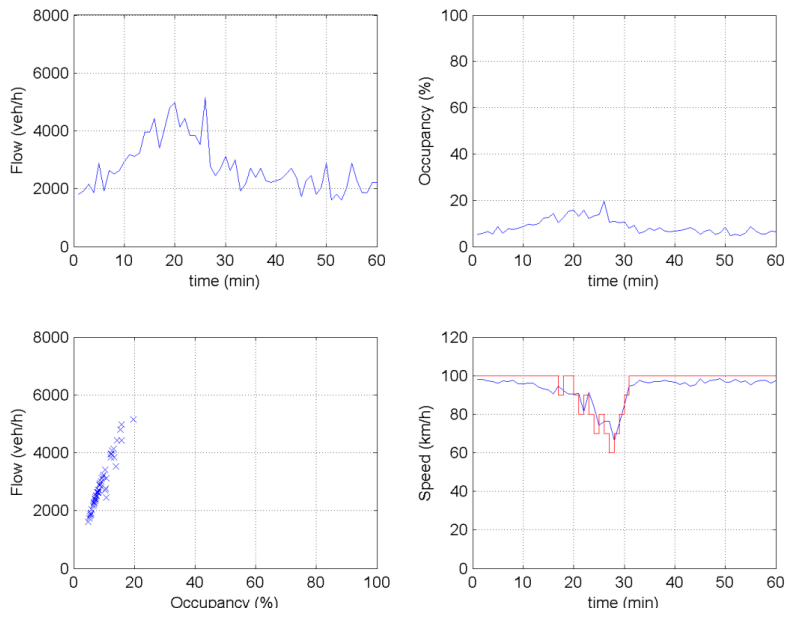
Figure L.7: Flow, Density, Speed-Time & Flow-Density at the Application area (ID 358), VSL decisions (red), LCC 100% & VSL
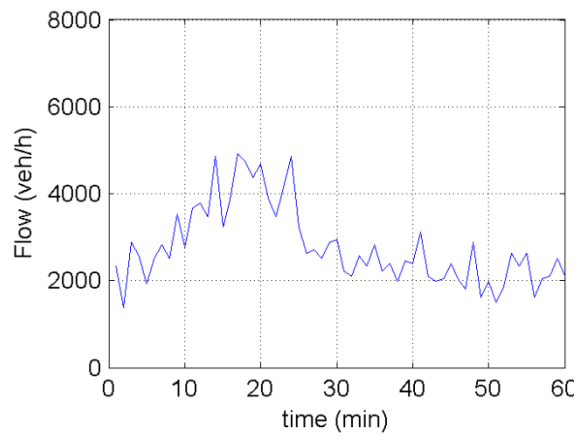

Figure L.8: Demand entering the network (ID 338)
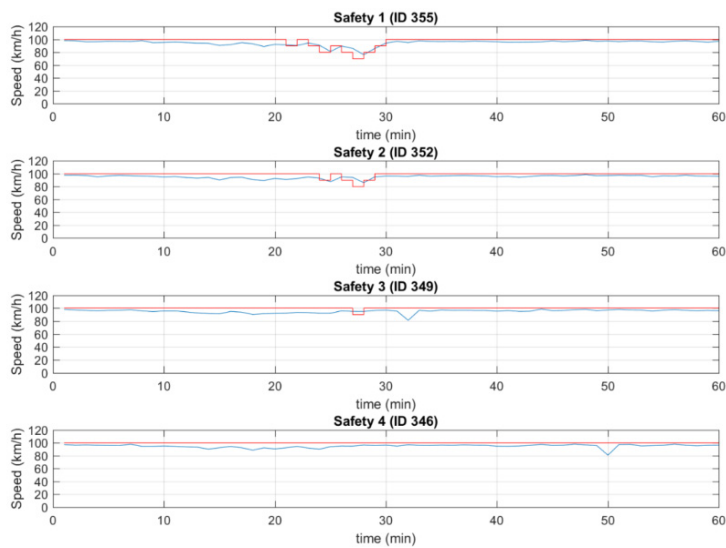
Figure L.9: Speed (blue) and VSL decisions (red) in Safety area, LCC 100% & VSL

91

References

AG Planung Transport Verkehr (2011). *Vissim 5.40-01 user manual.*

Anderson, B. D. O. & Moore, J. B. (1971). *Linear optimal control*, Prentice-Hall.

Barcelo, J. & Casas, J. (2005). *Dynamic network simulation with AIMSUN.*

Bekiaris, N., Roncoli, C. & Papageorgiou, M. (2016). Highway Traffic State Estimation With Mixed Connected and Conventional Vehicles. *IEEE Transactions on Intelligent Transportation Systems,* 17**,** 3484-3497.

Carlson, R. C., Papamichail, I. & Papageorgiou, M. (2011). Local Feedback-Based Mainstream Traffic Flow Control on Motorways Using Variable Speed Limits. *IEEE Transactions on Intelligent Transportation Systems,* 12**,** 1261-1276.

Carlson, R. C., Papamichail, I. & Papageorgiou, M. (2013). Comparison of Local Feedback Controllers for the Mainstream Traffic Flow on Freeways Using Variable Speed Limits. *Journal of Intelligent Transportation Systems,* 17**,** 268-281.

Chevallier, E. & Leclercq, L. (2009). Do microscopic merging models reproduce the observed priority sharing ratio in congestion? *Transportation Research Part C: Emerging Technologies,* 17**,** 328-336.

Courant, R., Friedrichs, K. & Lewy, H. (1928). Über die partiellen Differenzengleichungen der mathematischen Physik. *Mathematische Annalen,* 100**,** 32-74.

Diakaki, C., Papageorgiou, M., Papamichail, I. & Nikolos, I. (2015). Overview and analysis of vehicle automation and communication systems from a motorway traffic management perspective. *Transportation Research Part A: Policy and Practice,* 75**,** 147-165.

FHWA, U.S. Department of Transportation (1997). *CORSIM User's Manual*, FHWA, U.S. Department of Transportation

Gipps, P. (1981). A behavioural car-following model for computer simulation. *Transportation Research Part B: Methodological,* 15**,** 105-111.

Gipps, P. (1986). A model for the structure of lane-changing decisions. *Transportation Research Part B: Methodological,* 20**,** 403-414.

Hespanha, J.P. (2009). *Linear systems theory*, Princeton University Press

Kesting, A. & Treiber, M. (2008). Calibrating car-following models by using trajectory data: Methodological study. *Transportation Research Record: Journal of the Transportation Research Board*, 148-156.

Panwai, S. & Dia, H. (2005). Comparative evaluation of microscopic car-following behavior. *IEEE Transactions on Intelligent Transportation Systems,* 6, 314-325.

Papageorgiou, M. (2004). Overview of Road Traffic Control Strategies. *IFAC Proceedings Volumes,* 37, 29-40.

Papageorgiou, M., Diakaki, C., Dinopoulou, V., Kotsialos, A. & Yibing, Wang (2003). Review of road traffic control strategies. *Proceedings of the IEEE,* 91, 2043-2067.

Papageorgiou, M. & Kotsialos, A. (2000). Freeway ramp metering: an overview. *In ITSC2000. 2000 IEEE Intelligent Transportation Systems. Proceedings (Cat. No.00TH8493)*. 228-239.

Papamichail, I., Papageorgiou, M. & Stamatakis, I. (June 6-8, 2017). Feedback traffic control at highway work zones using variable speed limits. *15th IFAC Symposium on Control in Transportation Systems (CTS 2018),* Savona, Italy.

Park, B. & Qi, H. (2006). In Microscopic simulation model calibration and validation for freeway work zone network-a case study of VISSIM. *Intelligent Transportation Systems Conference, 2006. ITSC'06. IEEE*. IEEE, 1471-1476.

Perraki, G. (2016). *Evaluation of a model predictive control strategy on a calibrated multilane microscopic model.* Master Thesis, Technical Univesity Crete

Roncoli, C., Bekiaris, N. & Papageorgiou, M. (November 1-4, 2016 2016). Optimal lane-changing control at motorway bottlenecks. *2016 IEEE 19th International Conference on Intelligent Transportation Systems* Windsor Oceanico Hotel, Rio de Janeiro, Brazil. ITSC, 1785-1791.

Roncoli, C., Bekiaris, N. & Papageorgiou, M. (2017). Lane-Changing Feedback Control for Efficient Lane Assignment at Motorway Bottlenecks. *Transportation Research Record: Journal of the Transportation Research Board,* 2625, 20-31.

Roncoli, C., Papageorgiou, M. & Papamichail, I. (2015). Traffic flow optimisation in presence of vehicle automation and communication systems – Part I: A first-order multi-lane model for motorway traffic. *Transportation Research Part C: Emerging Technologies,* 57, 241-259.

Roncoli, C., Papamichail, I. & Papageorgiou, M. (2014). Model predictive control for multi-lane motorways in presence of VACS. *In Intelligent Transportation Systems (ITSC), 2014 IEEE 17th International Conference on*. IEEE, 501-507.

Schrank, David, Eisele, Bill, Lomax, Tim & Bak, Jim (2015). 2015 urban mobility scorecard.

Transport Simulation Systems (2003). *GETRAM Getting Started.*, Transport Simulation Systems.

Transport Simulation Systems (2014). *Aimsun 8 Dynamic Simulators Users' Manual.,* Transport Simulation Systems.

Treiber, M., Hennecke, A. & Helbing, D. (2000). Congested traffic states in empirical observations and microscopic simulations. *Physical review E,* 62**,** 1805.

Vigos, G., Papageorgiou, M. & Wang, Y. (2008). Real-time estimation of vehicle-count within signalized links. *Transportation Research Part C: Emerging Technologies,* 16**,** 18-35.

Wang, J., Liu, R. & Montgomery, F. (2005). Car-following model for motorway traffic. *Transportation Research Record: Journal of the Transportation Research Board***,** 33-42.

Williams, R. L. & Lawrence, D. A. (2007). *Linear State-Space Control Systems.,* USA, John Wiley & Sons, INC.